NASA Contractor Report 3638

Atmospheric Backscatter Model Development for CO_2 Wavelengths

Adarsh Deepak, Geoffrey S. Kent,
and Glenn K. Yue
Institute for Atmospheric Optics and Remote Sensing
Hampton, Virginia

Prepared for
Marshall Space Flight Center
under Contract NAS8-34427

National Aeronautics
and Space Administration

**Scientific and Technical
Information Branch**

1982

TABLE OF CONTENTS

SUMMARY

This is the final report for NASA Contract NAS8-34427. The report presents the results of investigations into the problems of modeling atmospheric backscatter from aerosols, in the lowest 20 km of the atmosphere, at CO_2 wavelengths. It contains a summary of the relevant aerosol characteristics and their variability, together with a discussion of the measurement techniques and the errors involved. The different methods of calculating the aerosol backscattering function, both from measured aerosol characteristics, and from optical measurements made at other wavelengths, are discussed in detail and limits placed on the accuracy of these methods. The effects of changing atmospheric humidity and temperature on the backscatter are analyzed and related to the actual atmosphere. Finally, the results of modeling CO_2 backscatter in the atmosphere are presented and the variation with height and geographic location discussed, and limits placed on the magnitude of the backscattering function β_{CO_2}. Detailed conclusions regarding modeling techniques and modeled atmospheric backscatter values are presented in tabular form at the end of the report. The most significant of these conclusions are as follows:

1. The qualitative hehavior of β_{CO_2} can be modeled, including the variation with height and major geographic features.

2. Accurate calculation of β_{CO_2} requires an accurate knowledge of the particle size distribution to a particle radius of at least 1 μm, for stratospheric aerosols, and at least 5 μm for tropospheric aerosols.

3. Particles with radii greather than 0.5 μm are responsible for 50% to 95% of the scattering from tropospheric aerosols.

4. β_{CO_2} decreases from about 10^{-6} m^{-1} sr^{-1} at the Earth's surface to 10^{-11} m^{-1} sr^{-1} in the stratosphere. A minimum value of 10^{-11} m^{-1} sr^{-1} is also observed in the free troposphere over the remote ocean.

5. The variation of β_{CO_2} with wavelength between 9 μm and 11 μm is not significant, except for water soluble aerosols.

6. β_{CO_2} is not strongly dependent upon relative humidity, except for very high values well above the point of deliquescence for the water soluble component.

7. The major information gap is in the composition and size distribution of particles with radii greater than 1 μm, particularly above an altitude of 7 km.

8. It is recommended that simultaneous measurements be made on aerosols in the free troposphere and stratosphere using different particle sensors and CO_2 lidar.

1. INTRODUCTION

The recent introduction of coherent doppler lidar systems, for atmospheric wind measurements, has led to a need for detailed knowledge of the scattering characteristics of stratospheric aerosols, at the CO_2 laser wavelengths used in these experiments. In order to meet this need, a program of study has been carried out to assess the problems encountered in modeling atmospheric backscatter at a wavelength of 10.6 μm (and neighboring wavelengths) and to determine, within limits of error, the values of the aerosol backscattering function (β_{CO_2}) in the atmosphere.

Factors involved in the calculation of β_{CO_2} from measured aerosol characteristics are the size distribution and number concentration of the aerosol, its refractive index and the particle shape. Consideration must also be given to uncertainties in the measurement of these quantities and their natural variation in the atmosphere. These last two factors are particularly important and also difficult to assess, as a variety of different measurement techniques exist, yielding results that often agree qualitatively rather than quantitatively. Moreover, such measurements have tended to be made mainly over continental regions, and oceanic areas, particularly in the southern hemisphere have been poorly represented. We have also examined the possibility of using backscattering measurements made at other wavelengths (using visible and near infrared lidar), and extinction measurements, to estimate β_{CO_2}. Again, the same factors are found to influence the establishment of any simple rule for conversion of backscattering functions and extinction coefficients from one wavelength to another.

Several parallel approaches have been taken to examine these problems. We have used log-normal models of variable mode radius and width to simulate the naturally occurring aerosol size distributions, using both a flexible range of refractive indices and those corresponding to a set of common aerosol materials. In these and other calculations we have assumed spherical particle shape and used standard Mie theory to determine the optical properties. We have also carried out similar calculations using a very wide range of measured particle size distributions obtained from a comprehensive literature search. Calculations of the effects of varying certain atmospheric and optical parameters, e.g., humidity and wavelength, have been made using a limited number of measured size distributions, representative of certain classes of aerosol measurement.

The organization of this report is sequential. Section 3 summarizes measured aerosol characteristics and the models used to describe them. Variations of concentration with altitude and geographical location, as well as the effect of changes in humidity and temperature are covered. Section 4 summarizes potentially useful optical measurements made on aerosols, using visible and near infrared wavelengths, particularly those made using lidar. Sections 5 and 6 discuss the techniques used for the calculation of β_{CO_2} and the errors arising in these techniques. A fairly full and, as far as possible, quantitative discussion is given of the influence of the various factors listed above. Section 7 contains the results of our calculations on β_{CO_2} in the atmosphere, its variation with height and geographical location and its statistical fluctuation. Comparison is made of the rsults of the model calculations with available β_{CO_2} lidar data from NASA-Marshall Space Flight Center and from NOAA. Section 8 summarizes, in tabular form, our conclusions with regard to the various aspects of this work.

2. DATA BASE USED

As will be discussed in more detail later in this report, there are three basic methods of modeling β_{CO_2}. The first method is based on our knowledge of the characteristics of aerosol particles at all altitudes and geographical locations of interest. The characteristics of aerosol particles pertinent to β_{CO_2} are basically aerosol size distribution, concentration, chemical composition, and refractive index. The input data commonly used in this method consists of in situ measurments and aerosol particle models. The second and third methods utilize lidar data at visible and near infrared wavelengths, and extinction measurements, respectively. Although the later two methods are more indirect than the first method, the existence of large quantities of data in these two classes makes it worthwhile to investigate the possibility of utilizing the lidar data obtained by different research groups scattered around the globe. In contrast to the wide distribution of possibly useful lidar data, extinction measurements, that serve our purpose, are dominated by the single data set that has been obtained by the SAGE and SAM II satellite experiments (McCormick et al., 1979). This data is now in the process of being archived at the National Space Sciences Data Center at NASA-Goddard Space Flight Center, Greenbelt, Maryland.

The method of acquisition of data bases, to be used in subsequent studies discussed in this report, consisted mainly of literature searches and personal contact. A literature search was carried out under the major headings used in this study, using the NASA/RECON system. The subject of interest was divided into five major areas which are listed in Table 2.1. Details of the search procedure as well as the number of references identified are also shown in that table. Approximately 1500 sources have been identified in this way. The most important articles have been obtained and analyzed according to their potential value. Besides such research reports in open literature, some unpublished data belonging to the Institute for Atmospheric Optics and Remote Sensing and its staff scientists have also been examined.

Our data base has also been augmented by personal contact. This included correspondence, telephone calls, personal discussions, and a few visits, where possible. This action was confined mainly to the field of lidar studies and details of the results of this investigation are shown in detail in Section 4.1.

TABLE 2.1 LITERATURE SEARCH ON NASA/RECON SYSTEM

Subject area	Details of search				Number of references identified
	Set	No.		Description	
Aerosol models and size distributions	1	6546	6546	ST/aerosols	
	2	1217	1217	BT/particles	
	3	14598	14598	R8,R9 ST/aerosols	
	4	2550	2550	R10,R13 ST/aerosols	
	5	14	14	RT/SAGE satellite	
	6	2876	2876	ST/models	
	7	15502	15502	NT/atmospheric models	
	8	599	599	NT/environment models	
	9	1917	1917	(1+2+3+4)*(6+7+8)	
	10	848	848	MJ/models	
	11	7846	7846	MJ/atmospheric models	
	12	346	346	MJ/environment models	
	13	1003	1003	(1+2+3+4)*(10+11+12)	
	14	315	315	1*(10+11+12)	
	15	1396	1396	RT/dust	
	16	350	350	(1+2+15)*(10+11+12)	
	17	6390	6390	R1,R2 ST/size distribution	
	18	1551	1551	(1+2+15)*17	
	19	1380	1380	1*17	
	20	2299	2299	MJ/R1,R2 ST/size distribution	
	21	695	695	(1+2+15)*20	
	22	670	670	21-16	
	23	473	473	)22/75-81	473
Aerosol composition	1	6546	6546	ST/aerosols	
	2	1217	1217	BT/particles	
	15	1396	1396	RT/dust	
	28	744	744	R1,R2 ST/composition	
	29	25	25	(1+2+15)*28	
	30	7840	7840	ST/chemical composition	
	31	6597	6597	ST/chemical analysis	
	32	396	396	(1+2+5)*(30+31)	
	33	416	416	29+32	416
Aerosol refractivity	1	6546	6546	ST/aerosols	
	2	1217	1217	BT/particles	
	10	848	848	MJ/models	
	11	7846	7846	MJ/atmospheric models	
	12	346	346	MJ/environment models	
	15	1396	1396	RT/dust	
	16	350	350	(1+2+15)*(10+11+12)	
	20	2299	2299	MJ/R1,R2 ST/size distribution	
	21	695	695	(1+2+15)*20	
	22	670	670	21-16	
	23	473	473	)22/75-81	
	24	4771	4771	US/refractivity	
	25	233	233	(1+2+15)*24	
	26	220	220	25-16	
	27	188	188	25-23	188
Lidar measurements of atmospheric aerosols	1	2276	2276	US/optical radar	
	2	6546	6546	ST/aerosols	
	3	1217	1217	BT/particles	
	4	1396	1396	RT/dust	
	5	440	440	1*(2+3+4)	440
Extinction radiometry and optical depth	1	409	409	ST/extinction	
	2	4500	4500	ST/atmospheric attenuat	
	3	2988	2988	ST/atmospheric boundary	
	4	1763	1763	MJ/atmospheric optics	
	5	3844	3844	ST/radiometers	
	6	24	24	4*5	
	7	88	88	1*(2+3+4)	
	8	42	42	UTP/optical *3 depth	
	9	644	810	AX/optical *3 depth	
	10	80	115	(2+3+4)*(8+9)	
	11	184	219	6+7+10	184

Terms used in the search are combined together using the normal rules of Boolean algebra. Special symbols usesd are as follows:

AX	Key word occurring in abstract	RT	Related Term
BT	Broader Term	ST	Subject Term
MJ	Major Term	US	Use
NT	Narrower Term	UTP	Key word occurring in title

3. AEROSOL PROPERTIES—MODELS AND MEASUREMENTS

3.1 Survey

Aerosol properties such as composition, refractive index and size distribution are a function, not only of geographic location and height above the earth's surface, but also of season and the history of the air-mass in which the aerosol occurs. A simplified view of its dependance upon the first two of these parameters is shown in Fig. 3.1. In this figure the first 20 km of the earth's atmosphere has been divided into four main regions within which the variation of aerosol properties is less than it is for the whole globe.

Two classes of boundary layer aerosols are recognized, a maritime aerosol with a moist sea-salt aerosol as its main component and a continental aerosol consisting of a mixture of an insoluble component (mainly silicate dust and soil) and a soluble component (mainly ammonium sulphate and sulphuric acid)(WMO report No. WGP-12).* Exchange of material between these two regions will occur near the continental margins. Above the boundary layer, there exists a free tropospheric aerosol whose constituents are derived from, and are the same as, the continental boundary layer aerosol. This is approximately true whether we consider the free troposphere over the land or the ocean although, as we shall see later, the size distributions are different.

Above the troposphere there exists a background stratospheric aerosol consisting of a mixture of approximately 75% sulphuric acid and 25% water. This is distributed globally with a concentration that varies with height and latitude as shown in Fig. 3.2 (Rosen et al., 1975).

Also shown in Fig. 3.1 is the approximate height variation of the aerosol number concentration. This quantity is highly variable but, in general, exhibits two maxima, one near the surface of the earth and the other in the stratosphere. The concentration near the earth's surface depends on the amount of mechanical disturbance; that in the stratosphere depends on the recent history of volcanic eruptions which inject material into that region. The concentration in the free troposphere is also highly variable, particularly over the oceans, where it depends upon transport of material from over the continents.

Fig. 3.3 shows typical examples of the aerosol size distribution in different parts of the atmosphere. These have been plotted in two ways—as the number of particles per log radius interval (dN/d log (r)) and as the particle volume per log radius interval (dV/d log (r)). Both representations occur in the literature, the former being the more common and the latter more useful for conversion to mass aerosol loading. A significant feature of the boundary layer and free tropospheric distributions is their bimodal character (Patterson and Gillette, 1977, Patterson et al., 1980). Of most importance is the coarse particle mode. This consists of approximately 80% insoluble and 20% soluble material, has a volume mode maximum radius between 1 and 4 μm (in the free troposphere) and a minimum between it and the ac-

*Note: A third class of Urban-Industrial Aerosols is also recognized, which will not be considered in this report.

cumulation mode aerosol at about 0.2μm (Nilsson, 1979; Winkler, 1974). The stratospheric aerosol is usually considered to be uni-modal in character although recent measurements by Hofmann and Rosen (1981) have cast some doubt upon this.

Measurements on the size distribution of the boundary layer aerosol are well distributed over the globe; those in the free troposphere and stratosphere are much less so. Fig. 3.4 shows the locations of those free tropospheric and stratospheric aerosol measurements used in this report. Three continents only are represented, North America, Australia and Europe, and a limited amount of data is available over the Atlantic and Pacific oceans.

3.2 Size Distributions and Concentrations

3.2.1 In situ measurement techniques

The existence of a wide range of aerosol size distributions, concentrations and refractive indices presents formidable problems in the measurement of aerosol size spectra. The size range of aerosol particles in the atmosphere that may contribute to the backscatter at CO_2 wavelengths extends from about 0.01 μm to 30 μm and the overall concentration may vary from less than 1 cm^{-3} in the stratosphere to 10^7 cm^{-3} in a polluted area. Aerosol refractive indices vary from 1.18 - 0.0677i (for water at λ = 10.6 μm) to 2.22 - 0.73i (for soot at λ = 10.6 μm). The problem is further complicated by the fact that most measurement devices perturb the natural state of the atmospheric aerosols in advance of measuring the number concentration. Some particles may be lost on their passage through the narrow tube leading to the counter and the size and composition may be modified deliberately or inadvertently inside the instrument. Though theoretically the actual aerosol size distribution can be deduced from the measured result, in practice the conversion process depends on so many factors that different aerosol size distributions may be obtained from the same set of measurements. Consequently, the reported aerosol size distribution obtained from in situ measurements must be used with caution and the possible errors involved in the measurement should be considered carefully.

According to Lundgren (1976), aerosol measurement instruments can be divided into four categories: inertial impactor, light-scattering particle counters, electric mobile analyzers and condensation nuclei counters. A critical discussion of instruments in these four categories is given in the following paragraphs.

A. Inertial impactor

Inertial classification devices separate aerosol particles in an aerodynamic size dependent manner for subsequent analysis by other techniques. The measured aerodynamic size range is from about 0.25 μm to 2.5 μm in radius. Some possible sources of errors commonly associated with all inertial impactors are:

(a) Aerosols collected by this method may undergo evaporation, growth and other physical or chemical processes between the time and location of collection and the time and location of analysis; i.e., this method is not a truly in situ method.

(b) Aerosol particles may be lost in the walls of inlet system; i.e., isokinetic sampling can hardly be achieved.

(c) Since the aerosol size distribution is not obtained directly from the impactor device, different size distributions may be deduced from the same set of samples using different analyzing techniques.

B. Light scattering particle counters

The basic parameter measured in this class of devices is the amount of radiation scattered by the aerosol particle inside the counter. The number and height of the pulses generated by the scattered radiation is electrically converted to a particle number and particle size; most optical counters operate best for particles with radii between 0.25 μm and 2.5 μm. Some possible sources of error commonly associated with all optical particle counters are:

(a) Systematic errors in the electric and optical system such as the instability of the light source, lens system distortion and contamination of the optical system.
(b) Uncertainty of the properties of aerosol, including its shape and the wavelength dependence of its refractive index.
(c) Multi-valued light scattering versus particle size response and multi-particle scattering.

C. Electric mobile analyzer

This device measures the electric mobility of an unknown particle in a known electric field. Since the electric mobility of a gas borne particle in an electric field is a monotonic function of particle size, the size of aerosol particles can be determined from the measured electric mobility. There are three basic parts of an electric mobile analyzer: a diffusion charge section which places a charge on each aerosol particle; a mobility analyzer which collects particles with a mobility greater than a pre-set value; and an electrometer which measures the current flow by the remaining charged particles.

This method is applicable to the measurement of aerosol particles with radii less than about 0.25 μm. In order to measure larger sized aerosols, it is necessary, either to increase the field intensity in the condenser, or to reduce the rate of flow of the aerosol. Very intense fields may result in leakages, local discharge and, at low flow rates, other complications such as the generation of convection currents.

Other possible sources of error are the non-uniform charging of the aerosol particles and non-laminar flow through the condenser.

D. Condensation nuclei counter

The condensation nuclei counter (C.N.C.) is a device that counts the number of active nuclei in a supersaturated chamber. The counting can be done manually, or automatically, by measuring the extinction of light caused by the presence of liquid droplets containing condensation nuclei.

Two types of errors may occur. One is the instrumental error and another is caused by the nature of the particle being measured. The traditional technique for detecting condensation nuclei is to make them grow to sizes where they are efficient scatterers of light, by supersaturating the sampling air. Since the number of active scattering nuclei increases dramatically in response to a slight increase of supersaturation, the supersaturation in the chamber must be accurately determined. Furthermore, the growth of condensation nuclei depends on their physical characteristics, including composition and shape. If the concentration is deduced by measuring extinction, one additional parameter, namely the index of refraction is involved. If the characteristics of the in situ aerosol particles are quite different from those used for a calibration, large errors may be produced.

A very brief summary of the common in situ measurement techniques is given in Table 3.1. The list of names of users shown in the Table is of course incomplete. Most of the names listed are here because they have measured aerosol characteristics (particularly the aerosol size distribution), which are specifically discussed in this report.

3.2.2 Measured size distributions

Aerosol size distributions in the free troposphere show considerable differences when measurements made by independent workers, using different techniques, are compared. Fig. 3.5 shows a set of volume size distributions obtained by Blifford and Ringer (1969) at different altitudes over the continental U.S.A. using a single stage impactor. All the distributions show a mode maximum at a radius of about 2 μm. There is a decrease of concentration with altitude particularly for the smaller particles. Fig. 3.6 shows size distributions measured by Cress (1980) over Europe using a Royco optical counter. Although not exactly the same, the general characteristics of the curves are similar, the mode maxima for this set occurring around 3 μm. Fig. 3.7 shows a set of distributions obtained by Patterson et al. (1980) over the continental U.S.A. and the Pacific Ocean using a PMS optical counter. The boundary layer distributions have a shape similar to those obtained by Blifford and Ringer and by Cress but the free tropospheric distributions show significant differences. From the point of view of modelling β_{co_2}, the most important difference is that of the mode maximum for the large particle distribution, which is less than 1 μm for this data. The effects of these differences on the modelled values for β_{co_2} will be discussed in a later section.

In Section 3.1 we noted that the free tropospheric aerosol over the ocean was largely derived from that over the continent. This has important implications with regard to the size distribution due to the gradual sedimentation of the larger particles during transport over the ocean. This is illustrated in Fig. 3.8 which shows data obtained by three independent sets of research workers over the land and over the ocean. That of Savoie (1978) is related to the movement of Saharan dust over the Atlantic Ocean and the change in the mode radius between the size distribution over Sal Island (off the coast of West Africa) and Miami is very clear. The other two sets do not relate directly to a specific transport process but illustrate the general differences between the aerosol over the Pacific Ocean and the continental U.S.A. In both cases the free troposphere over the ocean contains far fewer large particles. It is also clear from recent work (Shaw, 1980; Duce et al., 1980) that desert dust is carried over the Pacific Ocean from Eastern Asia in a somewhat similar manner to that in which Saharan dust is carried over the Atlantic. At this time measurements on these dust streams have yet to be made in the free troposphere.

An alternative way to present the differences between the free troposphere over the ocean and the land is to show the height variation of the larger particles for both cases. This is shown in Figs. 3.9, 3.10 and 3.11 for data over Europe, U.S.A. and the Pacific Ocean, respectively. The rapid decrease in concentration above the marine boundary layer is most noticeable. This is in contrast to the continental cases where convection causes vertical mixing throughout the troposphere.

Patterson et al. (1980) have reported a strong latitudinal variation in the aerosol mass loading in the free troposphere over the Pacific Ocean. The variation, which is shown in Fig. 3.12, reflects the fact that the majority of the continental land mass and hence the most significant movement of continental dust over the oceans is in the Northern Hemisphere. (The scale on the right hand side of this figure, which shows the equivalent value of β_{co_2} will be discussed in Section 7.)

So far in this section we have been primarily concerned with the variation with height and geographical location of the mean value of the aerosol concentration. It is of importance to inquire about the variation that may be observed if these two parameters are held fixed. The same data sets, as previously used from Cress and Patterson et al., have been analyzed in order to obtain information on this variation. Fig. 3.13 shows the probability distributions

for the particle count obtained by Cress at three different altitude ranges for a nine month period over Europe. No division in particle size range has been attempted although the data indicate that there was slightly more variation for particles with radii greater than one micron than for particles smaller than this. Fig. 3.14 shows probability distributions obtained by Patterson et al. on flights at a height of 5-6 km over the western U.S.A. and the central Pacific. Although the data are somewhat limited, the range of statistical variation is similar to that obtained by Cress, namely that the 10% and 90% probability levels for the particle concentration lie approximately 1½ decades apart.

Background stratospheric aerosol size distributions are traditionally uni-modal (Russell et al., 1981) and approximately log-normal in shape with a maximum (in dN/d log r) near a radius of 0.1 μm. The concentration shows a latitudinal variation as already described in Fig. 3.2 and small seasonal fluctuations. The major factor controlling the concentration of stratospheric aerosols is, however, volcanic activity, which injects SO_2 (and ash) into the stratosphere. This is subsequently oxidized and combines with water to form H_2SO_4 which then associates to form aerosols. The lifetime of these aerosols is to be measured in months or years and the injection from a single volcano may eventually spread to cover the globe. The ash which is injected with the SO_2 consists of larger particles which sedimate out much more rapidly. Although stratospheric particle concentrations have been measured directly for the past twenty years, one of the best long-term records is that obtained using lidar techniques. This will be described later in Section 4.1. Recently, as noted in Section 3.1, Hofmann and Rosen (1981) have made measurements, using a specially designed large particle counter, of the concentrations of particles with radii between 1 and 2 μm. An example of these measurements is shown in Fig. 3.15, where it can be seen that, compared to the log-normal distribution, there is a significant excess of particles with radii within these limits. Unfortunately, no other workers have yet made any similar measurements and the nature and behavior of these particles still has to be established.

In subsequent sections of this report we shall make use of both number and mass concentrations of aerosols when modelling β_{CO_2}. In order to assist in the appreciation of those sections, Table 3.2 shows a brief list of typical values of these quantities for different altitudes and parts of the globe. A summary of the main features of aerosol size distributions and concentrations, most of which have been covered in this chapter, is given in Table 3.3.

3.3 Aerosol Models

In the past two decades, numerous in situ measurements of aerosol particles in the atmosphere have been reported. These experimental data show that, in general, the physical, optical and chemical properties of aerosol particles change with altitude, location and season of the year. In order to predict the behavior of aerosol particles in different regions of the atmosphere and under different ambient conditions, several investigators have summarized the reported aerosol measurements and derived analytical or numerical representations of aerosol properties. A survey of these global aerosol models shows that their number is surprisingly small (see Table 3.4). Furthermore, most of these investigators have concentrated their effort on the lower stratosphere and boundary layer; the free troposphere is the region with the least amount of information available. This is probably due to the fact that aerosol particles in the free troposphere are more difficult to measure than those in the boundary layer, and the variation of aerosol properties in the free troposphere is much larger than in the lower stratosphere. We have also found that most of the reported aerosol models consist of information on the size distribution and refractive index but not on the number concentration. On the other hand, even though aerosol size distributions in the stratosphere are

meticulously simulated, the size ranges of interest are usually for the smaller particles, the occasionally reported existence of larger particles (> 1 μm) in the stratosphere has never been included in the stratospheric models. In summary, we found that the properties of aerosol particles in the free troposphere, the number concentration of aerosol particles, and the size distribution of larger particles in the stratosphere are three areas of information not adequately simulated in the reported aerosol models.

Some of the global aerosol models important for β_{CO_2} studies are summarized in Table 3.4. As indicated earlier the atmosphere of interest can be divided into three regions: lower stratosphere (from tropopause to 30 km), the free troposphere (from $\sim$2 km to tropopause), and boundary layer (from ground to $\sim$2 km). Two types of aerosols in the stratosphere are modeled—background and post-volcanic. Aerosols in the boundary layer can be summarized in three categories: maritime, clean air continental, and polluted continental.

It should be noted that aerosol models listed in Table 3.4 are by no means inclusive. Some models, such as the Junge power law and the Deirmendjian modified gamma are not listed separately because these have been utilized and incorporated into the aerosol models developed by later investigators. It may also be noted that many models are based on experimental data obtained over limited regions of the earth's surface, e.g., the stratospheric model of Toon and Pollack is based only on data from the USA and Australia. Care must be taken in applying such models to conditions outside those from which they have been developed.

3.4 Composition and Refractive Index

As mentioned in Section 3.1 of this report, the composition of aerosol particles depends on several parameters, including the geographical location, height, season and history of the air mass containing the aerosol particles. Roughly speaking, the variation of aerosol composition decreases with height. In the boundary layer, the continental aerosols consist of a mixture of soluble components (mainly ammonium sulfate and sulfuric acid) and an insoluble component (mostly silicate dust and soil); maritime aerosols are mainly sea-salt particles but a continental component may also be present. Above the boundary layer, but below the tropopause (free troposphere), the composition of the aerosol particles is similar to that in the continental boundary layer. Above the tropopause, the aerosol particles are mainly sulfuric acid solutions (approximately 75%H_2SO_4 and 25%H_2O).

One of the important input parameters in calculating β_{CO_2} from the Mie code is the complex refractive index of the aerosol at the wavelength under consideration. The wavelength dependence of the complex refractive indices of some common aerosol materials are listed in Tables 3.5 and 3.6. In Table 3.5 most of the refractive indices are for visible or near infrared wavelengths. In addition, the refractive indices at 5.0 μm and 10.6 μm are also listed for the sake of comparison. In Table 3.6 the wavelength of radiation is limited to CO_2 laser wavelengths, ranging from 9.1 μm to 11.1 μm. It should be kept in mind that for some substances there are slight discrepancies between refractive indices given by different investigators. When this is the case, we have chosen one representative set of values to be listed in the tables. Furthermore, some of the limited values are obtained by interpolation and some are obtained by very rough estimation from graphs published by the authors. It should also be noted that the refractive indices listed (except water) are those of dry aerosols at room temperatures. A change of the ambient parameters such as relative humidity and temperature will certainly affect the refractive index. The influence of these on the refractive index will be examined in the next subsection.

From the listed refractive indices shown in Tables 3.5 and 3.6, the following conclusions can be drawn:

(a) In general, the refractive indices are quite sensitive to CO_2 wavelengths but not sensitive to visible or near infrared wavelengths.

(b) In general, the imaginary parts of the refractive indices at visible wavelengths are so small that they can be ignored in Mie calculations; however, the imaginary parts of the refractive indices at CO_2 wavelengths, for most materials except NaCl, are quite large and the absorption by aerosols at these wavelengths should not be ignored in any Mie calculation.

(c) At visible wavelengths the variation of refractive index with wavelength is monotonic, but at CO_2 wavelengths the variation is not monotonic for some materials. Consequently, interpolation of the refractive indices at CO_2 wavelengths must be carried out with caution.

(d) At CO_2 wavelengths, the refractive indices of common aerosol materials are, in general, larger than those at visible wavelengths. Furthermore, for some aerosol materials, the refractive index (at certain wavelengths) may be much larger than at neighboring wavelengths [e.g., for $(NH_4)_2SO_4$ at wavelength $\lambda = 9.5$ μm]. The backscatter at such a wavelength may be quite different from that at other wavelengths.

3.5 Humidity and Temperature Effects

As the relative humidity increases, water vapor may be absorbed by aerosol particles suspended in the atmosphere. Laboratory experiments and theoretical calculations have shown that the properties of aerosol particles do not change until the ambiednt humidity has reached a threshold value which depends on the deliquescent property of the aerosol compound under consideration. The condensed water will change the optical properties in two ways: the first is to increase the size of the aerosol particles and the second is to change their effective refractive index.

The variation of the size of aerosol particles with ambient humidity can be modeled in several ways. The easiest way is to utilize the published growth factors which take into account the change of aerosol size with relative humidity. Unfortunately, most of the published data on growth factors are limited to certain types of aerosols in the boundary layer. For pure hygroscopic compounds in the atmosphere, the growth factor can be calculated as follows.

Since the mass of solute in an aerosol droplet before and after changes of ambient humidity should be the same, we have.

$$v\varrho x = v'\varrho' x' \tag{1}$$

where v is the volume of one aerosol particle, ϱ its density and x the weight percentage of solute in the solution. The symbols without and with prime refer to the initial, and final condition, respectively.

From Eq. (1) we have

$$\frac{v'}{v} = \frac{\varrho x}{\varrho' x'} \tag{2}$$

and for the growth factor, defined as the ratio of radii after and before the change of ambient conditions.

$$f = \frac{r'}{r} = \left(\frac{\varrho x}{\varrho' x'}\right) \tag{3}$$

The new density ϱ' is a function of x' and the new composition x' can be estimated by considering the fact that the ambient water vapor pressure should be in equilibrium with the water vapor pressure above the surface of the droplet solution with composition x'.

As mentioned earlier, the change of ambient humidity may change the aerosol composition, resulting in a change in its effective refractive index. The variation of refractive index with relative humidity is given by the following equation (Hanel, 1976).

$$n = n_w + (n_o - n_w) + \left(1 + \frac{\varrho_o}{\varrho_w} \cdot \frac{m_w}{m_o}\right)^{-1} \tag{4}$$

where n is the real or imaginary part of the complex index of refraction of the aerosols at the relative humidity under consideration, n, ϱ, and m with subscripts refer to the real or imaginary part of the complex index of refraction, density and mass, respectively, subscript w refers to water and subscript o refers to the pure substance at 0% relative humidity. The values of m_w and m_o are functions of the ambient relative humidity and they can be determined once the value of x' has been found with the method described earlier.

So far we have discussed only the effect of humidity on aerosol size and refractive index. If we assume the water content of the atmosphere remains constant, the relative humidity will change following a change in ambient temperature. Consequently, due to the change in relative humidity, aerosol size and refractive index should vary with the ambient temperature. Additionally, there may be some direct changes in the aerosol density and refractive index with temperature, though such changes are generally small. The change of densities of pure substances are given by standard references such as the International Critical Tables and the effect of temperature on the index of refraction can be derived from the well-known Lorentz-Lorenz formula (Longhurst, 1964):

$$\frac{n^2 - 1}{(n^2 + 2)\varrho} = \text{constant} \tag{5}$$

The value of n at temperature T is then given by

$$n(T) = \left[\frac{2C\,\varrho(T) + 1}{1 - C\,\varrho(T)}\right]^{1/2} \tag{6}$$

Where the constant C can be calculated from the known index of refraction n' at temperature T'

$$C = \frac{n'^2(T') - 1}{[n'^2(T') + 2]\,\varrho(T')} \tag{7}$$

TABLE 3.1: IN SITU INSTRUMENTS USED TO MEASURE AEROSOLS IN THE ATMOSPHERE

TYPE	NAME	USERS
INERTIAL IMPACTOR	FILTER COLLECTION	SAVOIE (1978), PROSPERO (1972)
	PARTICLE IMPACTOR ON SLIDES	BLIFFORD & RINGER (1969), DELUISI et al (1976), HOBBS et al (1976)
	PARTICLE IMPACTOR ON SCREENS	GRAS AND AYERS (1979), BIGG (1980)
	WIRE COLLECTOR	FARLOW et al (1981)
	QUARTZ CRYSTAL MICROBALANCE (QCM)	WOODS (1979)
LIGHT SCATTERING PARTICLE COUNTER	ROYCO OPTICAL COUNTER	CRESS (1980)
	SINGLE PARTICLE OPTICAL COUNTER	PATTERSON (1980)
	DUSTSONDE	HOFMANN and ROSEN (1981)
	KNOLLENBERG PROBE	HOBBS et al (1976)
	INTEGRATED NEPHELOMETER	CRESS (1980)
	POLAR NEPHELOMETER	GRAMS & PATTERSON (1980)
ELECTRIC MOBILE ANALYZER	ELECTRIC AEROSOL ANALYZER (EAA)	HOBBS et al (1976)
CONDENSATION NUCLEI COUNTER	GARDNER SMALL PARTICLE COUNTER	HOBBS et al (1976)
	CCN COUNTER	PUESCHEL (1980)
	ICE NUCLEI COUNTER	HOBBS et al (1976)
	STRATOSPHERIC AITKEN NUCLEI DETECTION SYSTEM (SANDS)	HABERL (1975)

TABLE 3.2: TYPICAL AEROSOL CONCENTRATIONS

NUMBER CONCENTRATIONS

TYPE	AUTHOR	RADIUS, r	$N(>r)$, cm^{-3}
STRATOSPHERIC, PRE-VOLCANIC	ROSEN & HOFMANN (1975)	.25 μm	~ .25
STRATOSPHERIC, POST-VOLCANIC	GRAS (1976)	.22 μm	~1.0
CONTINENTAL, 5 KM	BLIFFORD (1970)	.13 μm	~1.0
MARINE, 5 KM	BLIFFORD (1970)	.13 μm	~0.1
CONTINENTAL, 5 KM	PATTERSON et al (1980)	.5 μm	~0.3
CONTINENTAL, 0 → 6 KM	CRESS (1980)	.4 μm	0.1 →>10

MASS CONCENTRATION

TYPE	AUTHOR	M, $\mu g\ m^{-3}$
MARINE, 5 KM	PATTERSON et al (1980)	.02 → 1.0
CONTINENTAL, 5 KM	PATTERSON et al (1980)	~ 1.0
ATLANTIC DUST, 3 KM	PROSPERO & CARLSON (1972)	50
ATLANTIC DUST, 0 KM	PROSPERO & CARLSON (1972)	1 ⟶ 20
PACIFIC DUST, 0 KM	DUCE et al (1980)	1 ⟶ 2
PACIFIC DUST, 2-3 KM	SHAW (1980)	~50
SOUTH POLE, 0 KM	BIGG (1979)	>0.14

TABLE 3.3: SUMMARY OF THE MAIN PROPERTIES OF AEROSOLS AND THEIR DISTRIBUTION

1. GEOGRAPHICAL DISTRIBUTIONS ARE HARD TO DETECT BUT SIGNIFICANT DIFFERENCES EXIST BETWEEN THE FREE TROPOSPHERIC AEROSOL OVER THE LAND AND THE OCEAN.

2. THE FREE TROPOSPHERIC AEROSOL OVER THE OCEAN IS HIGHLY VARIABLE IN CERTAIN REGIONS DUE TO TRANSPORT OF CONTINENTAL DUST.

3. THE PRINCIPAL VARIATION IN AEROSOL CONCENTRATION IS THAT WITH ALTITUDE. IT IS DIFFERENT OVER LAND AND OCEAN. THE SMALL PARTICLE CONCENTRATION FALLS MORE RAPIDLY THAN THE LARGE PARTICLE CONCENTRATION

4. THE CONCENTRATION OF STRATOSPHERIC AEROSOL IS RELATED TO VOLCANIC ACTIVITY, REACHING A PEAK SHORTLY AFTER A MAJOR ERUPTION AND FALLING QUASI-EXPONENTIALLY WITH A TIME CONSTANT OF 6-12 MONTHS.

5. THE UPPER TROPOSPHERE IS NOT WELL DOCUMENTED BUT MATERIAL IS PROBABLY EXCHANGED THROUGH THIS REGION BETWEEN THE STRATOSPHERE AND LOWER TROPOSPHERE.

6. SIGNIFICANT VERTICAL STRATIFICATION AND HORIZONTAL VARIATION EXISTS.

7. DIFFERENT MEASUREMENT TECHNIQUES YIELD SIGNIFICANTLY DIFFERENT VALUES FOR DN/D(LOG R)

TABLE 3.4: Summary of Global Aerosol Models Important for β_{CO_2} Studies

No.	Author	Title	Year	Applicable Regions	Height Range & resolution	Environmental Conditions	Comments
1	Report of the meeting of JSC experts (Geneva, 27-31 Oct 1980) Chairman: H.J. Bolle	Aerosols and Climate	1980	stratosphere	>12 km	a) background b) volcanic	considerable detail of size distribution
				free troposphere	2 → 12 km	a) free tropospheric b) convective tropospheric	
				planetary boundary layer		a) continental b) urban - industrial c) maritime	
2	Hanel & Bullrich	Physical Properties of Four Types of Tropospheric Aerosols	1977	lower troposphere	0 → 2 km	maritime maritime & desert dust pollution continental clean	Size distribution given as a function of relative humidity
3	Kuznetsov and Izhovkina	Two Models of the Atmospheric Aerosol	1972	whole atmosphere	0 → 30 km (resolution 1 km)	a) oceanic b) continental	particle size distribution, number concentration and refractive index all varies with height & with size range
4	McClatchy et al	Optical Properties of the Atmosphere (third edition)	1972	whole atmosphere	0 → 100 km	a) clear b) haze	given the variation of aerosol number concentration with height

(Continued)

No.	Author	Title	Year	Applicable Regions	Height Range & resolution	Environmental Conditions	Comments
5	Pinnick et al.	Stratospheric Aerosol Measurements IV. Optical Model Calculation	1976	stratosphere	18 → 20 km	over Laramie 1971 - 1974	analytic aerosol size distribution and refractive index based on own measurements
6	Russell et al.	Satellite and Correlative Measurements of the Stratospheric Aerosol. I. An Optical Model for Data Conversions	1981	stratosphere	T+2 → 30 km	a) background b) post volcanic eruption global avg.	summarizes models used previously
				tropopause	0.7T → T+2	global average	
				troposphere	0.3T → 0.7T	global average	
					T = tropopause height		
7	Shettle & Fenn	Models of the Aerosols of the Lower Atmosphere and the Effects of Humidity Variations on Their Optical Properties, AFGL-TR-79-0214	1979	troposphere lower altitudes	above boundary layer boundary layer	a) rural b) urban c) maritime	size distribution is the sum of two log-normal distributions
8	Toon and Pollack	A Global Average Model of Atmospheric Aerosols for Radioactive Transfer Calculations	1976	stratosphere	12 → 45 km (resolution 3 km)	a) background b) post-volcanic eruption	size distributions are Zold and power law
					0 → 12 km (resolution 3 km)	global average	

TABLE 3.5: REFRACTIVE INDICES OF COMMON AEROSOL MATERIALS AT CO_2 WAVELENGTHS

AEROSOL MATERIAL	COMPLEX INDEX OF REFRACTION wavelength in microns								AUTHORS
	9.1	9.2	9.5	9.8	10.0	10.59	11.0	11.1	
Water	1.259 - 0.0405	1.255 - 0.0415	1.243 - 0.0444	1.229 - 0.0479	1.218 - 0.0508	1.179 - 0.0723	1.153 - 0.0968	1.138 - 0.106	Hale & Querry (1973)
Water soluble	2.380 - 0.395	2.200 - 0.420	1.950 - 0.160	1.870 - 0.095	1.820 - 0.09	1.760 - 0.07	1.720 - 0.05	1.710 - 0.049	Shettle & Fenn (1979)
Dust-like	1.710 - 0.145	1.720 - 0.150	1.730 - 0.162	1.740 - 0.162	1.750 - 0.162	1.620 - 0.120	1.620 - 0.105	1.614 - 0.104	Shettle & Fenn (1979)
Soot	2.175 - 0.700	2.180 - 0.700	2.190 - 0.710	2.200 - 0.715	2.210 - 0.720	2.220 - 0.730	2.230 - 0.730	2.232 - 0.732	Shettle & Fenn (1979)
Sea Salt	1.630 - 0.027	1.610 - 0.026	1.580 - 0.018	1.560 - 0.016	1.540 - 0.015	1.500 - 0.014	1.480 - 0.014	1.480 - 0.014	Shettle & Fenn (1979)
Clay	- 0.3	- 0.35	- 0.65	- 0.6	- 0.5	- 0.2	- 0.18	- 0.16	Patterson (1981)
75% H_2SO_4	1.651 - 0.554	1.615 - 0.546	1.681 - 0.699	1.944 - 0.538	1.915 - 0.396	1.737 - 0.273	1.676 - 0.410	1.739 - 0.463	Palmer & Williams (1975)
Al_2O_3	1.172 - 0.3093	1.114 - 0.010	1.06 - 0.013	0.976 - 1.798	0.92 - 0.018	0.55 - 0.06	0.30 - 0.089	0.275 - 0.179	Toon *et al.* (1976)
NaCl	$1.499-0.1\times10^{-6}$	$1.498-0.1\times10^{-6}$	$1.495-0.1\times10^{-6}$	$1.492-0.1\times10^{-6}$	$1.49-0.1\times10^{-6}$	$1.49-0.1\times10^{-6}$	$1.49-1.9\times10^{-7}$	$1.489-1.9\times10^{-7}$	Toon *et al.* (1976)
$(NH_4)_2SO_4$	1.46 - 1.9	1.95 - 2.1	2.68 - 0.53	2.376 - 0.24	2.19 - 0.13	1.972 - 0.057	1.90 - 0.043	1.88 - 0.04	Toon *et al.* (1976)
Sahara dust	1.90 - 0.6	2.0 - 0.65	2.9 - 0.75	2.8 - 0.85	2.7 - 0.9	1.74 - 0.60	1.85 - 0.38	1.86 - 0.36	Volz (1973)
Volcanic dust	1.90 - 0.2	2.0 - 0.25	3.2 - 0.35	3.1 - 0.35	3.0 - 0.4	1.95 - 0.40	1.90 - 0.38	1.88 - 0.36	Volz (1973)

TABLE 3.6: REFRACTIVE INDICES OF COMMON AEROSOL MATERIALS

AEROSOL MODELS	COMPLEX INDEX OF REFRACTION wavelength in microns							AUTHORS
	0.488	0.55	0.6328	1.06	1.66	5.0	10.59	
Water	$1.336 - 1 \times 10^{-9}$	$1.333 - 1.96 \times 10^{-9}$	$1.332 - 1.5 \times 10^{-8}$	$1.326 - 5 \times 10^{-6}$	$1.316 - 9.43 \times 10^{-5}$	1.325 - 0.0124	1.179 - 0.0677	Hale & Querry 1973
Maritime	1.418 - 0.002	1.418 - 0.002	1.415 - 0.002	1.405 - 0.004	1.376 - 0.004	1.372 - 0.010	1.380 - 0.057	Selby 1976
Maritime/ Rural	1.475 - 0.005	1.474 - 0.004	1.473 - 0.004	1.463 - 0.009	1.408 - 0.010	1.381 - 0.012	1.550 - 0.071	Selby 1976
Rural	1.530 - 0.008	1.530 - 0.006	1.530 - 0.006	1.520 - 0.014	1.440 - 0.016	1.390 - 0.013	1.720 - 0.085	Selby 1976
Rural/ Urban	1.569 - 0.086	1.569 - 0.082	1.569 - 0.080	1.560 - 0.089	1.500 - 0.096	1.492 - 0.116	1.810 - 0.198	Selby 1976
Urban	1.607 - 0.163	1.607 - 0.158	1.607 - 0.154	1.600 - 0.163	1.559 - 0.175	1.593 - 0.218	1.895 - 0.310	Selby 1976
Water Soluble	1.530 - 0.005	1.530 - 0.006	1.530 - 0.006	1.520 - 0.017	$1.487 - 2 \times 10^{-2}$	1.450 - 0.012	1.760 - 0.07	Shettle & Fenn 1979
Dust-like	1.530 - 0.008	1.530 - 0.008	1.530 - 0.008	1.520 - 0.008	$1.367 - 8 \times 10^{-3}$	1.250 - 0.016	1.620 - 0.120	Shettle & Fenn 1979
Soot	1.750 - 0.450	1.750 - 0.440	1.750 - 0.430	1.750 - 0.440	1.78 - 0.469	1.970 - 0.600	2.220 - 0.730	Shettle & Fenn 1979
Sea Salt	$1.500 - 2 \times 10^{-8}$	$1.500 - 1 \times 10^{-8}$	$1.490 - 2 \times 10^{-4}$	$1.470 - 2 \times 10^{-4}$	$1.456 - 7 \times 10^{-4}$	1.470 - 0.0025	1.500 - 0.014	Shettle & Fenn 1979
Crustal	$- 7 \times 10^{-3}$	$- 6 \times 10^{-3}$	$- 2.5 \times 10^{-3}$	$- 2 \times 10^{-3}$	$- 2.5 \times 10^{-3}$	$- 2 \times 10^{-2}$	- 0.2	Patterson 1981
75% H_2SO_4	$1.432 - 2 \times 10^{-8}$	$1.431 - 2 \times 10^{-8}$	$1.429 - 2 \times 10^{-8}$	$1.420 - 1.5 \times 10^{-6}$	$1.398 - 2.72 \times 10^{-4}$	1.359 - 0.123	1.737 - 0.273	Palmer & Williams 1975
Al_2O_3	$1.77 - 2 \times 10^{-7}$	$1.77 - 2 \times 10^{-7}$	$1.77 - 2 \times 10^{-7}$	$1.76 - 6 \times 10^{-8}$	$1.74 - 5.5 \times 10^{-8}$	$1.62 - 3.1 \times 10^{-5}$	0.55 - 0.061	Toon & Pollack 1976
NaCl	$1.55 - 10^{-7}$	$1.55 - 10^{-7}$	$1.55 - 10^{-7}$	$1.53 - 10^{-7}$	$1.53 - 10^{-7}$	$1.515 - 10^{-7}$	$1.49 - 10^{-7}$	Toon & Pollack 1976
$(NH_4)_2SO_4$	$1.53 - 10^{-7}$	$1.52 - 10^{-7}$	$1.52 - 10^{-7}$	$1.51 - 2.4 \times 10^{-6}$	$1.49 - 1.8 \times 10^{-4}$	1.46 - 0.006	1.98 - 0.06	Toon & Pollack 1976
Sahara dust						1.56 - 0.015	1.74 - 0.40	Volz 1973
Volcanic dust						1.56 - 0.009	1.95 - 0.40	Volz 1973

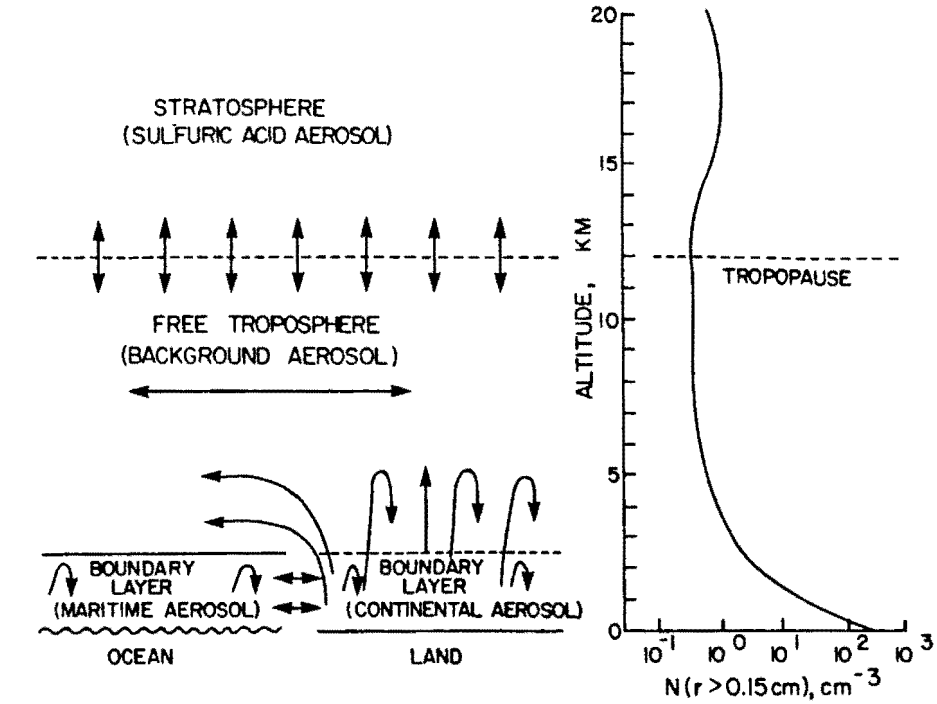

Figure 3.1 Schematic diagram showing the variation of aerosol properties with altitude.

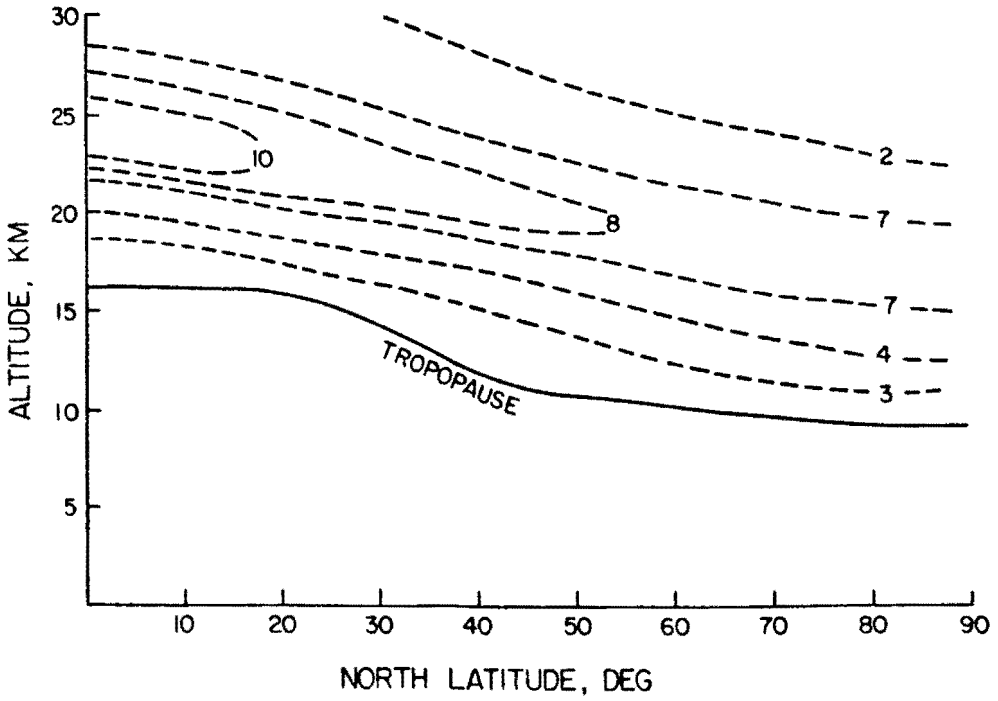

Figure 3.2 Latitude distribution of the variation of stratospheric aerosols (from Rosen et al., 1975). Numbers on the diagram give the number of aerosol particles per mg of air.

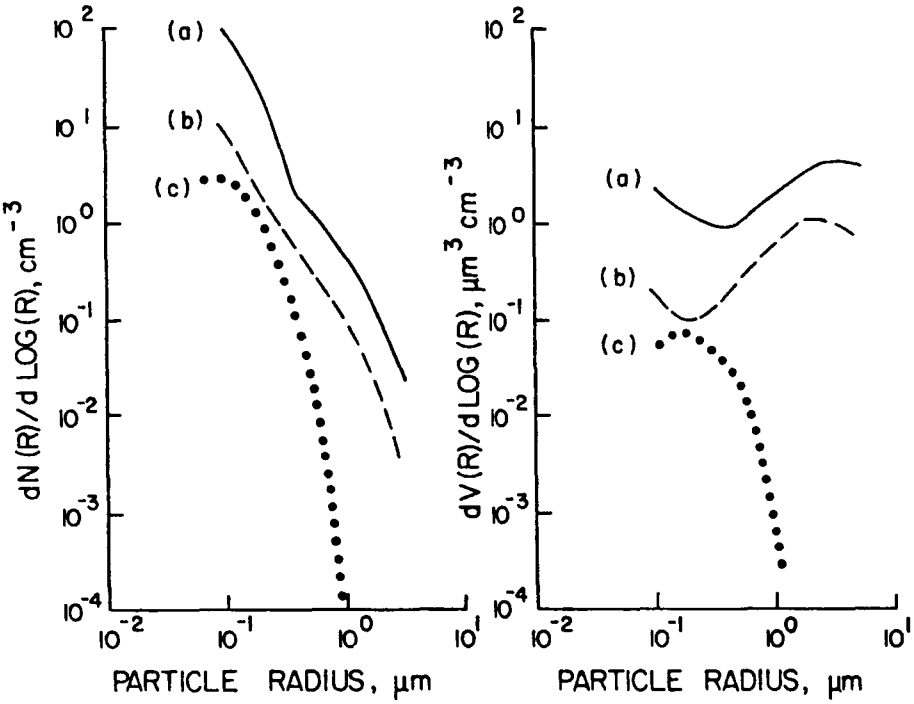

Figure 3.3 Typical samples of aerosol size distribution in different regions of the atmosphere: (a) boundary layer; (b) free troposphere; (c) stratosphere.

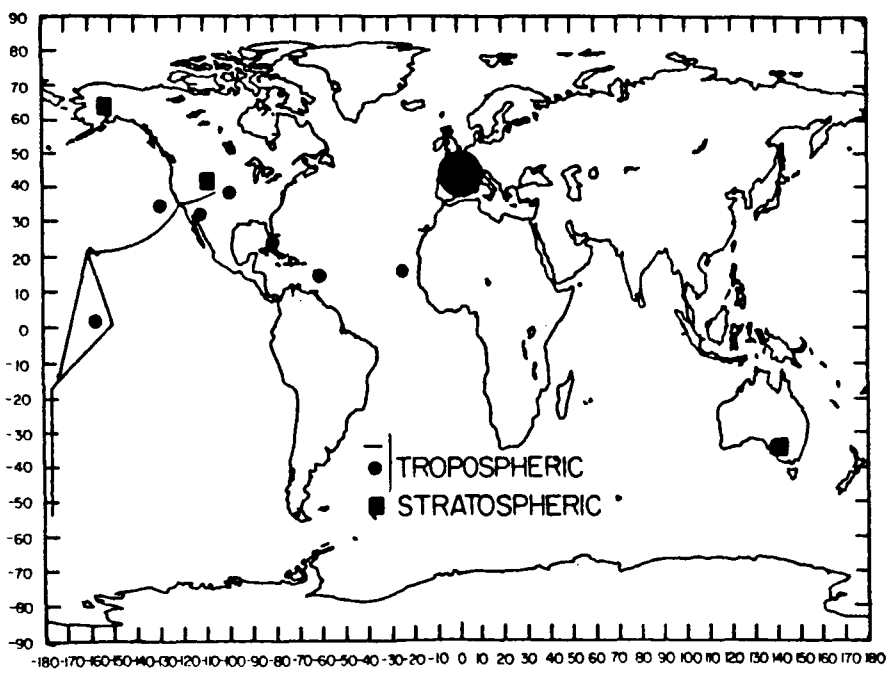

Figure 3.4 Location of free tropospheric and stratospheric aerosol measurements used in this report.

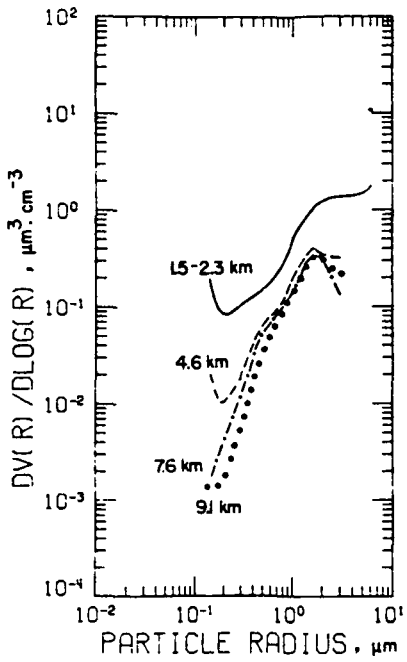

Figure 3.5 Aerosol volume distributions measured over the USA by Blifford and Ringer (1969).

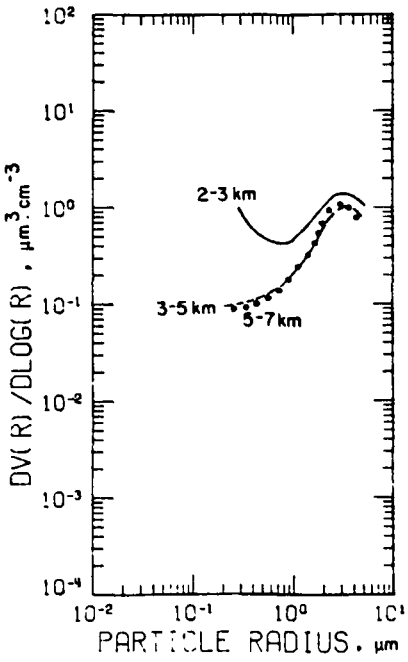

Figure 3.6 Aerosol volume distributions measured over Europe by Cress (1980).

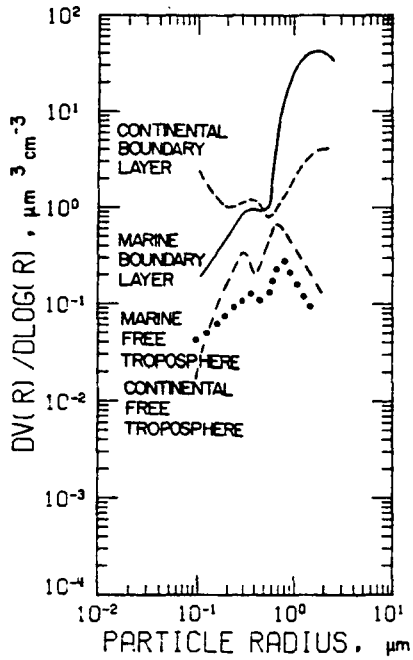

Figure 3.7 Aerosol volume distribution measurements made over the USA or the Pacific Ocean by Patterson et al. (1980).

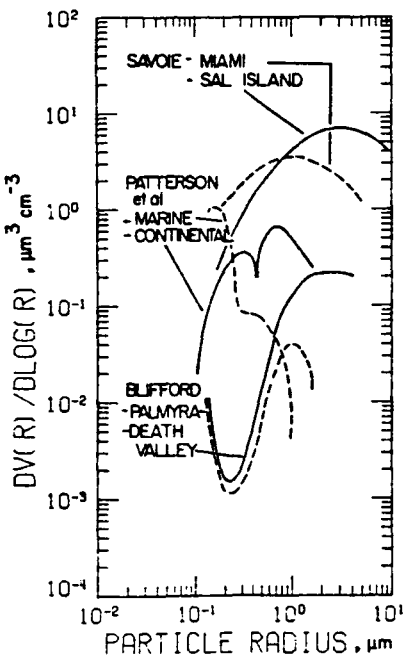

Figure 3.8 Volume size distributions measured by different research workers over land and ocean (Blifford, 1970; Savoie, 1978; Patterson et al., 1980).

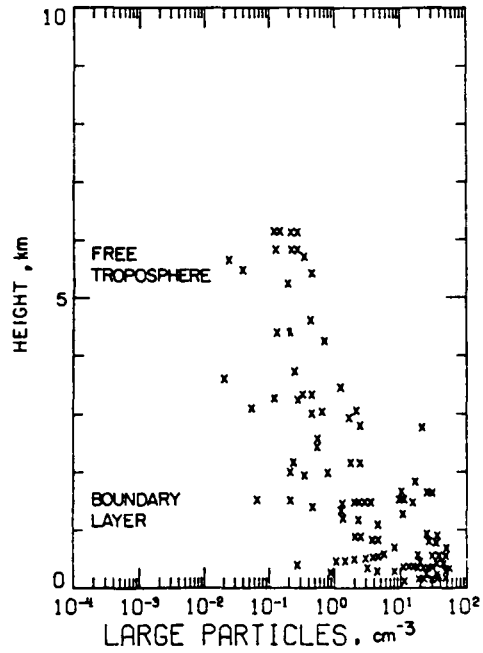

Figure 3.9 Altitude variation of large particle concentrations ($r > 0.2$ μm) over Europe (Cress, 1980).

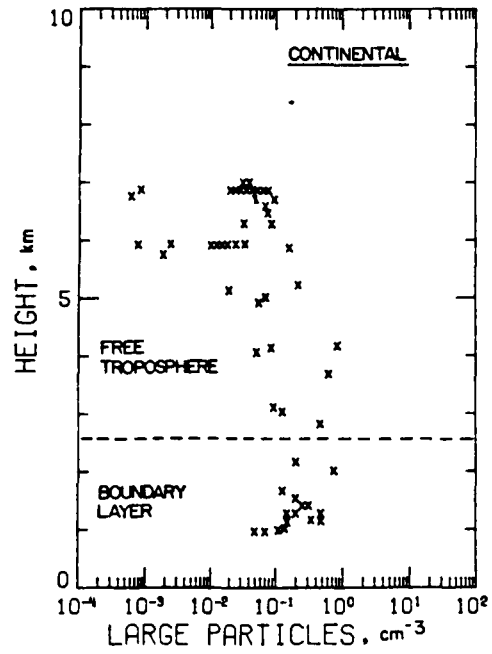

Figure 3.10 Altitude variation of large particle concentrations ($r > 0.5$ μm) over the USA (Patterson et al., 1980).

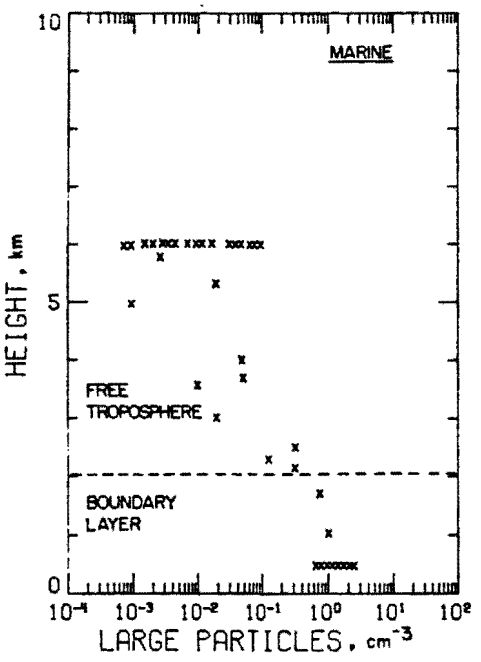

Figure 3.11 Altitude variation of large particle concentration ($r > 0.5$ μm) over the Pacific Ocean (Patterson et al., 1980).

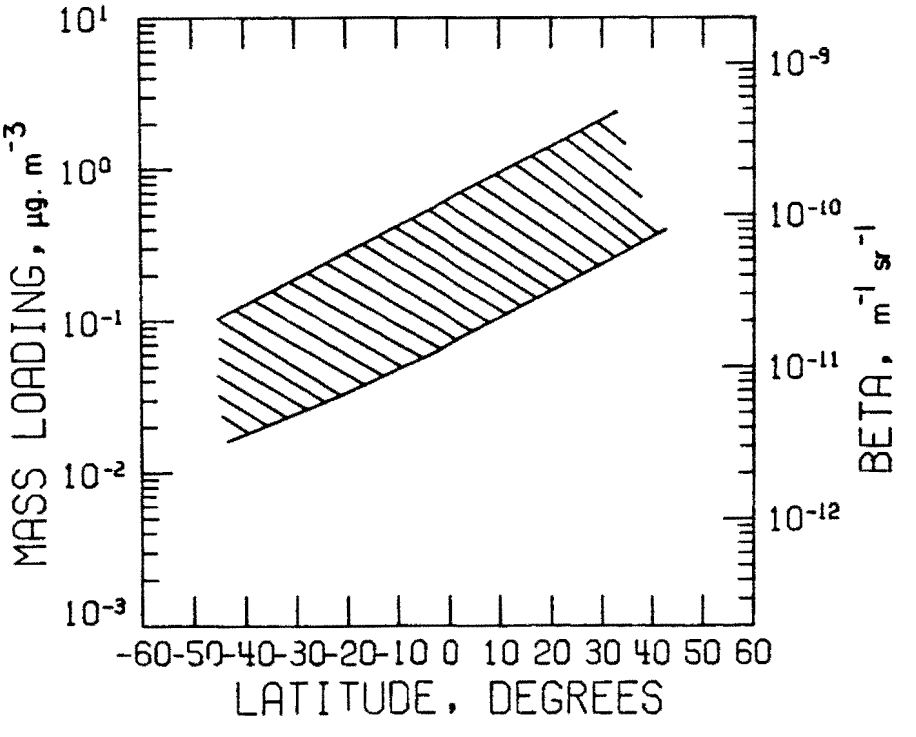

Figure 3.12 Latitude variation of aerosol mass loading in the free troposphere over the Pacific Ocean (Patterson et al., 1980) and the equivalent β_{CO_2}.

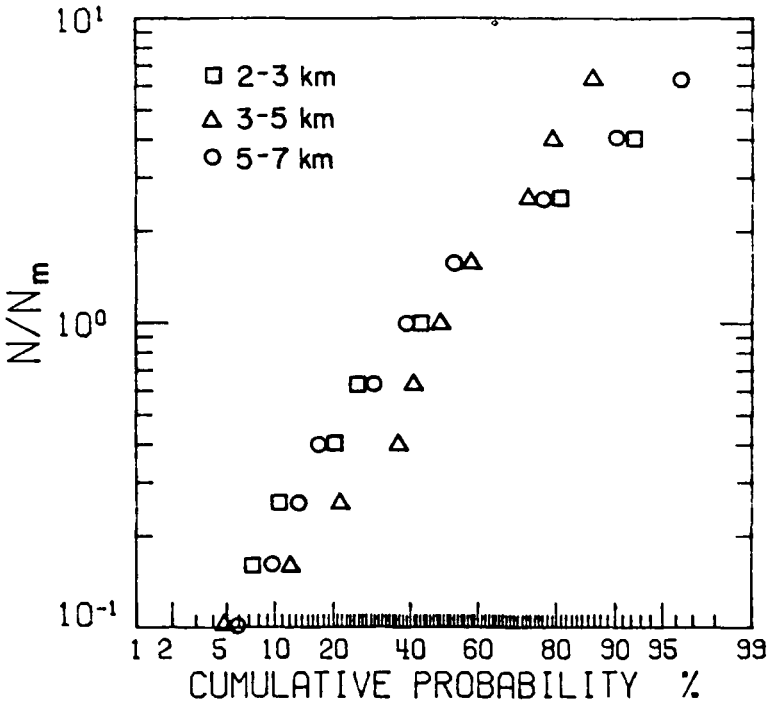

Figure 3.13 Cumulative probability distribution for the aerosol particle concentrations over Europe (Cress, 1980). N/N_m represents the ratio of the aerosol number concentration to the mean concentration.

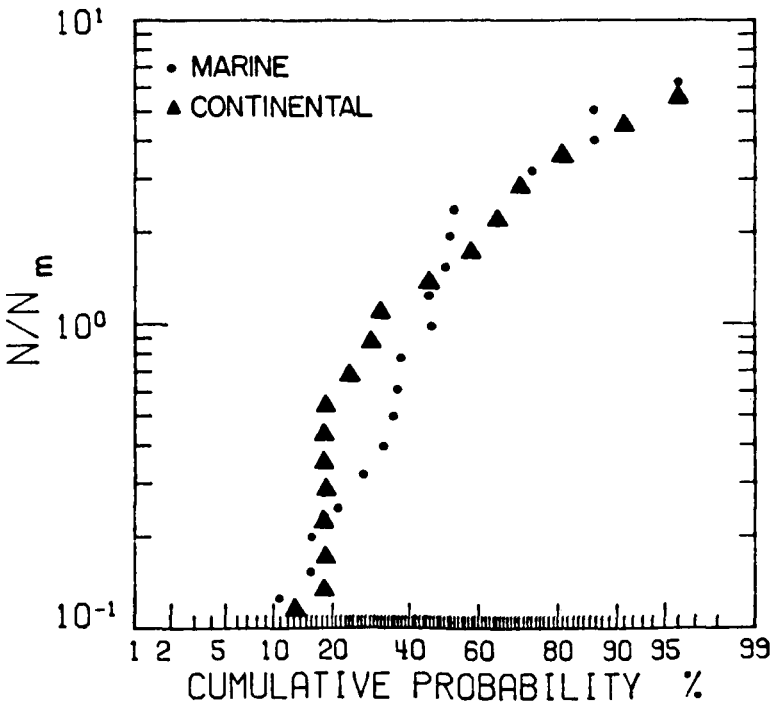

Figure 3.14 Cumulative probability distribution for the aerosol particle concentration over the USA and the Pacific Ocean (Patterson et al., 1980). N/N_m represents the ratio of the aerosol number concentration to the mean concentration.

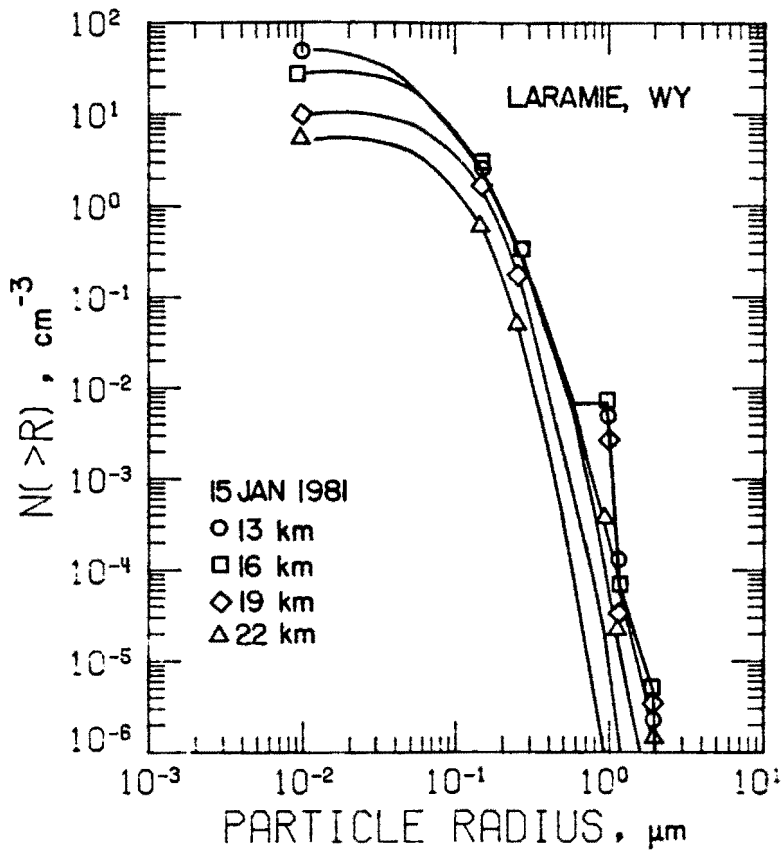

Figure 3.15 Cumulative aerosol size distributions obtained by Hofmann and Rosen (1981).

4. OPTICAL MEASUREMENTS OF AEROSOLS

4.1 Lidar Measurements

Lidar measurements have now been made for approximately twenty years and have developed from very simple experiments, designed to record total molecular and aerosol backscatter, to a very wide range of techniques for studying different atmospheric species and parameters. Of particular interest to this report are measurements of aerosol backscatter. These measurements, in one form or another, go back to the beginning of lidar as a technique and a small number of data sets exist that extend over many years. The most consistent and reliable of these are those for stratospheric aerosols and the records that exist clearly show the aerosol increases due to volcanic eruptions and the subsequent slow decreases. Tropospheric data, although extending back as far as stratospheric, presents a much less orderly picture. There are two reasons for this. In the lower troposphere, large variations occur in aerosol concentration. Relatively few systematic comparisons have been made of lidar returns with aerosol source and history and there are no long-term comparisons. In the upper troposphere the aerosol concentration is low. Unfortunately, lidar systems are difficult to calibrate directly and the returned signals are most commonly normalized by assuming that the scattering is entirely molecular at a selected altitude in the atmospehre. For tropospheric measurements, the altitude most often chosen is that just below the tropopause, rendering it impossible to assess the aerosol contribution at that height.

Early lidar measurements were made using ruby lidar systems operating at a wavelength 694 nm. Ruby systems are still much used although they are considerably supplemented by Neodymium Yag at 1.06 μm and, much less commonly, by harmonics of those wavelengths. A few recent observations exist at 10.6 μm but virtually no observations have been made for wavelengths between 1.06 and 10.6 μm. The geographic spread of lidar observations is poor, being heavily concentrated in North America, Europe, and Japan. This is shown in Fig. 4.1, which indicates those stations making tropospheric and lower stratospheric aerosol measurements using visible or near-infrared wavelengths.

In order to assess the situations as regards available data sets on aerosol scattering using lidar, letters were written to research workers believed to have made such measurements, particularly those outside the USA. Table 4.1 summarizes the replies and other information gained, either by direct contact or from published reports (Names and addresses of those persons supplying information are included in the appendix to this report.) Section (a) of the table is a very brief summary while Section (b) gives more detailed information. For the sake of completeness the table also contains information about CO_2 lidar measurements on aerosols and lists stations making measurements on fog, cloud, etc. It may be noted that only one research group in the USA, namely, that of Marshall Space Flight Center, is at present making airborne measurements of CO_2 wavelengths. Stations making lidar measurements on gaseous atmospheric species only, are not listed.

Earlier in this Section it was noted that a few good long-term data sets existed of lidar measurements of the stratospheric aerosol. One such, probably the best, obtained at Hampton, Virginia, is shown in Fig. 4.2 (Swissler et al., 1982). The figure shows the peak backscatter cross section at a wavelength of 0.6943 μm between 1974 and 1979. (The scale on the right-hand side of the figure which shows the equivalent backscatter at a wavelength of 10.6 μm will be discussed in Section 7.) The effects of the eruptions of Fuego and Mount St. Helens can be seen very clearly. Table 4.2 shows a list of those volcanoes in the past three years known to have ejected material into the stratosphere. This has been a period of very considerable volcanic activity, culminating in April 1982 in the eruption of El Chinchon, probably the most significant eruption (as far as the stratosphere is concerned) since that of Agung in 1963. A short table listing the most important conclusions concerning lidar measurements is included in Section 8.

4.2 Extinction Measurements

Extraterrestrial radiation passing through the atmosphere will be absorbed and scattered by air molecules (including ozone, water vapor, CO_2 and other absorbing species) and atmospheric aerosols, resulting in a reduction in intensity according to the Lambert-Beers law (at a single wavelength). Since the extinction in radiation is directly related to the optical properties of the aerosol, the aerosol size distribution and/or its concentration can be obtained by inverting the measured extinction, provided we can assume some other properties of the aerosol, such as its index of refraction.

Atmospheric aerosol extinction measurements can be divided into two general classes: in the first the total extinction due to all aerosols along the path between the sources and the detector device is measured; in the second the extinction from aerosols along a path of unit length is measured or deduced. Atmospheric turbidity, visibility and total optical depth measurements belong to the first class. These measurements are relatively easy to make and so provide good continuity. However, results of these measurements are usually related to the mean aerosol properties, and the distribution of aerosol properties along the path of radiation is almost impossible to obtain from the experimental data. On the other hand, those measurements belonging to the second class, such as extinction or attenuation coefficient measurements, conducted on the ground or by detection devices mounted on space craft can provide information on aerosol properties with, in the latter case, a resolution of about 1 km. For the purpose of this study we are more interested in the extinction data obtained by measurements of this second class mentioned above.

Although aerosol extinction or attenuation coefficient profiles obtained by numerical modeling have been reported in the litrature (Elterman, 1970; Kneizys et al., 1980), we are aware of only a very few measured extinction profiles (e.g., Elterman, 1966). So far the largest data base on aerosol extinction coefficients is undoubtedly that obtained by the SAM II and SAGE satellite experiments. The SAM II instrument consists of a single channel sun photometer, centered at 1.0 μm wavelength, mounted on the Nimbus-7 satellite which was launched on October 23, 1978. Aerosol extinction coefficient profiles, with a 1 km vertical resolution, are being obtained by this method. The SAGE instrument consists of four radiometric channels centered at 1.0 μm, 0.6 μm, 0.45 μm, and 0.385 μm, mounted on the Application Explorer Mission-B (AEM-B) satellite, which was launched on February 18, 1979. The four-channel extinction measurement obtained by SAGE can be inverted to obtain aerosol extinction coefficients at 1.0 μm and 0.45 μm. Due to the orbital characteristics of the Nimbus-7 satellite, SAM II measurements are limited to two latitude bands ranging from 64°S to 81°S, and 65°N to 83°N. In contrast, the highly processing orbid of the AEM-B satellite allows the SAGE measurements to cover global areas in the latitudes between about

79°S and 79°N. Though the majority of data obtained by both SAGE and SAM II is confined to stratospheric regions below 30 km, under favorable conditions without cloud coverage, extinction data to the surface of the earth can sometimes be inverted. If the conversion of SAGE and SAM II extinction data to β_{CO_2} is proven to be feasible, the spatial and temporal variation of β_{CO_2} over the globe can be accurately modeled.

TABLE 4.1: LIDAR MEASUREMENTS ON AEROSOLS, FOG AND CLOUD IN THE LOWER ATMOSPHERE

(a) Summary

	MADE USING VISIBLE OR NEAR INFRARED WAVELENGTHS							MADE USING CO_2 WAVELENGTHS	
	(i) Aerosol Measurements						(ii) Fog, Cloud or Precipitation Only		
	Available Data Sets								
Continent	No. of stations	No. of airborne	Extensive tropospheric	Limited tropo-spheric	Extensive stratospheric	Limited stratos-spheric	No. of stations	No. of stations	No. of airborne systems
North America and Pacific	13	2	4	5	1	3	4	3	1
South America and Caribbean	2					2			
Europe	8	2	1	7	1	2	3	4	1
Asia	6		1	4	1		2		
Australia	2		1	1	1				

Notes: 1) Stations and airborne systems no longer operating are not listed unless there exists a considerable data base.
2) Extensive stratospheric observations imply a data base of several years; extensive tropospheric observations imply several sets of experiments.

(b) Detailed Information

Station	Principal Research Worker(s)	Wavelengths Used	Period of Operation	Source of Information	Notes
North America and Pacific					
U. of Wisconsin Meteorol. Dept. Madison, WI	E. Eloranta J. Weinman	694 nm		Conference Proceedings, Publications Phone conversation Nov. 30, 1981	Extensive studies of convective boundary layer using scanning lidar system. High spectral resolution airborne lidar for separation of aerosol and molecular scattering.
Air Force Geophysics Laboratory, Hanscom AFB, MA 01731 U.S.A.	D. E. Bedo K.S.W. Champion	1,064,355 nm		Conference Proceedings	Proposed balloonborne lidar system for high altitude studies.
Photometrics Inc. Woburn, MA 01801	G. Davidson	0.53 μm	1981	Conference Proceedings	Backscatter measurements in falling snow.
Atmos. Sci. Center SRI International Menlo Park, CA 94025, USA	E. Uthe P. Russell	694 nm (also CO_2 laser)	1960s → present	Publications, reports	1) Numerous lidar systems developed including mobile and airborne 2) Main field of study is tropospheric, particularly boundary layer 3) Shipborne measurements made in 1977 in Atlantic and Mediterranean 4) Considerable work done on modelling of aerosols.

Station	Principal Research Worker(s)	Wavelengths Used	Period of Operation	Source of Information	Notes
NASA-Langley Research Center Hampton, VA 23665, USA	E. V. Browell	600 nm	1980	Conference reports, personal contact	Airborne system has been used to obtain downward looking profiles from altitudes of about 3 km. Aerosols, ozone, and atmospheric water vapor studied.
NASA-MSFC Huntsville, AL 35802	J. Bilbro	10.6 μm	1981-82	Conference proceedings, personal contact	Airborne aerosol backscatter and doppler shift measurements.
NASA/Goddard Space Flight Center, Code 913, Greenbelt, MD 20771	J. D. Spinhirne	532 nm	1979-82	Conference proceedings	Investigation of cloud structure.
U. of Arizona Dept. of Elec. Eng.* or Institute of Atmos.+ Physics U. of Arizona Tucson, AZ 85721 U.S.A.	*J. Reagan +R. Schotland	694 nm 8-12 μm	1970 → present	Publications, personal contact	Monstatic and bistatic lidar, several experiments conducted in and closely above the boundary layer combining several observational techniques. Recent CO_2 lidar measurements.
Atmospheric Sciences Lab White Sands Missile Range, NM 88002	J.S. Randhawa E. Measure	694 nm (also CO_2 lidar)	1979 → present	Conference reports, personal visit	Application mostly to smoke and dust, ongoing data collection comparing visible and CO_2 backscattering and extinction. Measurements in U.S.A. and Europe.
U.S. Army Atmospheric Sciences Laboratory Atmospheric Sensing Division White Sands Missile Range, NM 88002	W.J. Lentz	1.06 μm	1981-82	Conference proceedings	Main interest is in inversion of data to obtain extinction profiles.

Station	Principal Research Worker(s)	Wavelengths Used	Period of Operation	Source of Information	Notes
Jet Propulsion Laboratory California Institute of Technology Pasadena, CA 91109	R. T. Menzies	10.6 μm		Conference proceedings, personal contact	Lidar returns from aerosols and topographic targets.
Environmental Monitoring Systems Laboratory U.S. Environmental Protection Agency P. O. Box 15027 Las Vegas, NV 89114	J.L. McElroy	1.06, 0.53 μm		Conference proceedings	Downward looking airborne lidar to study air pollution transport.
NASA-Langley Research Center Hampton, VA 23665	M.P. McCormick T.J. Swissler J. Goad	694 nm (ground-based) 694 & 1060 nm (airborne)	1974 - present	Numerous publications and reports, personal contact	1) Good back-log of data on stratospheric aerosol 2) Detailed study of stratospheric volcanic effects 3) Operational airborne system, upward & downward looking from aircraft 4) Polarization studies.
Environmental Research Labs. NOAA Boulder, CO 80303	V. Derr J. deLuisi F. Hall W. Eberhard R. Schweisow	694 & 347 nm (also CO_2 lidar)	1973 - present	Publications and conference presentation, personal contact	Stratospheric data following Mt. St. Helens eruption, May 1980 (CO_2 and visible lidar comparison). Studies of plume dispersion CO_2 aerosol measurements from 1980, including backscattering and doppler shif
Aeronomy Laboratory Dept. of Elec. Eng. U. of Illinois Urbana, IL 61801	C.S. Gardner C.F. Sechrist	596 nm	1980	Conference presentation; recent correspondence (Dec. 1981)	Studies of mesopheric sodium, stratospheric aerosol observations following Mt. St. Helens eruption, May 1980.
Barrow, Alaska c/o NOAA Env. Res. Labs. Boulder, CO 80303	J. deLuisi			Recent correspondence (November 1981)	System set up but not yet operational, long-term future uncertain.

Station	Principal Research Worker(s)	Wavelengths Used	Period of Operation	Source of Information	Notes
NOAA Air Res. Laboratory Hilo, HI 95616	J. deLuisi R.W. Fegley F. Fernald	694 nm	1973 - present	Recent correspondence (November 1981) and conference presentation	Several years data, processing incomplete; continuing to monitor stratospheric aerosols.
University of Utah Dept. of Meteorology Salt Lake City, UT 94112	K. Sassen	694 nm	1982	Conference proceedings	Studies of scattering characteristics of clouds (including polarization).
Defense Research Establishment, Valcentier P. O. Box 8800 Courcelette, Quebec, Canada	R.E. Kluchert	1.06 μm		Conference proceedings	System used to map pollution plumes
York University 4700 Keele St. Pownsview, Ontario, Canada M3J 1P3	A. Carswell		1977-82	Publications and conference proceedings	Studies of scattering in clouds and fogs.
Defense Research Establishment, Valcentier P. O. Box 8800 Courcelette, Quebec, Canada	E.T. Evans	1.06 μm		Conference proceedings	Lidar mapping a of smoke aerosols.
South America and Caribbean					
INPE-C.P. Sao Jose dos Compos Sao Paulo Brazil	B.R. Clemesha	694 and 589 nm	1970 - present	Recent correspondence (November 1981)	Continuous data base to 1977 on stratospheric aerosols, β-profiles for 1970-77 between 10 & 50 km published.
Dept. of Physics U. of the West Indies Kingston 7 Jamaica	M. Shams	694 nm	1965-1980	Personal operation	Intermittent data on stratospheric aerosol for 1965-1980. Total data base is extensive. Present status uncertain.

Station	Principal Research Worker(s)	Wavelengths Used	Period of Operation	Source of Information	Notes
Europe					
Instituto di Ricera sulle Onde Electromagnetische of CNR Via Paniatichi 64 Firenze 50127 Italy	L. Stefanutti P. Bruscaglioni	1.06 μm 0.53 μm	1975 - present	Conference reports; recent correspondence (Dec, 1981)	Main research has been on properties of fogs. Data base on aerosols limited.
National Swedish Environment Protection Board S-611 82 Nyköping Sweden	K. Fredriksson	1.06 μm and dye laser	1978 - present	Conference reports; recent correspondence (Dec. 1981)	Main interest is in urban pollution (SO_2, NO_2, O_3, H_2O). No absolute measurements of aerosol cross-section.
Department of Electrical Measurements Chalmers University of Technology S-412, 96 Güteberg Sweden	S. Lundquist	10.6 μm		Recent correspondence (Feb., 1982)	Measuring diffuse reflectivity coefficients.
National Defence Research Institute Department 3 Box 1165, S-581 11, Linköhing, Sweden	A. Hägard	9.2 → 10.8 μm	1982	Conference proceedings, personal contact	Aerosol scattering and extinction from fog, snow, rain, etc.
University of Bergen Norway	I. Singstad	694 nm	1982	Conference proceedings	Measurement of Stokes Parameters in scattering from clouds.
Physics Lab TNO The Hague The Netherlands	C.W. Lamberts	1.06 μm	1978 - present	Conference reports; recent correspondence (Dec. 1981)	Program of measurement of extinction and backscatter caused by tropospheric aerosols. Future work comparing 1.06 μm and 10.6 μm scattering and extinction planned.

Station	Principal Research Worker(s)	Wavelengths Used	Period of Operation	Source of Information	Notes
Service d'Aeronomie BP3 91370 Verrieres-Buisson France	A. Hauchecorne L. Chanin G. Megie	1.06 μm, 530, 353 nm and various dye lasers	1970 - present	Publications and conference reports; recent correspondence (Feb. 1982)	An extensive range of measurements is being conducted on a wide range of atmospheric properties. Information on scattering from volcanically enhanced stratospheric layers has been published but no other aerosol data base.
Direction de la Meteorologie -EERM 78470 MAGNV Les Hameaux, France	J.L. Gausset	694 nm	1982	Conference proceedings	Measurements of visibility in fogs.
Meteorologie Nationale, EERM, 78470 St-Rémy-les-Chevreuse France	D. Renaut	347,266 nm	1981 - present	Conference proceedings	Raman measurements of aerosols, water vapor and gaseous pollutants in the boundary layer.
Deutscher Wetterdienst Meteorologische Observatorium Hamburg Frahmredder 95 2000 Hamburg 65 FRG	F. Kasten E. Klaphack		1979 - present	Conference report, letter written; recent correspondence (Nov. 1981)	Studies of tropospheric and anthropogenic aerosols (0-2 km altitude) using steerable lidar system. Data not yet available.
DFVLR - Inst. for Optoelectronics D-8031 Oberpfaffenhofen FRG	Ch. Werner F. Köpp	1.06 μm (airborne system) 694 nm ground based, 10.6 μm	1970	Conference reports, publications, personal experience; recent discussions (June, 1982)	Extensive observations and system development over a period of many years. Interest mainly on tropospheric aerosols. Operational airborne system. CO_2 system in use for doppler shift measurements. Ship-borne studies of plume dispersion.

Station	Principal Research Worker(s)	Wavelengths Used	Period of Operation	Source of Information	Notes
DFVLR - Inst. for Atmospheric Optics D-8031 Oberpfaffenhofen FRG	W. Renger	1.06 μm, 530 nm in airborne system		Conference reports, personal discussion; recent correspondence (March, 1982)	Operational downward looking airborne system for the study of aerosols and pollution. Measurements over Alpine regions.
Fraunhofer Institute for Atmos. Env. Res. D-8100 Garmisch-Partenkirchen, FRG	R. Reiter	694, 347, 530 nm	1976 - present	Conference proceedings; publications; recent correspondence (Nov. 1981)	Published data on back-scattering profiles for both tropospheric (1-3 km) and stratospheric (10-30 km) aerosols. Study of volcanic effects. Making extensive, multi-wavelength transmission measurements in the boundary layer; data not yet published.
SRC Rutherford & Appleton Laboratories Ditton Park Slough, Berks SL3 9JX England	L. Thomas*	694 nm and dye lasers	1966 - present	Publications; recent correspondence (March, 1982)	Series of experiments over many years. Main interest stratosphere and mesosphere. Some data on aerosol scattering published.
Royal Signals and Radar Establishment, St. Andrews Road Great Malverson, Wores WR13 3PS England	J. Vaughan	10.6 μm	1981-82	Recent correspondence (Feb., 1982)	Considerable body of back-scatter data from airborne system. Not yet published.
Department of Applied Physics, University of Hull Hull, United Kingdom	E.L. Thomas	10.6 μm		Recent correspondence (Nov., 1981)	No absolute measurements of volume backscattering coefficient yet, but future measurements planned.

* Now at The University College of Wales, Aberystwyth, Wales.

Station	Principal Research Worker(s)	Wavelengths Used	Period of Operation	Source of Information	Notes
Asia and Australia					
The Institute of Atmospheric Optics U.S.S.R. Academy of Sciences, Siberian Branch, Tomsk U.S.S.R.	V.E. Zuev	1.06 μm 530, 490 nm	1972 - present	Conference reports; recent correspondence (April, 1982)	Extensive work carried out on scattering and extinction by tropospheric aerosols.
Institute of Atmospheric Physics Academic Sciences Beijing, China	X.J. Zhou Y.Z. Zhao	694 nm	1972 - present	Conference reports; recent discussion (June, 1982)	Interest is in tropospheric aerosols and their extinction. Extent of data base unknown. DIAL measurements of atmospheric water vapor. Recent visibility measurements.
Water Research Inst. Nagoya University Chikusa-hu Nagoya Japan	K. Nagaya Y. Iwasaka	694 nm and other wavelength	1979 - present	Conference reports; recent correspondence (March 1982)	Interest in tropospheric aerosols 0-2 km. Published data on aerosols from dust-storms over China. Stratospheric data available also.
Dept. of Physics Kyushu University Fukuoka 812 Japan	M. Hirono M. Fujiwara	1.06 μm 530 nm	1972 - present	Publications and conference presentations; recent correspondence (March, 1982)	Has good continuous data base on stratospheric aerosols. Planning measurements of aerosol profiles from 6 km upwards.
Research Institute of Elec. Communications Tohuku University Katshiva 2-1-1 Sendai 980 Japan	H. Inaba			Conference proceedings	Main interest is in water droplets in fogs and clouds.

Station	Principal Research Worker(s)	Wavelengths Used	Period of Operation	Source of Information	Notes
National Inst. for Environmental Studies Yatabe, Tsukuba Ibaraki, 305 Japan	N. Takeuchi	1.06 m 532 nm	1979? - present	Conference presentations; recent correspondence (March, 1982)	Main interest is in spatial and dynamic structure of air pollution. Using large atmospheric multi-purpose lidar.
Department of Atmospheric Sciences The Hebrew University of Jerusalem, Jerusalem, Israel	A. Cohen			Publications, conference proceedings	Studies of scattering in the lower atmosphere and in clouds.
Space Physics Division Vikram Sarabhlai Space Centre, Trwinitrum - 695022, India	B.V. Krishna Murthy	514.5 nm	1982	Conference proceedings	Bistatic aerosol studies.
Dept. of Physics U. of Adelaide Adelaide Australia	S.A. Young W.G. Elford	694 nm	1969-73 (at least)	Publications, personal contact; recent correspondence (Nov., 1981)	Good data base on scattering from tropospheric and stratospheric aerosol. No longer operational.
CSIRO Division of Atmos. Physics Aspendale Victoria Australia	C.M.P. Platt	694 nm	1971 - present	Publications, conference and workshop reports, personal contact; recent correspondence (Feb., 1982)	Main interest has been on scattering properties of clouds. Some boundary layer backscatter cross-sections.

TABLE 4.2: RECENT VOLCANIC ERUPTIONS AFFECTING THE STRATOSPHERE

DATE	VOLCANO	LOCATION	COLUMN HEIGHT
April 17, 1979	Soufriere	13.3 N, 61.2 W	18 - 20 km
November 13, 1979	Sierra Negra	0.8 S, 91.2 W	> 14 km
May 18, 1980	St. Helens	46.2 N, 122.2 W	> 23 km
Oct 7, 1980	Ulawun	5.0 S, 151.3 E	10 km
April 27, 1981	Alaid	50.8 N, 155.5 E	15 km
May 15, 1981	Pagan	18.1 N, 145.8 E	13 - 20 km
Dec-Jan, 1982	Possibly Pagan	-	Lidar at 10 N shows peak at 17 km
March 19, 1982	St. Helens	46.2N, 122.2W	14 km
March 28 - April 4, 1982	El Chinchon	17.3 N, 93.2 W	26 km

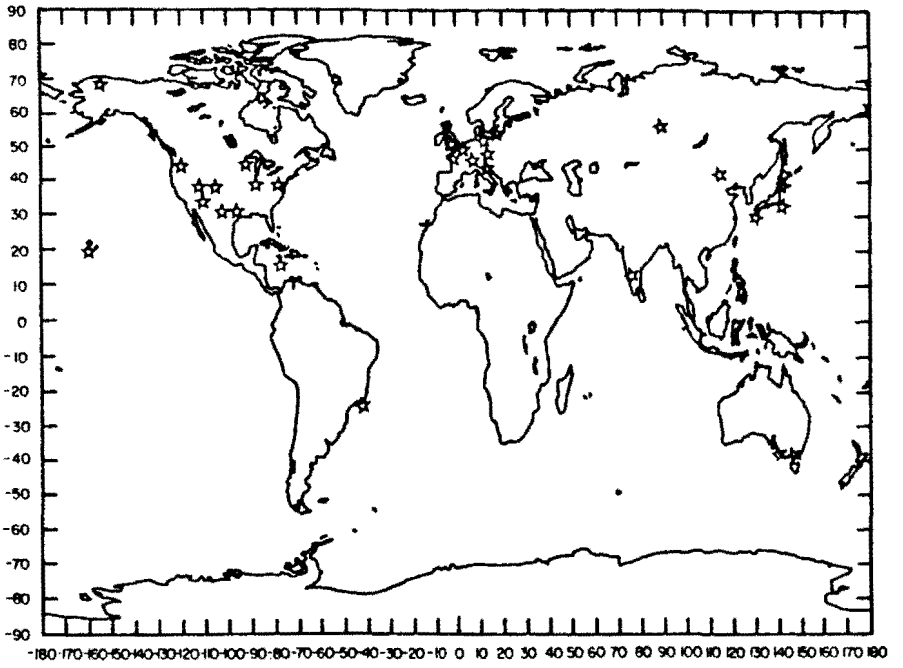

Figure 4.1 Map showing lidar stations making tropospheric and lower stratospheric aerosol measurements using visible or near infrared wavelengths. Lidar stations are marked by a ☆.

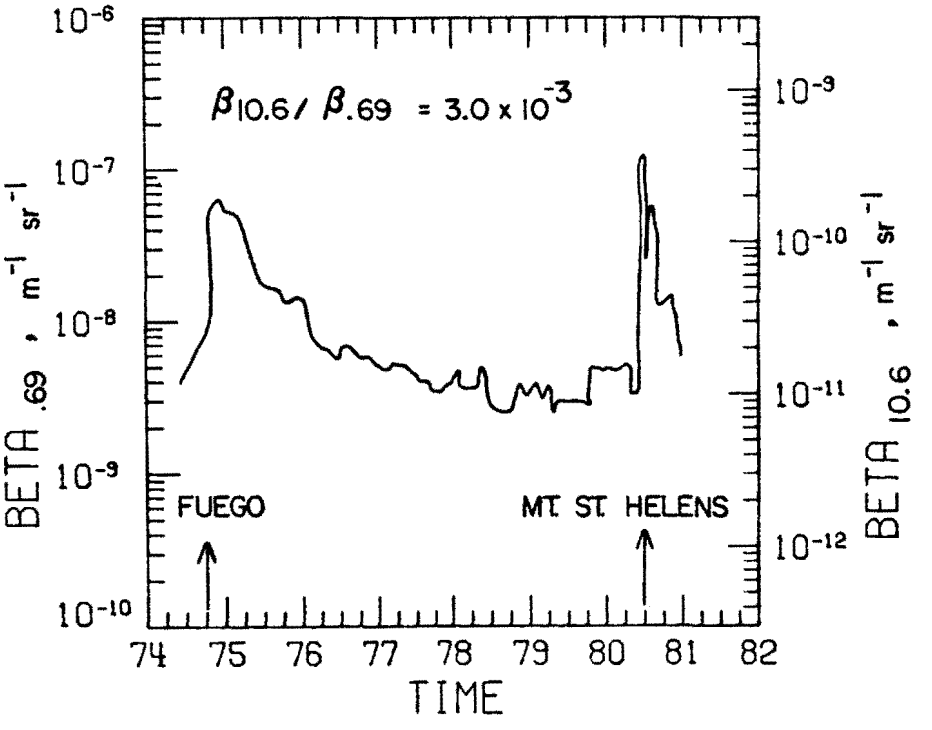

Figure 4.2 Stratospheric lidar record at Hampton, Virginia (Swissler et al., 1982) and the equivalent 10.6 μm backscatter.

5. TECHNIQUES FOR THE CALCULATION OF β_{CO_2}

5.1 Introduction

It is possible to model β_{CO_2} by the following three techniques:

(a) Direct calculation of the β_{CO_2} values from the reported aerosol properties including size distribution, concentration, and composition or complex refractive index.

(b) Extrapolating the existing backscattering data at visible or near infrared wavelengths to CO_2 laser wavelengths (e.g., $\lambda = 10.6\ \mu m$).

(c) Converting the existing aerosol extinction data to backscattering values at the same wavelength or, more directly, to the CO_2 wavelength that we are most interested in. A more detailed discussion of these three methods will be given in subsections 5.2, 5.3, and 5.4, respectively.

In our calculations, we assume that the aerosol particles are spherical so that a Mie code can be used. The assumnption is justified because most of the reported aerosol particles in the atmosphere have size ranges from about 0.01 μm to a few microns. Particles of that size range are usually spherical with the possible exception of those larger particles close to a few micron radius. The errors involved by assuming the sphericity of these larger particles will be discussed in Section 6.2.4.

The majority of our calculations have been carried out by the scattering code AGAUS developed by the Atmospheric Sciences Laboratory of US Army at White Sands Missile Range, New Mexico. As a check, the results of this code have been compared with that of an older scattering code developed by N. Logan. We are completely satisfied with the AGAUS code because results from their code are different from Logan's results by less than about 1%, even when integrations over complete size distributions are carried out. The original AGAUS code can only accept commonly used analytical expressions for aerosol size distributions or else numerical concentrations specified at equal size ranges. It outputs several optical properties, including extinction coefficients and backscattering functions. In order to suit our purpose we have slightly modified the original program so that it can accept measured aerosol size distributions in formats reported in open literature as well as use different methods to extrapolate the input data to larger sizes.

Since large variations occur in aerosol size distributions, most of our analyses have been conducted with three approaches. The first is to conduct calculations using a log-normal size distribution and different mode radii. A semi-quantitative conclusion can be drawn from this aproach. Our second approach has been to use some typical aerosol size distributions measured in different regions of the atmosphere. The third is to calculate the backscatter functions for a large number of possible size distributions and interpret the values obtained.

5.2 From Measured Aerosol Size Distributions and Models

The two input parametrs of β_{CO_2} calculation are the size distribution (including total concentration) and the refractive index of the aerosol material at the CO_2 wavelength.

As mentioned earlier, our first approach is to assume aerosol particles have a log-normal size distirbution. The width of the mode is fixed at 2.0 μm and the mode radii range from 0.05 μm to 5.0 μm. Our second approach is to use the aerosol size distributions obtained by in situ measurements. A list of some of the reported aerosol size distributions used in this study is given in Table 5.1. From the size range listed in this table, it can be seen that, with the exception of Cress' data, most measurements are cut off at a few microns particle radius. In order to study the effect of large particles on the value of β_{CO_2}, we have also calculated β_{CO_2} with aerosol size distributions extrapolated to 10 μm, or even larger sizes, using both linear and log-normal extrapolation. A comparison of the resultant β_{CO_2} values will be presented in the next section.

Some of the reported aerosol size distributions are not smooth but show fluctuations in the larger size range. In some of these cases we have drawn envelopes to the reported aerosol size distribution and calculated the corresponding lower and upper limits of β_{CO_2}.

The aerosol materials under investigtion are sulfuric acid solution with 75% H_2SO_4 by weight, water soluble, dust, soot, clay, and $(NH_4)_2SO_4$. Their corresponding indices of refraction at 10.6 μm are listed previously in Table 3.5.

5.3 From Lidar Measurements

Lidar measurements made at visible or near-infrared wavelengths may be used to calculate the equivalent value for β_{CO_2} provided a suitable conversion factor for the ratio ($\beta_{CO_2}/\beta_{visible\ or\ near\ infrared}$) may be found. This factor will depend upon the wavelengths used but, more significantly, it will depend upon the refractive indices and size distributions of the aerosols under study. These will normally not be known well, and the conversion factor will not be exact. The question of whether visible lidar measurements form a useful data base for conversion to CO_2 wavelengths depends therefore on whether useful limits may be placed on this factor whose values vary from 10^{-4} to 10^{-1}, depending upon particle size, wavelength and refractive index. In particular, it is relevant to ask whether more accurate results may be obtained by this technique than by carrying out calculations based directly upon the estimated aerosol parameters themselves. This question will be directly addressed in Section 6.2.2.

5.4 From Extinction Measurements

The conversion of extinction measurements, made at CO_2 or other wavelengths, to equivalent backscattering function at CO_2 wavelengths is essentially similar to the conversion of lidar measurements made at other wavelengths. The caveats with regard to the establishment of a suitable conversion factor, discussed in relation to lidar in the previous section, apply equally well to extinction. Our conclusions with regard to this problem will be discussed in Section 6.2.3.

The problem with regard to the use of optical depth measurements is more complex. Optical depth is equivalent to the total extinction integrated between the two points of reference. For many measurements this is the whole atmosphere from space to the point of measurement. The extinction coefficient will vary along the path and the characteristics of aerosol, as shown by the optical depth measurement, will be heavily biased toward the region of maximum extinction. For example, multi-wavelength radiometer measurements made at the earth's surface are used to deduce the mean aerosol particle size distribution along the path (Reagan et al., 1977). Since, in many cases, the maximum aerosol concentration will be near the point of measurement, the size distribution found will correspond most closely to this region, and give relatively little information about the aerosol at other points

along the path. This is not to say that optical depth measurements may not give useful information about the aerosol in the free troposphere when measurements are made from a point about the boundary layer (e.g., Shaw, 1980). Once the region in which the extinction is occurring has been established, conversion to β_{CO_2} may be attempted, with additional inaccuracies arising because it is an optical depth rather than an extinction measurement. This necessitates assumptions about the size of the region and the variations of relative extinction within the region.

TABLE 5.1: Examples of reported aerosol size distributions used in this study

Date	Region and Height	Type	Size Range	Author
January 15, 1981	Laramie, Wyoming 16 km	stratospheric	0.01 μm to 1 μm, but larger size aerosols exist	Hofmann and Rosen (1981)
February 10, 1978	Mildura, Australia 10, 16, 23 km	stratospheric	0.05 μm to about 0.9 μm	Gras and Ayers (1979)
May 1, 1976 May 7, 1976	Sherborne, England 1-6 km	European continental	~0.2 μm to ~8 μm	Cress (1976)
1977, 1978	U.S.A & Pacific 0-6 km		0.1 to 3 μm	Patterson et al (1980)

6. ERRORS AND UNCERTAINTIES IN THE CALCULATION OF β_{CO_2}

6.1 Sources of Error

Since it is not feasible to obtain complete and accurate information about all the relevant properties of aerosols for β_{CO_2} modeling, errors are expected to occur. It is therefore essential to identify the sources of error and estimate the magnitude of the uncertainties incurred from such errors.

We can identify three types of errors: those associated with the measuring instruments, those associated with the analysis technique, and those associated with the properties of the aerosol particles themselves. The possible errors associated with the measuring instruments have been discussed in Section 3.2. Here we just wish to point out that, due to the instability of the measuring systems, noise may occur in the measured aerosol property, especially in the size distribution. As also pointed out in that section, some in situ measurements are effectively not in situ; the properties of aerosol particles that we are interested in have to be deduced in the laboratory from the samples collected in the field. As will be discussed later in this section, different aerosol properties can be deduced from the same measured results using different analyzing techniques. The incompleteness and inaccuracy of the reported aerosol properties are another source of error. Due to the limitation of conventional measuring devices, the small number concentration of particles in the coarse-particle mode is hard to measure. Consequently, their properties are usually not reported along with those of smaller sizes. This is not a serious problem for modeling extinction and backscatter at visible wavelengths, due to their expected small contribution to the overall value. However, for radiation of longer wavelengths (such as CO_2 laser), the presence of larger particles may greatly increase the overall β_{CO_2} values, as will be reported later in this section. The incompleteness of aerosol size distributions can be partially solved by extrapolating the reported size range to larger sizes if that seems feasible. However, error may be generated by using a wrong extrapolation method. The composition (or more directly the complex refractive index) and shape are other sources of error that will also be discussed later in this section.

6.2 Effects of Errors on the Calculated β_{CO_2}

As explained in Section 5.1, three main techniques have been used to estimate errors and to assess the dependence of β_{CO_2} upon an exact knowledge of the parameters involved in its calculation.

The first of these involve the use of log-normal models and the principle features of these are summarized in Fig. 6.1 which shows the key parameters and the relationship between the number distribution and the volume distribution. In the following subsections, modeling has been carried out for values of mode radius r_g between 0.03 μm and 5 μm, covering that of the commonly observed range of particle size distributions in the lowest 20 km of the atmosphere. A limited amount of calculation has been done varying the geometric mean standard deviation σ_g between 1.5 and 2.5.

Three size distributions have been selected as typical for the free troposphere. These are shown in Fig. 6.2. They consist of a continental distrribution with a large number of the larger particles (Cress, 1980, spring average), a continental distribution with fewer large particles (Patterson et al., 1980) and a marine free tropospheric distribution with very few large particles (Patterson et al., 1980). Most aerosol size distributions found in the literature lie between the limits represented by these three.

6.2.1 β_{CO_2} calculated from measured size distributions and refractive index

Using the three size distributions shown in Fig. 6.2 as a starting point, histograms have been calculated showing the relative contribution to β_{CO_2} from different particle size ranges. These are shown in Figs. 6.3, 6.4, and 6.5. (Note: the size ranges used in the three figures are not the same.) Also shown in these figures are similar histograms for the backscattering function at 0.69 and 1.06 μm and the extinction coefficient at 1.0 μm. The main points shown by these figures are:

(a) That, even for the Cress spring average aerosol size distribution which contains a relatively large number of the larger particles, most of the scattering at 10.6 μm is from particles with radii less than 2.5 μm. In this example, very little scattering comes from particles with radii less than 1.0 μm.

(b) That, for the marine free troposphere, an appreciable fraction of the scattering comes from particles with radii less than 0.5 μm.

(c) In all cases, the size ranges corresponding to peak scattering at the shorter wavelengths differ from those responsible for the peak scattering at 10.6 μm.

These histograms and the points noted above will be useful in understanding the source of the errors and uncertainties in modeling β_{CO_2}, to be discussed in the following subsections.

6.2.1.1 Errors related to refractive index uncertainties

Calculations have been made of the β_{CO_2} at 10.6 μm for each of the three aerosol size distributions described in Section 6.2 and a range of refractive indices. These are shown in Figs. 6.6, 6.7, and 6.8 where the real part of the refractive index is allowed to vary between 1.1 and 2.2 and the imaginary part from 0 to 1.0. (The figures correspond to the Cress spring average, the Patterson et al. continental, and the Patterson et al. maritime aerosol size distributions, respectively.) The curves (for constant imaginary component of the refractive index) are similar in all three figures, although more overlapping occurs in the Cress spring average size distribution than with the other two and the mean level is very different between the figures. Also shown on these figures are the scattering and refractive indices for five common arosol materials and for water. The following are the main characteristics common to these three figures.

(a) For a zero imaginary component of refractive index β_{CO_2} varies by about two orders of magnitude as the real component of refractive index varies from 1.1 to 2.2.

(b) For an imaginary component of refractive index of the order of unity (this may occur near an absorption band), the scattering is independent of the real component of the refractive index. What is in fact happening is that the particle has become totally reflecting.

(c) For imaginary components of refractive index of less than 0.1, the scattering from the two Patterson et al. distributions is effectively the same as for a totally nonabsorbing particle.

(d) If we except water and carbon from the set of aerosol materials shown, the remaining four materials have fairly close backscattering functions. Carbon is normally a minor constituent although it may be important at certain times and locations. Water is of course not a minor constituent and its omission implies that we are dealing with low humidity conditions. The importance of the low backscattering functions for water will be taken up again in Section 7.4. The fact that the backscattering functions of the remaining four aerosol materials are fairly close implies that errors in refractive index may not have too great an effect on β_{CO_2}, a point that will be discussed again in the next section.

6.2.1.2 Errors related to size distribution uncertainties

The effect of changing aerosol radius on the values of β_{CO_2} has been examined using log-normal models with constant $\sigma_g = 2.00$ and varying r_g from 0.03 to 5 μm. The resultant behavior of β_{CO_2} is shown in Fig. 6.9 for the five different aerosol materials used in Section 6.2.1.1. Also shown in Fig. 6.9 are the ranges of log-normal mode maxima found to exist in the free troposphere and stratosphere. These have been determined both by actual fitting to published size distributions and by noting values quoted by other researech workers. (The ranges for the stratospheric and tropospheric accumulation modes are not quite the same but have been assumed to be so for the purposes of this figure.) It can be seen that the range of β_{CO_2} is at least six orders of magnitude. Calculation, using actual measured size distributions shows a range about as great as this, even though almost all tropospheric aerosol distributions consist of a mixture of the two dominant modes. In contrast, as noted in the previous section, the change in β_{CO_2} for different aerosol materials is much less than the change produced even by a small shift in mode radius. This point is further emphasized in Fig. 6.10 where the values of β_{CO_2} for sulfuric acid, water soluble aerosol (Shettle and Fenn, 1979) and ammonium sulfate have been plotted as a ratio to β_{CO_2} for the dust aerosol (Shettle and Fenn, 1979). Since the soluble content of the tropospheric aerosol varies with aerosol radius, curves have been plotted for both the four materials and also for a standard mixture (Winkler, 1974; Nilsson, 1979). Over the common range of mode radius (.03 → 1.0 μm) the variation of β_{CO_2} for the mixed aerosol does not differ by more than a factor of 2½ from that for a pure dust aerosol, even for the extreme case of ammonium sulphate. In general, therefore, it may be concluded that the effects of uncertainties in aerosol composition are small compared to those caused by uncertainties in particle size.

Fig. 6.10 shows two scales, one for the mode radius of the fitted number log-normal distribution and one for the equivalent log-normal volume distribution. It may be noted that these differ by approximately a factor of four. It is possible to extend this concept and plot β_{CO_2}, not for one particle per unit volume but for unit volume of aerosol per unit volume of air. This has been done in Fig. 6.11, and it may be seen that the change in β_{CO_2} is very much less than in Fig. 6.9. This is an important result, as it means that an uncertainty in the maximum of a volume distribution will produce less variation in the modelled β_{CO_2} than a simular uncertainty in the maximum of a number distribution. It also means that aerosol volumes or mass concentrations may be converted to β_{CO_2} with not more than two orders of magnitude possible error, even if no size information is available. There may be a considerable improvement over this figure if a reasonable guess at the type of size distribution is possible. A further development of this point is illustrated in Table 6.1. In the calculations described above, we have assumed that $\sigma_g = 2.0$. In practice σ_g for the best fit log-normal distribution may vary from 1.5 to 2.5. Table 6.1 shows the effect of this variation in σ_g on the modelled values for β_{CO_2}. For calculations based on a fixed number distribution mean, the effect is severe; for calculations based on a fixed volume distribution mean the effect is small.

All the analysis presented thus far in this sub-section has been based on log-normal models. It is useful to consider the errors in β_{CO_2} produced by uncertainties and noise within a single research worker's data or by uncertainties arising because of contradictions between data obtained by different research workers. It is also necessary to consider the fact that many measured distributions do not include particles of sufficiently large radii, and such distributions must either be discarded, or extrapolated to larger radii.

Fig. 6.12 shows examples of noise in data obtained by Cress (1980). At the large particle end of the size distributions considerable statistical fluctuation is evident. Table 6.2 shows values of β_{CO_2} calculated for the profiles at heights of 1.6 and 5.6 km, using both the upper and lower envelopes of the size distributions. The modeled values for β_{CO_2} differ by more than a factor of two in these cases. (Note the values shown in the Table are for extrapolated curves; the effect of extrapolation is discussed below.) Another source of uncertainty is shown in Fig. 6.13; this shows impactor data obtained, at three different altitudes, for stratospheric aerosols by Gras and Ayers (1979) and analyzed using two different techniques, a third curve in each diagram shows data obtained on the same aerosols using an in situ white light technique. All three curves are different at each altitude, particularly c from either a or b. Table 6.3 shows the corresponding values for β_{CO_2}, which, at two of the altitudes, differ by more than an order of magnitude.

An even more graphic illustrationn of the uncertainties in β_{CO_2} is obtained by considering the stratospheric data of Hofmann and Rosen which was discussed in Section 3.2.2. In that section we saw that Hofmann and Rosen have reported the existence of particles with radii between 1 and 2 μm in greater numbers than had previously been expected. Fig. 6.14 shows value of β_{CO_2} modeled from an example of Hofmann and Rosen's data. In this example, β_{CO_2} has been calculated for: (a) a log-normal distribution fitted to the cumulative number distributions obtained at radii of .15 and .25 μm; (b) a slightly truncated log-normal distribution with the appropriate number of particles removed and placed in the radius ranges 0.95 $\rightarrow$ 1.2 μm and 1.2 $\rightarrow$ 1.8 μm. Corresponding values for β_{CO_2} are also shown for each section of the distribution. It can be seen that inclusion of the large particles increases β_{CO_2} from 2.5 x 10^{-11} m^{-1} sr^{-1} to 55.6 x 10^{-11} m^{-1} sr^{-1}. Analysis of another example of Hofmann and Rosen's data produced a similar, although not quite as large, increase.

One problem that occurs is whether it is permissible to use size distribution data that does not extend to sufficiently large radii. It is necessary to inquire whether such distributions may be extrapolated to larger particle sizes with success. Two methods of extrapolating measured size distributions have been considered, which are shown in Fig. 6.15. Since the particle size distribution approximates to a double log-normal, it might be expected that a log-normal extrapolation would be more accurate than a power law extrapolation. This is normally the case and indeed a power law extrapolation can be very unreliable. It has to be fitted to the last two or three measured points in the distribution, which as we have seen, can be noisy. The resultant extrapolation may lead to very erroneous results. A log-normal extrapolation is normally more reliable but, if the data are noisy, it may not be possible to fit a log-normal. In this case the data are better without extrapolation and possibly should not be used at all. Table 6.4 shows the effects of both a log-normal and a linear (power law) extrapolation on three typical size distributions. The distribution measured by Cress extends to a radius of 5 μm. Both a linear and a log-normal extrapolation are possible, neither changes the modeled value for β_{CO_2} by a very large factor. The distribution of Gras and Laby is very different; it does not extend beyond a radius of 1 μm. A log-normal extrapolation is not possible and the linear extrapolation produces a value of β_{CO_2} that is an order of magnitude greater than the unextrapolated value. It is clear that the distribution should not be used, either extrapolated or unextrapolated. The third distribution, although extending only to a

radius of 1.8 μm, can be extrapolated by both methods. Again β_{CO_2} is increased by extrapolation, but not greatly. In general, it can be said that extrapolation is possible and useful for tropospheric aerosol if the measured size distribution extends beyond the peak of the coarse particle mode. If the distribution does not extend that far, it should not be used at all.

6.2.2 β_{CO_2} calculated from lidar measurements

Fig. 6.16 shows the results of calculation of the ratios of the backscattering function at 10.6 μm to the backscattering function at 0.6943 μm for the same ranges of log-normal models and aerosol compositions as used previously. Fig. 6.17 shows similar curves for the ratios of the backscattering function at 10.6 μm to the backscattering function at 1.06 μm. In both cases, the range of variation is somewhat less than that shown in Fig. 6.9 but is, nevertheless, still about two orders of magnitude over the naturally observed range of log-normal modes, even when the curve for soot is excepted.

A similar range of conversion factors is found when calculations of these ratios are carried out for a large number of measured size distributions. The size distributions have been divided into three classes—stratospheric aerosol, marine free tropospheric aerosol and continental free tropospheric aerosol, and Figs. 6.18 and 6.19 show histograms of the frequency of occurrence of a given value for the ratio (calculated for sulfuric acid for the stratospheric aerosol, for dust for the other aerosols). This range of variation in the conversion factor has been foreshadowed in Section 6.2, where it was observed that the aerosol sizes responsible for the bulk of the scattering at 10.6 μm were not the same as those responsible for the bulk of the scattering at shorter wavelengths. Even though the data has been sub-divided into the classes shown, it is still highly scattered. The stratospheric ratios appear consistent except for the fact that these ratios have been calculated assuming no large particles with radii of the order of 1 μm. Inclusion of these particles increases the conversion factor by approximately one order of magnitude. The marine free tropospheric aerosol, in which the ratio of the numbers of large to small aerosols can vary over a very wide range, shows a large variation in the conversion factor. Values for the continental free tropospheric aerosols show consistency, but this should be used with caution, as many of the values at the peak of the histogram come from a single measurement technique (single stage impactor) and may be artificially concentrated.

6.2.3 β_{CO_2} calculated from extinction and optical depth measurements

Calculations have been carried out for the ratios of $\beta_{10.6}$ to extinction at 1.0 μm in an exactly analogous manner to those presented in the previous section. The results of these calculations are shown in Figs. 6.20 and 6.21. The same comments and conclusions apply to these graphs as to the earlier ones and need not be repeated. Fig. 6.22 shows the results of calculation of the ratio of the backscattering function at 10.6 μm to the extinction coefficient at 10.6 μm. A considerable range of variation (about 1½ orders of magnitude) is observed, even though both values are calculated at the same wavelengths.

Detailed calculations of $\beta_{10.6}$ from optical depth measurements have not been attempted.

6.2.4 Effects of uncertainties in shape

Although the smaller sized aerosol particles, especially the liquid phase aerosols, can be assumed to be spherical, most naturally occurring scattering particles are not always perfect spheres. The shape of aerosol particles can be seen by scanning electron microscope photomicrographs or other techniques. An analysis of the samples collected from cascade impactors aboard aircraft has shown that the small particles are more nearly spherical in shape but are not really smooth spheres and the large particles are irregularly shaped agglomerates (Wood, 1979).

In spite of the fact that most natural aerosols are not perfect spheres, a vast amount of theoretical calculation has been made for perfect spheres. This is because Mie theory calculations are easy to perform and in some cases the qualitative, and even quantitative, characteristics of particle scattering are adequately represented by equivalent spheres. For most irregularly shaped particles, the calculation of exact backscatter is almost impossible even with the use of today's high speed computers.

.A recent report by Huffman (1981) shows that the measured volume extinction coefficients for Al_2O_3 are in general slightly larger than those calculated from Mie theory, with the exception that, near the absorption line at $\lambda = 13.3$ μm, the calculated volume extinction coefficient is about ten times the measured value. A comparison between the measured angular scattring pattern at $\lambda = 0.6328$ μm for irregular particles with those calculated by Mie theory shows that the calculated backscatter is about two to three times the measured value (Chylek, 1976). For comparisons at 10.6 μm, the experimentally measured backscatter from an ice cloud containing minute crystals (2.3 μm mean dimension) is only slight smaller than that predicted from Mie theory (Sassen, 1981).

Since the backscattering cross section is a function of the size parameter $\alpha = (2\pi r)/\lambda$ where r and λ are radius of the particle and wavelength of radiation, respectively, and the size parameter of aerosols at $\lambda = 10.6$ μm is equal to only 1/10 of the size parameter of the same aerosols at visible wavelengths, we expect the effect of shape on backscatter at 10.6 μm should be far less significant than that at visible wavelengths. As mentioned earlier, at the visible wavelength $\lambda = 0.6328$ μm, the difference between the measured backscatter and the backscatter predicted by Mie theory is only a factor of about 2. We tentatively conclude therefore that the errors produced by β_{CO_2} due to the irregularity of shape in aerosol particles are small in comparison with other sources of error. Only if the wavelength is close to that of an absorption line, may the actual backscatter from irregularly shaped particles be significantly different from the value predicted by the Mie theory.

TABLE 6.1: EFFECT OF VARYING THE WIDTH OF THE LOG-NORMAL MODEL

$\lambda = 10.6$ μm, DUST AEROSOL

(A) FIXED NUMBER DISTRIBUTION MEAN, $r_g = 0.631$ μm, 1 PARTICLE PER cm^3

ρ_g	β
1.5	8.73×10^{-9} m^{-1} sr^{-1}
1.75	19.56×10^{-9} m^{-1} sr^{-1}
2.00	31.79×10^{-9} m^{-1} sr^{-1}
2.25	46.94×10^{-9} m^{-1} sr^{-1}
2.5	65.14×10^{-9} m^{-1} sr^{-1}

(B) FIXED VOLUME DISTRIBUTION MEAN, $r_V = 2.51$ μm, 1 μm^3 PER cm^3

ρ_g	β
1.5	4.10×10^{-9} m^{-1} sr^{-1}
1.75	3.39×10^{-9} m^{-1} sr^{-1}
2.00	3.68×10^{-9} m^{-1} sr^{-1}
2.25	3.49×10^{-9} m^{-1} sr^{-1}
2.5	3.34×10^{-9} m^{-1} sr^{-1}

TABLE 6.2: A COMPARISON OF β_{CO_2} VALUES CALCULATED FROM THE LOWER AND UPPER ENVELOPES OF THE REPORTED AEROSOL SIZE DISTRIBUTIONS WITH NOISE AT THE LARGE PARTICLE END[1]

Height (km)	β_{CO_2} (m^{-1} sr^{-1})[2]	
	calculated from lower envelope	calculated from upper envelope
1.6	0.816×10^{-8}	1.57×10^{-8}
5.6	0.671×10^{-8}	1.42×10^{-8}

[1]The aerosol size distributions are given by Cress [AFGL-TR-80-0178 (1980)] at 0850 Z on July 7, 1977. (See Fig. 6.12)

[2]Aerosol size distributions are extrapolated to 30 μm and aerosols are assumed to be dusts.

TABLE 6.3: A COMPARISON OF β_{CO_2} VALUES CALCULATED FROM AEROSOL SIZE DISTRIBUTIONS DEDUCED WITH DIFFERENT SIZING TECHNIQUES[1]

Height (km)	β_{CO_2} (m^{-1} sr^{-1})		
	from Gras & Ayer technique	from Bigg & Ono technique	from *In situ* white-light scatter
10	1.568×10^{-11}	4.068×10^{-12}	1.376×10^{-11}
16	3.716×10^{-12}	2.184×10^{-13}	2.866×10^{-12}
23	6.062×10^{-12}	3.785×10^{-13}	3.037×10^{-12}

[1]Size distribution of aerosol particles are obtained on February 10, 1978 at Mildura (34.2°S, 142.1°E) by Gras and Ayers (1979). Aerosol particles are assumed to be 75% H_2SO_4. (See Fig. 6.13)

TABLE 6.4: EFFECT OF EXTRAPOLATION ON THE CALCULATED VALUES OF β_{CO_2}

Data Source	Maximum Particle Radius Measured	Altitude	β_{CO_2} (10^{-9} m^{-1} sr^{-1})		
			No. Extrap.	Log-normal Extrap.	Linear Extrap.
Cress, 1980	5 μm	6 km	1.78	1.93	2.11
Gras & Laby 1981	1 μm	4-10 km	0.017	not possible	0.16
Patterson et al. 1980	1.8 μm	5 km	0.60	0.66	0.72

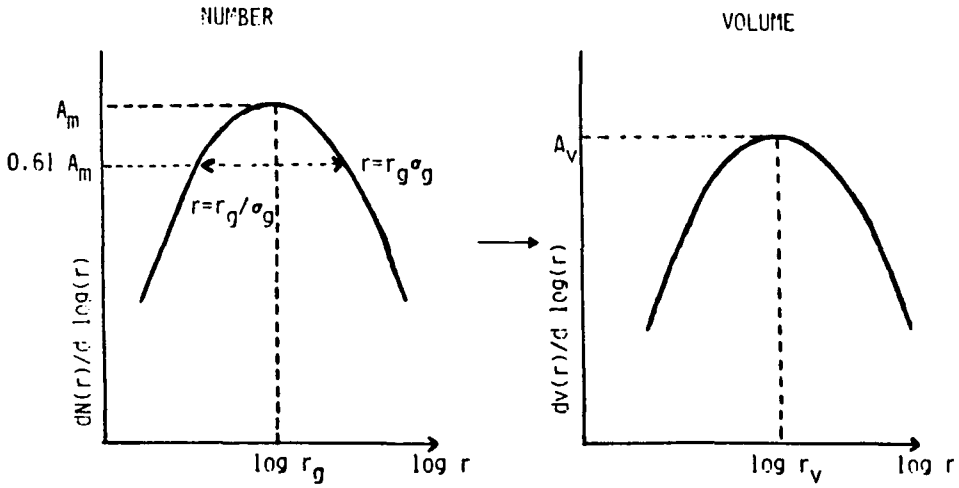

Figure 6.1 Key parameters of log-normal size distributions and the relationship between the number and volume distribution. $dN(r)/d\log(r) = A_m \exp[-k \ln^2 (r/r_g)]$; $k = 1/(2 \ln^2 \sigma_g)$; $r_v = r_g \exp 3(\ln \sigma_g)^2$, *if* $\sigma_g = 2.00$; $r_v = 4.23\, r_g$.

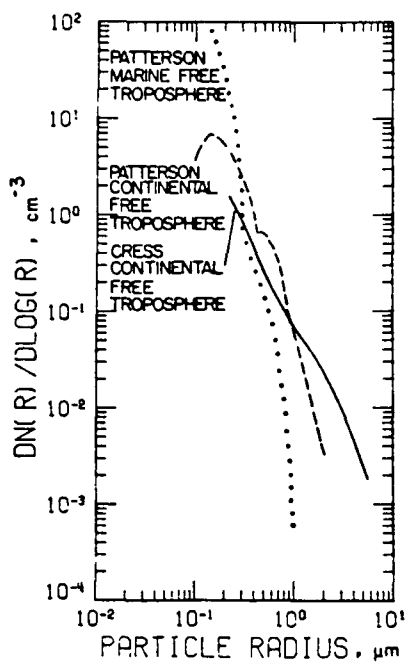

Figure 6.2 Size distributions selected as typical of those occurring in the free troposphere (Cress, 1980; Patterson et al., 1980).

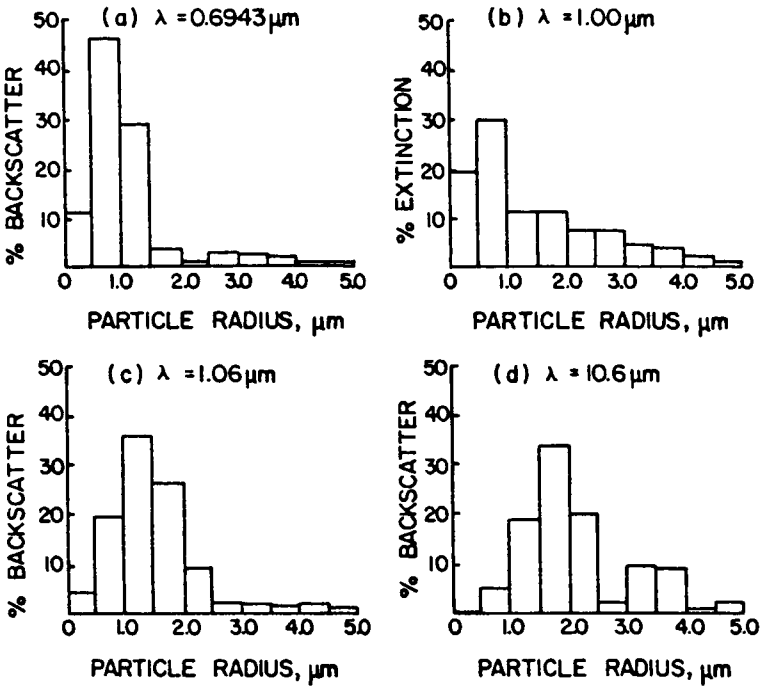

Figure 6.3 Histograms showing the relative backscatter and extinction, at four different wavelengths, from different particle size ranges for the Cress spring average size distribution.

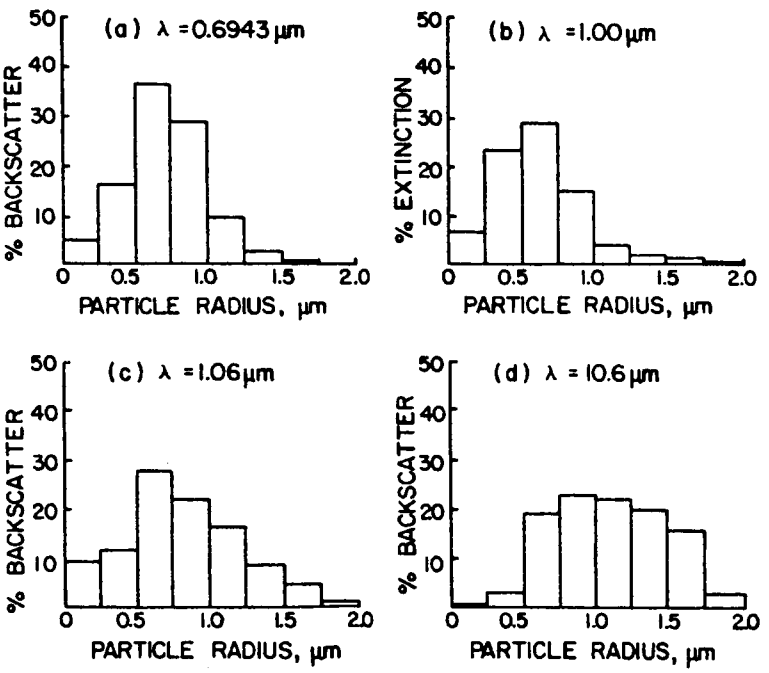

Figure 6.4 Histograms showing the relative backscatter and extinction, at four different wavelengths, from different particle size ranges for the Patterson et al. (1980) continental free troposphere size distribution

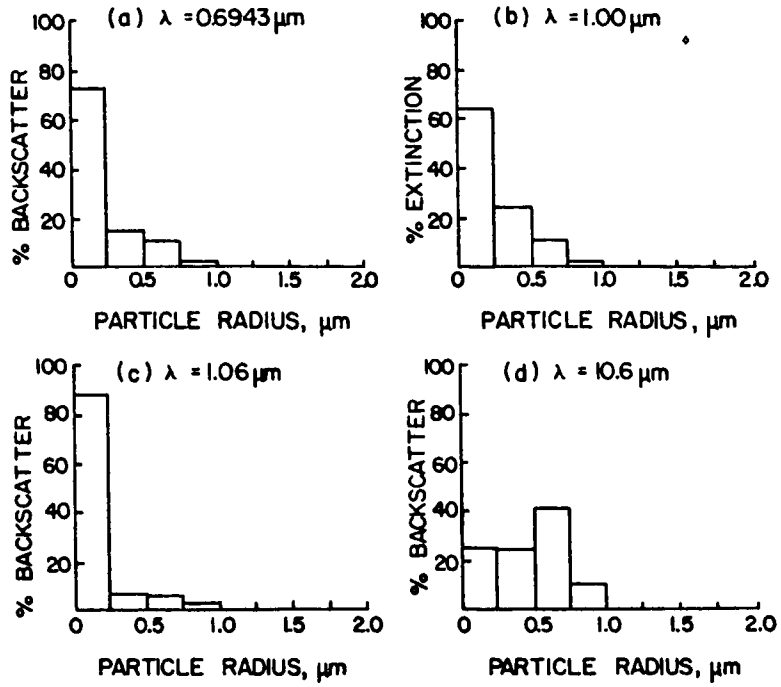

Figure 6.5 Histograms showing the relative backscatter and extinction, at four different wavelengths, from different particle size ranges for the Patterson et al. (1980) marine free troposphere size distribution.

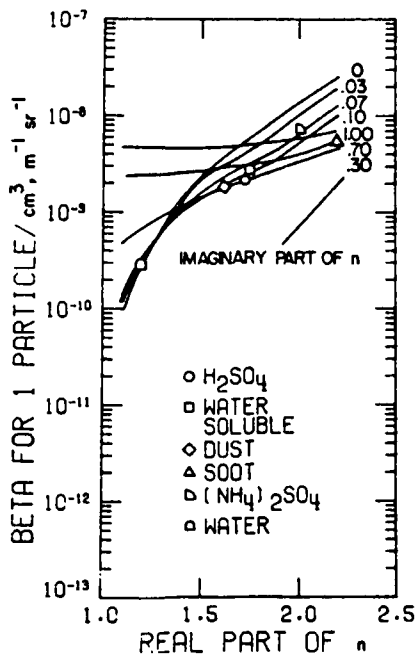

Figure 6.6 Variation of β_{CO_2} with refractive index for the Cress spring average size distribution.

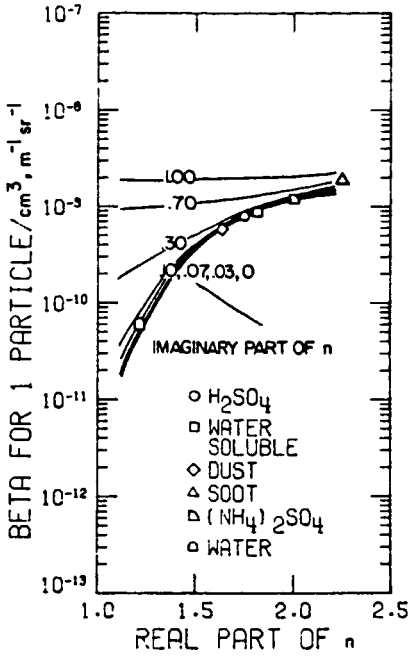

Figure 6.7 Variation of β_{CO_2} with refractive index for the Patterson et al. (1980) continental size distribution.

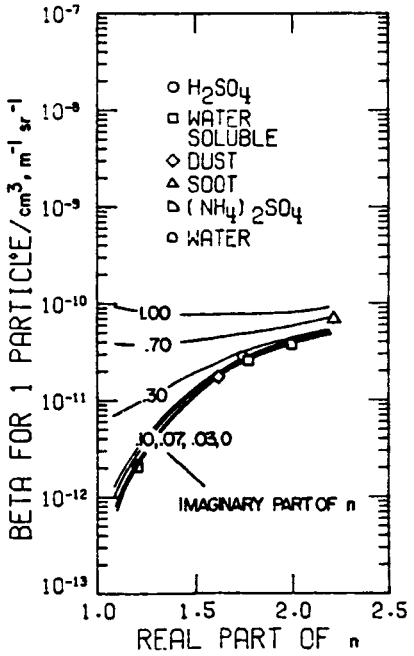

Figure 6.8 Variation of β_{CO_2} with refractive index for the Patterson et al. (1980) marine free troposphere size distribution.

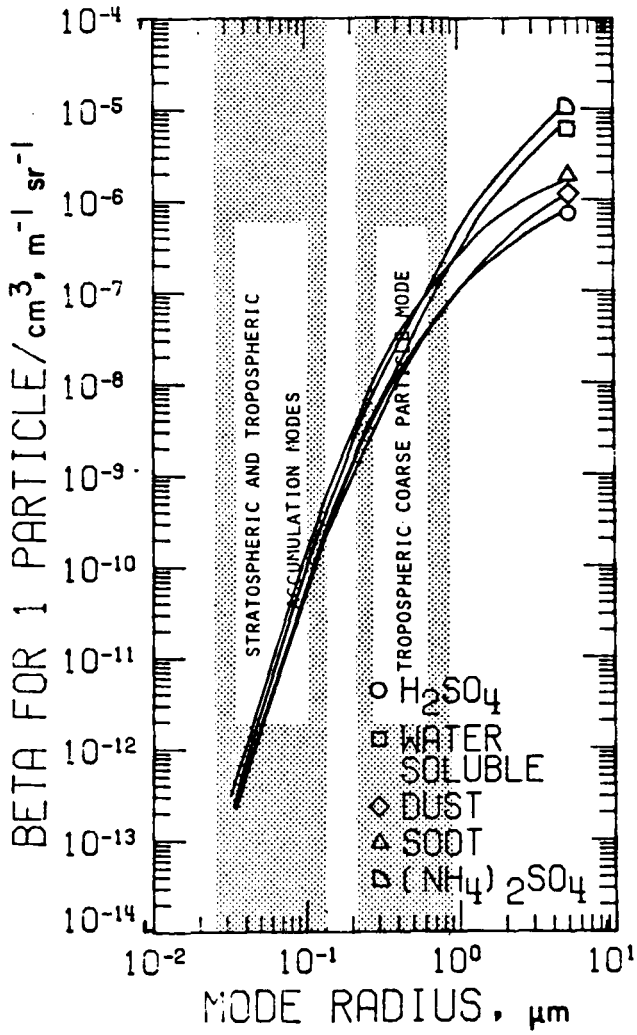

Figure 6.9 Variation, with mode radius of β_{CO_2} for constant number density for log-normal size distributions and five common aerosol materials.

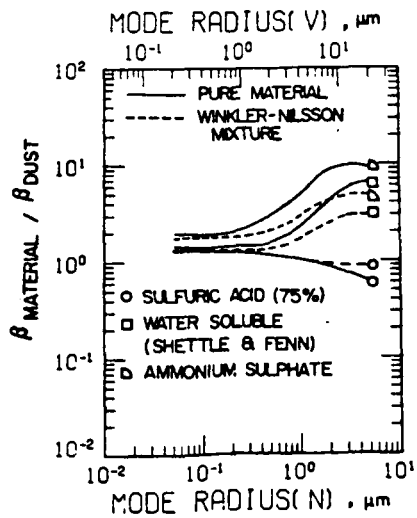

Figure 6.10 Ratios of β_{CO_2} for different aerosol materials to that for dust. This ratio is shown as a function of log-normal distribution mode radius.

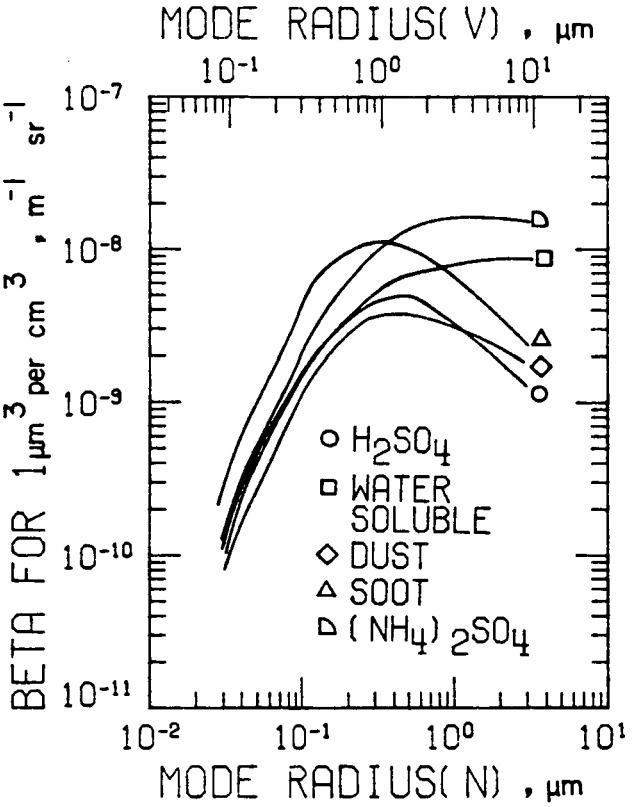

Figure 6.11 β_{co_2} *per unit volume of aerosol for log-normal size distributions, shown as a function of number and volume mode radius.*

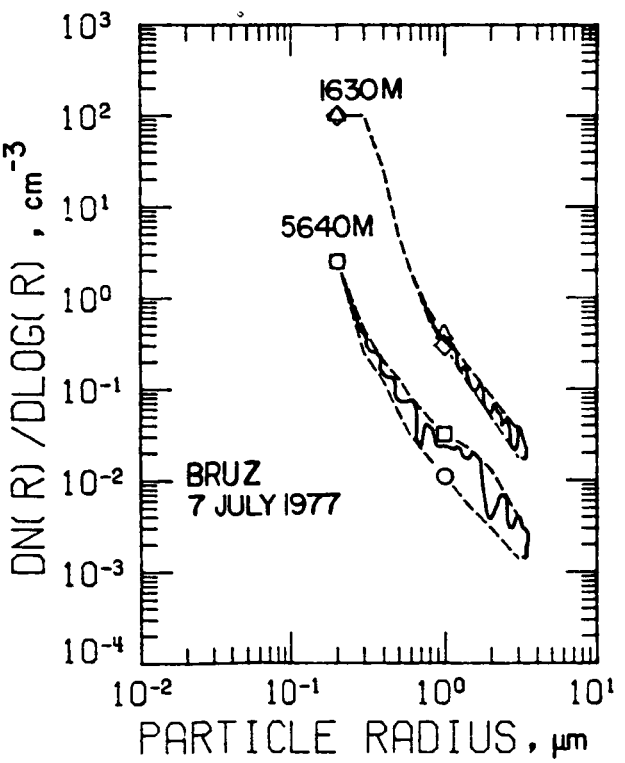

Figure 6.12 Example of aerosol size distribution measurements showing statistical noise at the larger radii particles (Cress, 1980).

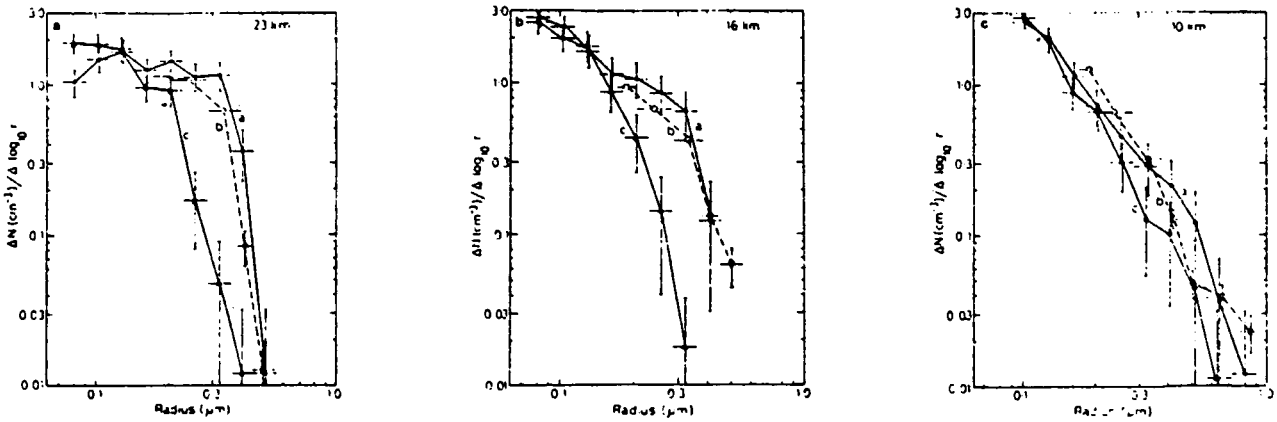

Figure 6.13 Stratospheric aerosol size distributions attained by Gras and Ayers (1979) at Mildura, Australia. Distributions marked a and c were determined from impaction samples, those marked a using a new sizing model and those marked c the Bigg and Ono (1974) model. Distributions marked b were determined independently using in situ white-light scatter sizing of individual particles.

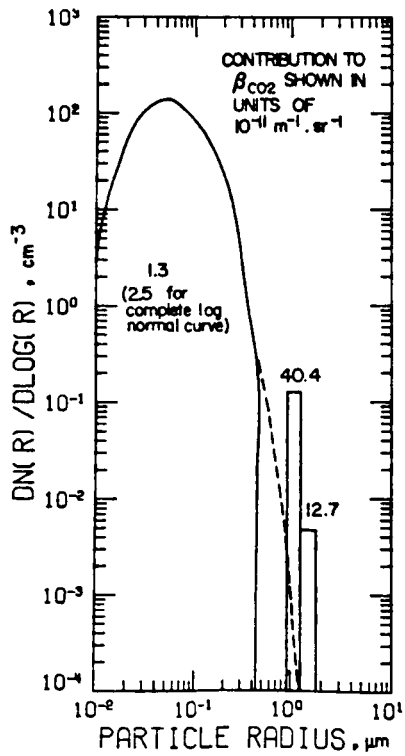

Figure 6.14 Contributions to β_{CO_2} for the Hofmann and Rosen cumulative size distribution at an altitude of 13.7-15.8 km shown in Fig. 3.15

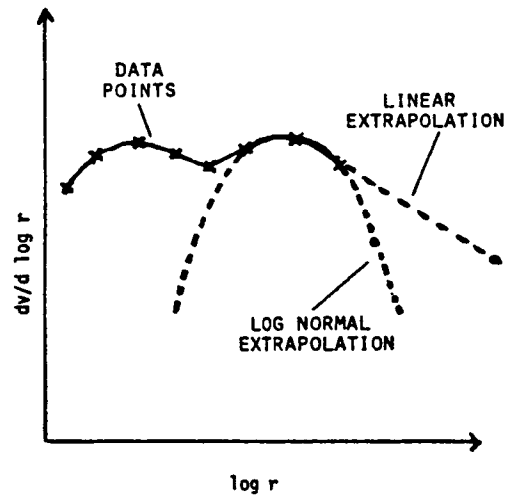

Figure 6.15 Methods of extrapolating measured size distributions.

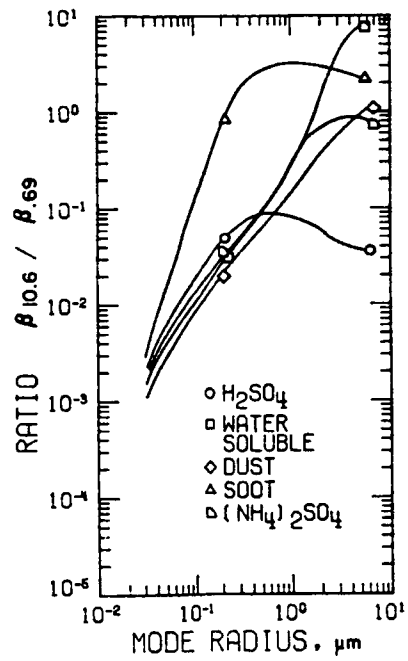

Figure 6.16 Backscatter ratios $\beta_{10.6}/\beta_{0.69}$ shown as a function of log-normal mode radius.

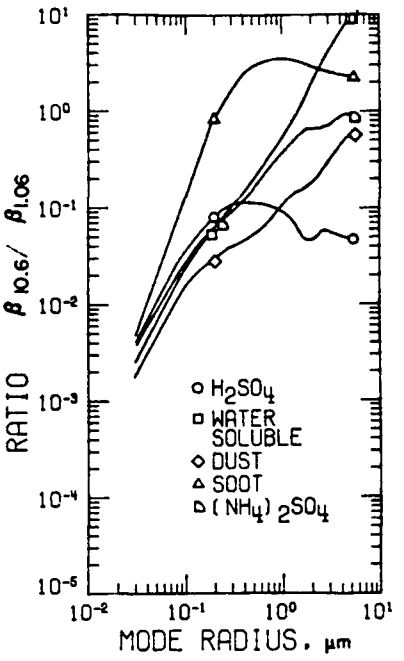

Figure 6.17 Backscatter ratios $\beta_{10.6}/\beta_{1.06}$ shown as a function of log-normal mode radius.

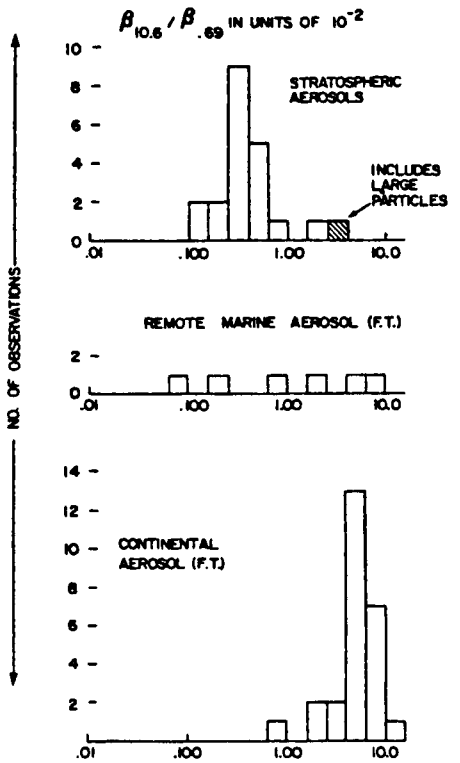

Figure 6.18 Histograms of the frequency of observation of various values of the ratio $\beta_{10.6}/\beta_{0.64}$.

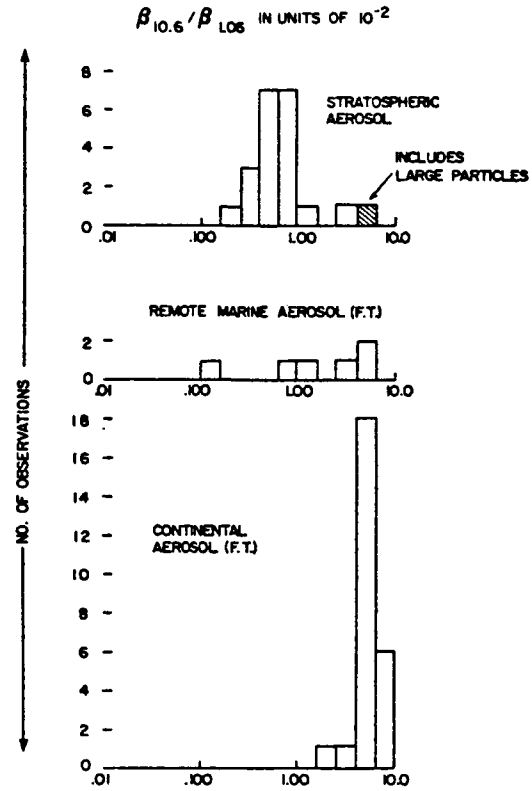

Figure 6.19 Histograms of the frequency of observation of various values of the ratio $\beta_{10.6}/\beta_{1.06}$.

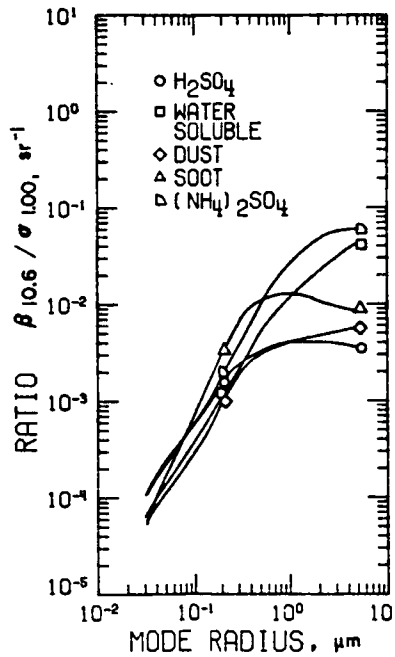

Figure 6.20 Back scatter to extinction ratios $\beta_{10.6}/\sigma_{1.00}$ *shown as a function of log-normal mode radius.*

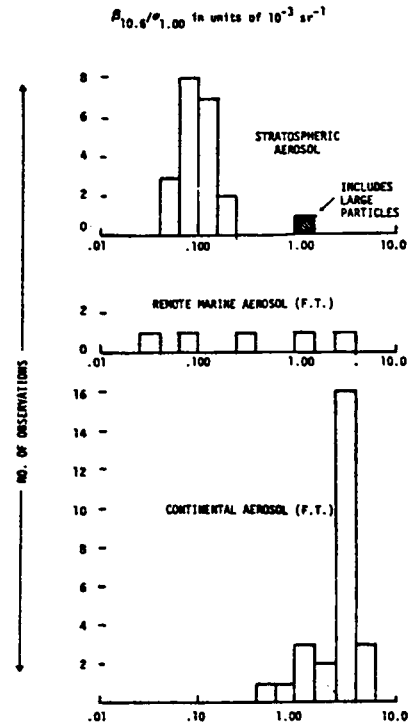

Figure 6.21 Histograms of the frequency of observation of various values of the ratio $\beta_{10.6}/\sigma_{1.00}$.

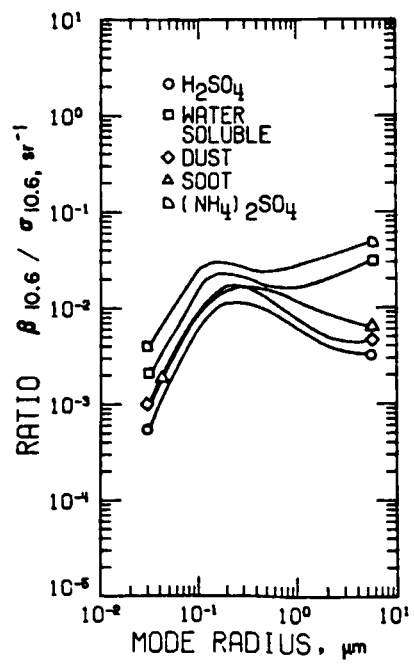

Figure 6.22 Back scatter to extinction ratios $\beta_{10.6}/\sigma_{10.6}$ *shown as a function of log-normal mode radius.*

7. DETERMINATION OF β_{CO_2}

7.1 General Behavior

Fig. 7.1 shows a scattered plot of the calculated values of β_{CO_2} for a large number of published size distributions (Bigg, 1975; Grass and Laby, 1981; Farlow et al., 1981; Rosen and Hofmann, 1981; Hofmann and Rosen, 1981; Patterson et al., 1980; Cress, 1980; Blifford and Ringer, 1969; Blifford, 1970; DeLuisi et al., 1976). Values in the troposphere have been calculated assuming a mixed dust/water soluble aerosol and those in the stratosphere have been calculated assuming a sulfuric acid/water aerosol. The figure has been sub-divided into regions and it is of particular interest to note that the values for the remote Pacific Ocean fall in a β_{CO_2} region quite distinct from that in which the continental free tropospheric values fall. (The continental free tropospheric region includes values obtained over the ocean close to continental land masses.) It is also important to note that a minimum value of approximately 10^{-11} m^{-1} sr^{-1} is found for both the stratosphere and the remote free troposphere. Stratospheric values in the figure are somewhat confused as we have shown the results of calculations based on the Hofmann and Rosen data with and without the inclusion of the larger particles. Data from Farlow et al. has also been shown with an arrow and two values in order to illustrate the effect of the relatively small uncertainty of 15% in the mode maximum which is discussed in their paper. Relatively little boundary layer data has been included, but the vertical arrows in the bottom right-hand corner of the figure show results of calculations based on DeLuisi et al.'s (1976) data, representing vertical averages including part of the boundary layer. It may also be noted from the figure that there is a scarcity of measured data between 7 km altitude and the tropopause. Also shown on the figure are experimental data obtained by MSFC (Bilbro, 1981) and NOAA (Post et al., 1982). This data were obtained in June and July 1981. One set of Rosen and Hofmann's data was obtained in July 1981 and it should be noted that the experimental curve passes between the two values representing calculations with and without the large particles. Agreement between the experimental and the modeled values is good in the upper troposphere and in the boundary layer but relatively poor in the lower free troposphere. It is quite likely that much of this discrepancy is due to a seasonal variation. Blifford and Ringer (1969) show a very strong seasonal variation in the continental aerosol over the USA, particularly in the lower free troposphere. This variation has its maximum in June and July when values about five times the annual mean were obtained. It is thus likely that the experimental data represents a summer maximum; the same is not true for the modeled values.

Effects due to humidity and temperature changes have not been included in this figure. As we shall see in Section 7.5, such effects are normally not of major importance in the free troposphere, provided regions of cloud are excluded.

7.2 Tropospheric Behavior

In Section 3.2.2 we presented data obtained by Patterson et al. (1980) for the mass aerosol loading in the free troposphere over the Pacific Ocean. This was shown in Fig. 3.7 and the

right-hand ordinate of the figure shows the corresponding values for β_{CO_2}. This has been obtained by calculating a mean conversion factor (shown in Table 7.1) from mass loading to β_{CO_2} using the size distributions obtained by Patterson et al. (1980) over the Pacific Ocean. This factor is undoubtedly variable, probably systematically with latitude and thus the scale shown should be taken as approximate only. Nevertheless, it shows clearly the major fact of the latitude variation and the probably spread in β_{CO_2}, the minimum value of which is again around 10^{-11} m^{-1} sr^{-1}.

In Section 3.2.2 we also showed Figs. 3.13 and 3.14 containing the probability distributions for two sets of aerosol observations. In Fig. 7.2 these are shown again, converted to the equivalent backscattering function. Also superimposed on this figure are the experimental probability distributions for β_{CO_2} obtained by Post et al. (1982). Points to note are

(a) The similarity in slopes between the NOAA experimental data and the modeled results from Cress

(b) The lack of height variation in the values of β_{CO_2} based on the Cress data in contrast to the NOAA 4 km and 7 km data

(c) The differences between the values of β_{CO_2} based on the Patterson et al. and the Cress continental data reflecting the lack of large particles in the Patterson et al. data

7.3 Stratospheric Behavior

Fig. 4.2 shows the long-term stratospheric lidar aerosol variation between 1974 and 1981. A mean conversion factor for $\beta_{10.6}/\beta_{0.69}$ has been calculated using stratospheric aerosol data without the inclusion of the Hofmann and Rosen large particles (Table 7.1). This has been used to generate the β_{CO_2} scale shown on the right-hand side of the figure. Once again, a minimum value of β_{CO_2} of about 10^{-11} m^{-1} sr^{-1} is obtained. Shortly after a significant volcanic eruption this may increase to 10^{-10} or 10^{-9} for a period of a few months. (If Hofmann and Rosen's large particles are included in the modeling, even higher values will be obtained.) More measurements are required on the variations in the stratospheric particle size distribution, particularly for particles with radii $\sim$1 μm before this figure can be regarded as authoritative.

7.4 Effect of Wavelength Variation

The backscattering functions have been calculated for CO_2 wavelengths ranging from λ = 9.1 μm to 11.1 μm using different aerosol substances and size distributions. The Mie code has been used with the refractive indices given in Table 3.5. In the first set of calculations, we have assumed the aerosol concentration is one particle per cc and aerosol size distributions to be log-normal, with geometric mean standard deviation σ_g = 2.0 and mode radii varying from 0.05 μm to 5.0 μm. As illustrated in the plots shown in Figs. 7.3, 7.4, and 7.5, for some materials, such as sulfuric acid with 75% H_2SO_4 and 25% H_2O, and dust, the variation of β_{CO_2} with CO_2 wavelength is small (a factor of less than about 3) regardless of the assumed aerosol size distribution. However, for other materials, such as $(NH_4)_2SO_4$, the variation of β_{CO_2} with CO_2 wavelength is size dependent. For log-normal aerosol size distributions with mode radii at about 0.7 μm, the variation is less than a factor of 2. However, for aerosols with large or small radii, it is possible to get an order of magnitude variation. This observation can also be seen from the variation of β_{CO_2} with wavelength, based on measured aerosol size distributions (Figs. 7.6-7.8). The same three size distributions have been selected for this study as were mentioned in Section 6.2. They are, a spring averge continental distribution with a large number of the larger particles given by Cress (1980), a continental distribution with fewer large particles and a maritime free tropospheric distribution with even fewer

larger particles both by Patterson et al. (1980). For the Cress spring average size distrribution, the variation of the backscattering function with CO_2 wavelength is always less than a factor of 2, regardless of the aerosol substances. For the Patterson et al. size distribution, the backscattering functions for water soluble and $(NH_4)_2SO_4$ aerosols may vary by about an order of magnitrude with the CO_2 wavelength, but for other aerosol materials the variation is small.

7.5 Effects of Humidity and Temperature Variations

As mentioned previously in Section 3.5, a dry but hygroscopic aerosol particle will grow as soon as the ambient humidity passes the threshhold value required for deliquescence. When aerosols remain in the solution state, their water vapor pressure is in equilibrium with the ambient water vapor pressure. The size and effective index of refraction will change following a change in the ambient humidity and/or temperature. Consequently the backscattering function and extinction coefficients of the growing or evaporating aerosols change.

Previously we have developed a numerical model to study th growth and evaporation effects on the extinction of 1.0 μm solar radiation traversing stratospheric sulfuric acid aerosols (Yue and Deepak, 1981); we have now extended this model to study both the backscatter and extinction, to study not only the wavelength used in the SAGE and SAM II satellite experiment (λ = 1.0 μm) but other wavelengths of radiation including λ = 10.6 μm (CO_2 laser wavelength), λ = 1.06 (YAG laser), and λ = 0.6943 μm (Ruby laser). In addition, we are able to study not only H_2SO_4 aerosols, but NaCl and $(NH_4)_2SO_4$ as well.

We assume that initially all particles have the same composition and their size distribution is given by

$$n(r) = \frac{A}{r} \exp\left[- \frac{\ln^2(r/r_m)}{2(\ln\sigma_g)^2} \right] \tag{7.1}$$

where A is a constant, and r_m and σ_g are mode radius and standard deviation, respectively.

As ambient conditions change, the size of a particle changes from r to r′ as discussed in Section 3.5. Consequently, the aerosol size distribution changes to n′(r) given by

$$n'(r) \frac{A}{r} \exp\left[- \frac{\ln^2[r/(fr_m)]}{2(\ln\sigma_g)^2} \right] \tag{7.2}$$

where f is the growth factor defined in Section 3.5.

The percentage change of backscattering function when ambient conditions change is then given by

$$P = \frac{\Delta\beta}{\beta} \times 100\%$$

$$= \frac{\int_{fr_1}^{fr_2} \frac{a}{r} \exp\left\{ - \frac{\ln^2[r/(fr_m)]}{2(\ln\sigma_g)^2} \right\} dr - \int_{r_1}^{r_2} \frac{a}{r} \exp\left\{ - \frac{\ln^2(r/r_m)}{2(\ln\sigma_g)^2} \right\} dr}{\int_{r_1}^{r_2} \frac{a}{r} \exp\left\{ - \frac{\ln^2(r/r_m)}{2(\ln\sigma_g)^2} \right\} dr} \times 100\%$$

Some of the percentage backscatter changes, plotted as a function of temperature or relative humidity change, are presented in Figs. 7.9 to 7.12. These figures illustrate that the change of backscattering function due to a change in ambient conditions is negligibly small at low relative humidities. However, when the relative humidity is 90% or higher, the change

in the backscattering function may reach more than 100% for a few degrees change in temperature or a few percent change in relative humidity. The plotted curves also demonstrated that the change in backscattering function is size dependent; the smaller the aerosol particles, the higher the backscatter change corresponding to the same ambient condition change.

In order to see whether high relative humidity actually occurs in the atmosphere, we have studied the relative humidities reported by Cress (1980). The result is plotted in Fig. 7.13 where each dot in the height versus relative humidity plane represents a value reported by Cress. Also plotted in Fig. 7.13 are the median for Cress' data and the profiles of humidity in January and July reported by Newell et al. (1972). It can be seen that the higher the altitude, the less the chance of occurrence of high humidity. At high altitudes there still exists some instances where the relative humidity is close to 100%. Consequently, the effect of humidity on backscatter should not be ignored, especially for aerosols near the ground.

The percentage ocurrence of humidity at 1 km is plotted in the form of histogram in Fig. 7.14. Also plotted in Fig. 7.14 are the ratios of backscattering function at a given relative humidity to the backscattering function at 0% relative humidity, using the Cress spring average aerosol size distribution with two aerosol materials: $(NH_4)_2SO_4$ and NaCl. The deliquescence starts at a relative humidity equal to about 77% and 82% for NaCl and $(NH_4)_2SO_4$, respectively. The ratio of the backscattering functions for $(NH_4)_2SO_4$ drops down to less than 1 before it increases and gradually reaches values greater than 1 at a relative humidity greater than 95%. This surprising phenomenon is due to the fact that the refractive index of dry $(NH_4)_2SO_4$ is about 1.98 but that of H_2O is only about 1.18. Although the absorption of water after passing the deliquescent point increases the cross section of the particles, the decrease in refractive index plays a more dominant role, resulting in a decrease in backscattering function. The behavior of NaCl aerosols is less unexpected, showing a large change in backscattering function following the same change in relative humidity in a humid environment.,

TABLE 7.1: CONVERSION FACTORS USED TO OBTAIN β_{CO_2}

Atmospheric Region	Conversion Factor
MARINE FREE TROPOPAUSE AEROSOL	β_{CO_2} FOR 1 μGM^{-3} = $2.0 \times 10^{-10} M^{-1} SR^{-1}$
STRATOSPHERIC AEROSOL	$\beta_{10.6}/\beta_{0.69}$ = 3.0×10^{-3}
	$\beta_{10.6}/\sigma_{1.00}$ = $1.0 \times 10^{-4} SR^{-1}$

NOTE

AEROSOL DENSITY IN $\mu G.M^{-3}$ = AEROSOL VOLUME CONCENTRATION IN $\mu M^3.CM^{-3} \times \rho$

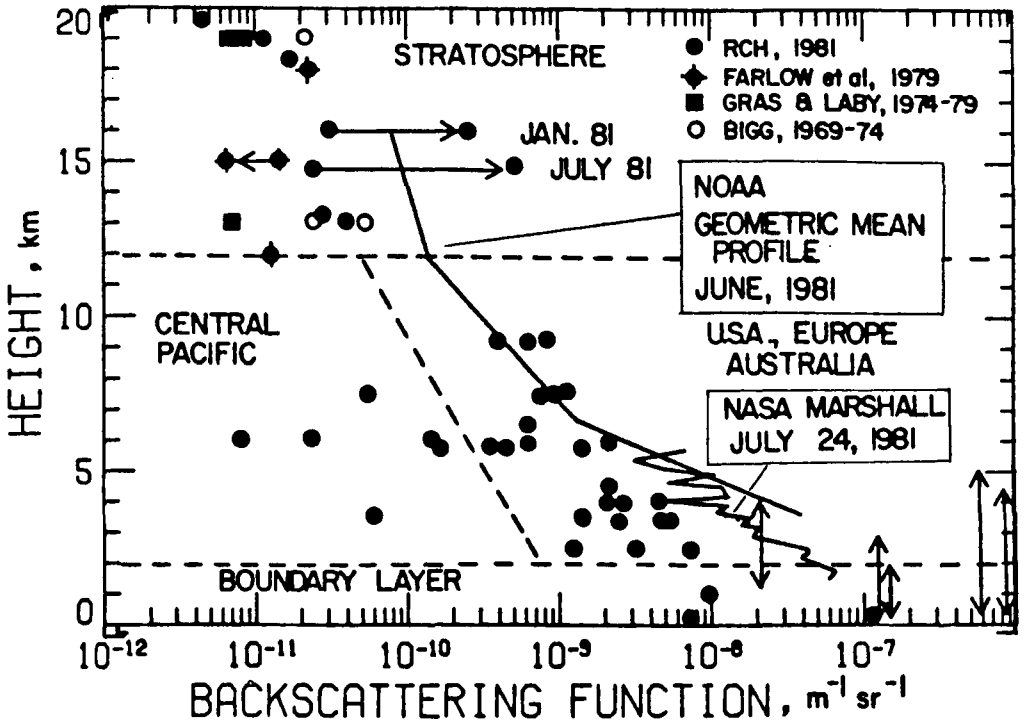

Figure 7.1 Modeled backscattering functions as a function of altitude for a large number of particle size distributions (see text for full references). Also shown are two curves for experimental determined values of β_{CO_2} (Bilbro, 1982; Post et al., 1982).

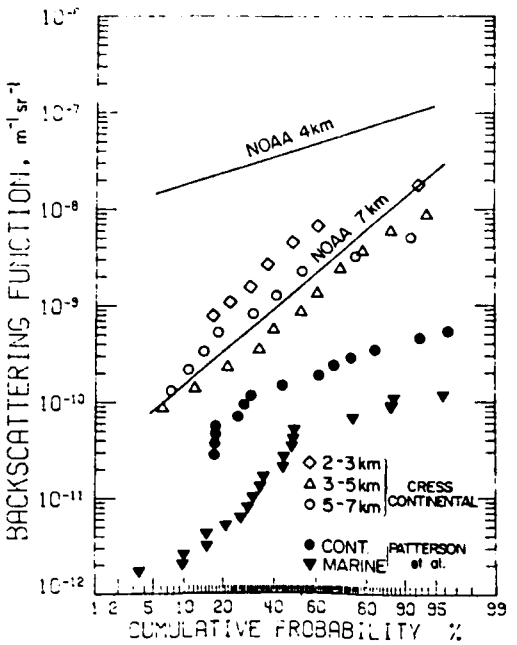

Figure 7.2 Cumulative probability distribution for modeled β_{CO_2} derived from the data shown in Figs. 3.13 and 3. 14. Also shown are the cumulative probability distributions obtained by NOAA (Post et al., 1982).

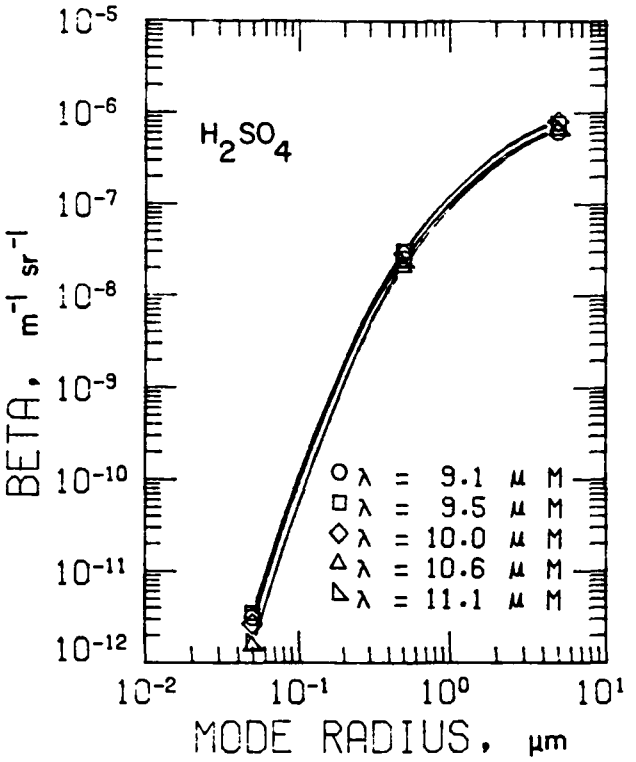

Figure 7.3 β_{CO_2} *versus mode radius for* H_2SO_4 *aerosols and different* CO_2 *wavelengths.*

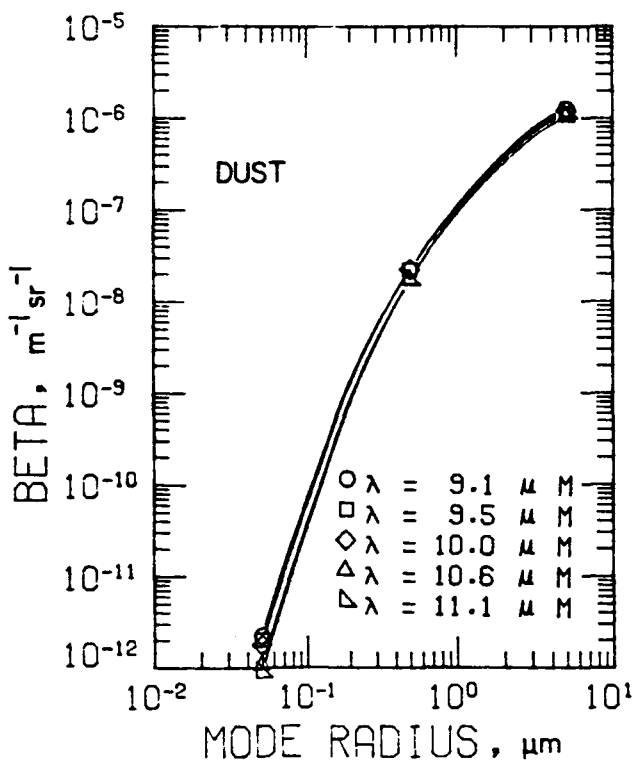

Figure 7.4 β_{CO_2} *versus mode radius for dust aerosols and different* CO_2 *wavelengths.*

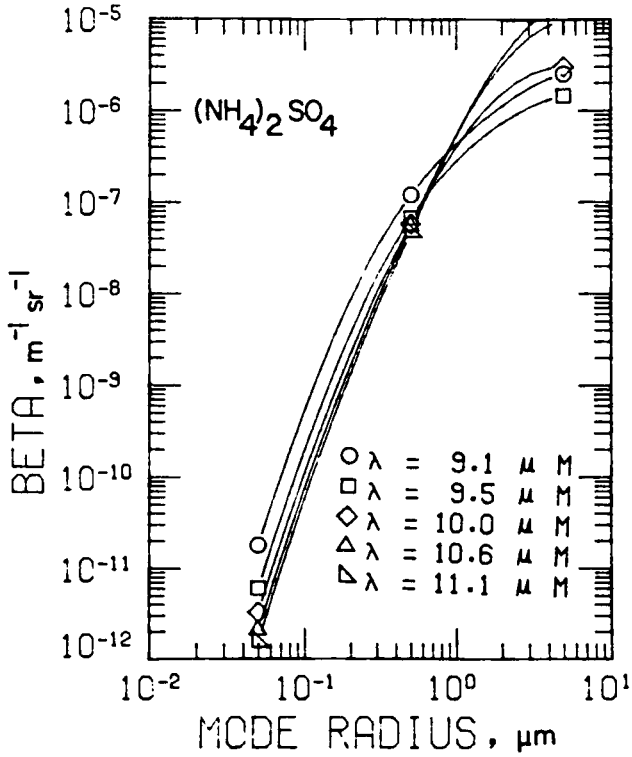

Figure 7.5 β_{CO_2} versus mode radius for $(NH_4)_2SO_4$ aerosols and different CO_2 wavelengths.

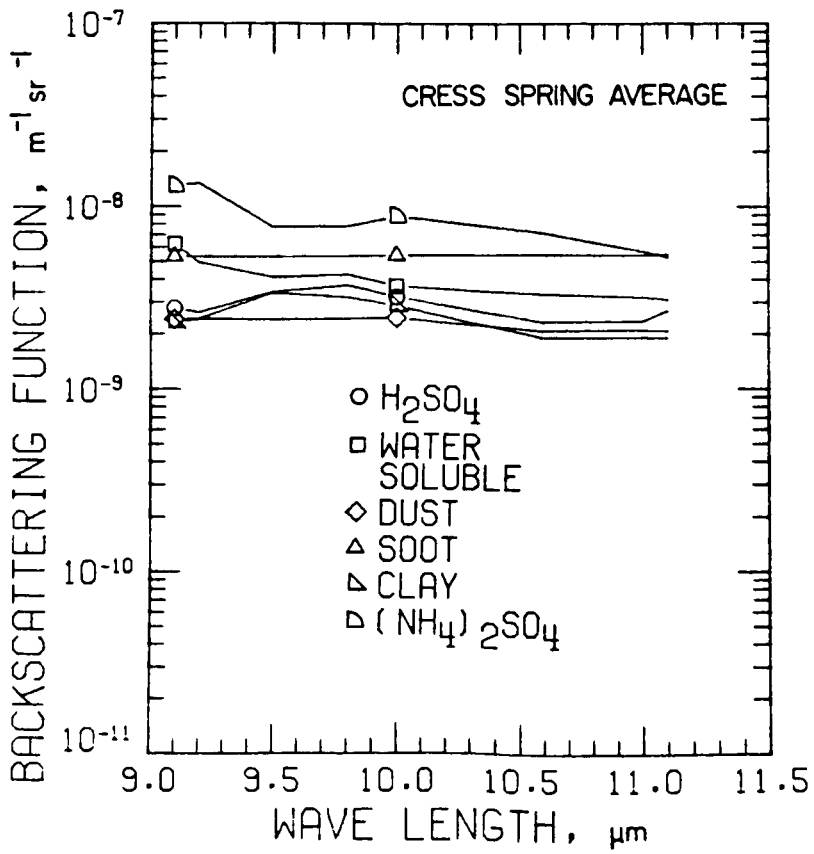

Figure 7.6 β_{CO_2} versus wavelength for the spring average aerosol size distribution reported by Cress (1980) and for different aerosol compositions.

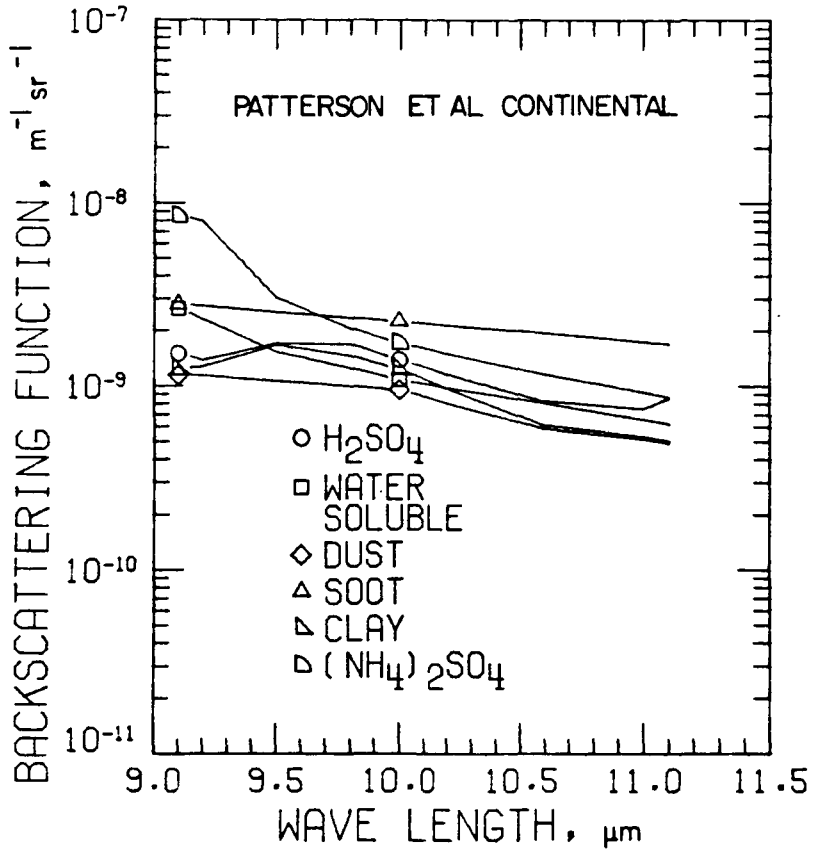

Figure 7.7 β_{CO_2} versus wavelength for continental aerosol size distributions reported by Patterson et al. (1980) and for different compositions.

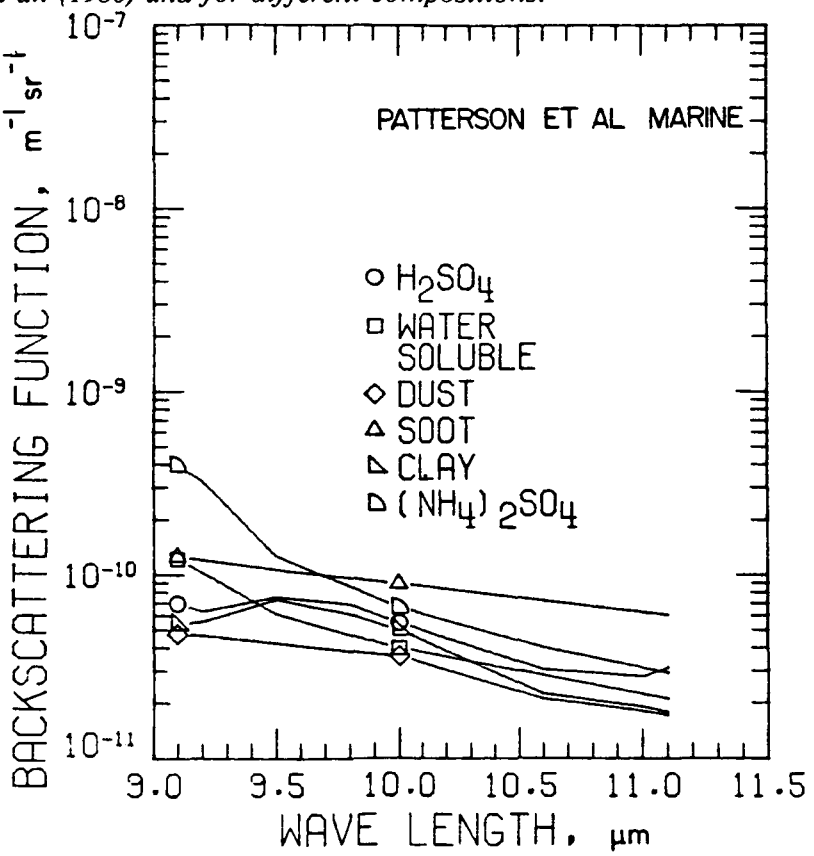

Figure 7.8 β_{CO_2} versus wavelength for marine aerosol size distributions reported by Patterson et al. (1980) and for different aerosol compositions.

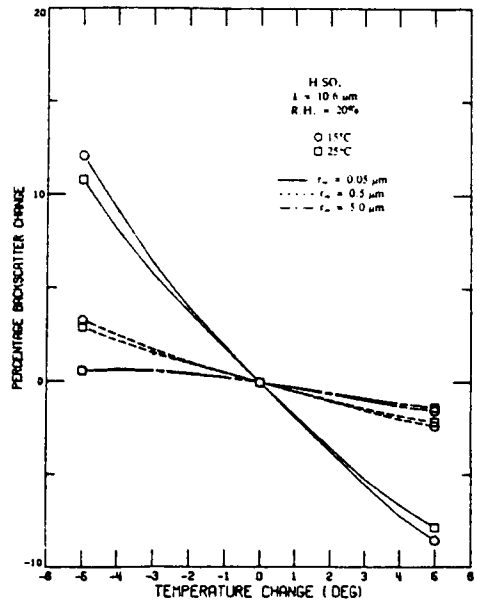

Figure 7.9 Percentage β_{CO_2} change versus temperature change for H_2SO_4 aerosols, using log-normal size distributions with mode radii equal to 0.05, 0.5, and 5.0 μm, at temperatures 15°C and 25°C and at a relative humidity of 20%.

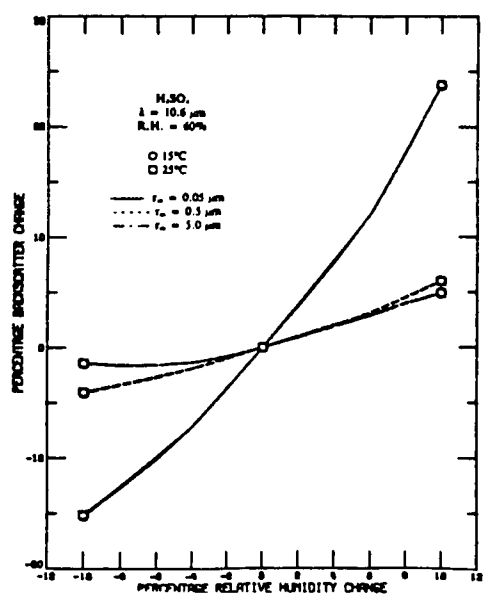

Figure 7.10 Percentage β_{CO_2} change versus relative humidity change for H_2SO_4 aerosols, using log-normal size distributions with mode radii equal to 0.05, 0.5, and 5.0 μm, at temperatures 15°C and 25°C, and at a relative humidity of 60%.

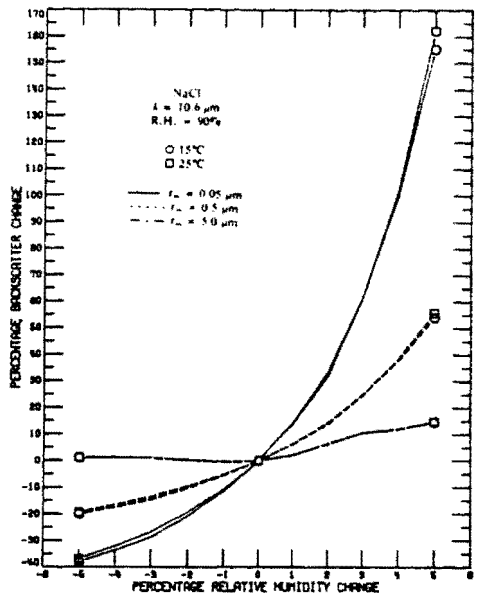

Figure 7.11 Percentage β_{CO_2} change versus percentage relative humidity change for NaCl aerosols, using log-normal size distributions with mode radii equal to 0.05, 0.5, and 5.0 μm, at temperatures 15°C and 25°C, and at a relative humidity of 90%.

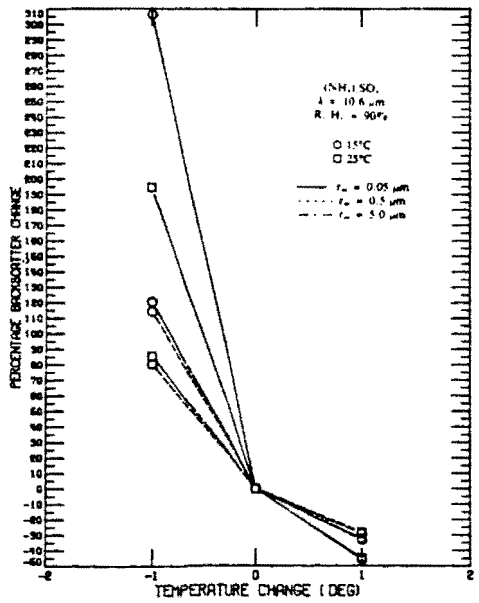

Figure 7.12 Percentage β_{CO_2} change versus temperature change for $(NH_4)_2SO_4$ aerosols using log normal size distributions with mode radii equal to 0.05, 0.5, and 5.0 μm, at temperatures 15°C and 25°C, and a relative humidity of 90%.

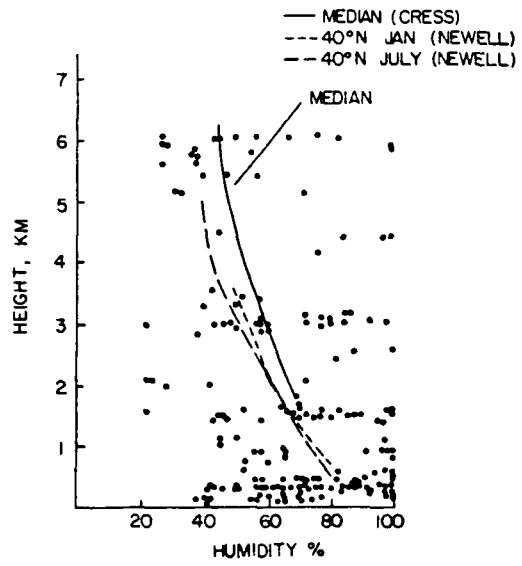

Figure 7.13 The humidities at different heights as reported by Cress (1980) and Newell (1972). Each dot represents an ambient condition reported by Cress and the solid line is the median value for this data. The short- and long-dashed lines are the 40°N January and July values presented by Newell et al. (1972), respectively.

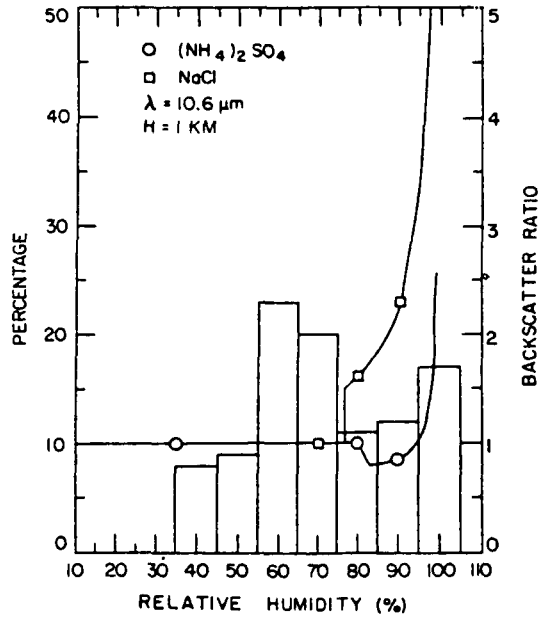

Figure 7.14 Histogram of the percentage of cases of a given relative humidity at an altitude of 1 km, reported by Cress (1980). The curves represent the ratio of β_{CO_2} at a given relative humidity to β_{CO_2} at 0% relative humidity. O is for $(NH_4)_2SO_4$ aerosols and □ is for NaCl aerosols.

8. CONCLUSIONS

Our conclusions from this study have been assembled in the form of tables, each covering a separate aspect of the work. The division is as follows.

TABLE 8.1: *Deduction of β_{CO_2} from Aerosol Measurements.* This table summarizes the main facts to emerge concerning the problems of modeling β_{CO_2}, using measurements of aerosol particle size and refractive index as a basis.

TABLE 8.2: *Main Features of Lidar and Extinction Measurements of Aerosols in the Lower Atmosphere.* This table summarizes the main characteristics of the available data set of lidar and extinction measurements made on atmospheric aerosols.

TABLE 8.3: *Deduction of β_{CO_2} from Backscattering Measurements at Other Wavelengths and from Extinction Measurements.* This table summarizes the problems of determining β_{CO_2} using other optical measurements as a basis.

TABLE 8.4: *General Remarks Concerning the Modeling of β_{CO_2}.* This table summarizes the range of accuracy achievable when modeling is done. It lists the major information gaps and makes recommendations for filling these gaps.

TABLE 8.5: *Effects of CO_2* Wavelength and Ambient Condition Changes on β_{CO_2}. This table summarizes the changes in the backscattering function due to a change in radiation wavelength from 9.1 μm to 11.1 μm, and identifies parameters affecting the change in β_{CO_2} when the ambient conditions change.

TABLE 8.6: *Sources of Error in the Calculation of β_{CO_2}.* This table lists (separately from what may already have been shown in the other tables) the possible sources of error in the calculation of β_{CO_2} and the magnitude of their effect on β_{CO_2}.

TABLE 8.7: *Modeled Values of β_{CO_2} in the Atmosphere.* This table summarizes the information that we have been able to obtain concerning the actual behavior of β_{CO_2} in the atmosphere, its magnitude, its variation, and the major information gaps and problems.

TABLE 8.1 DEDUCTION OF β_{CO_2} FROM AEROSOL MEASUREMENTS

1. At a wavelength of 10.6 μm, particles with radii greater than 0.5 μm are responsible for 50-95% of the scattering from tropospheric aerosols.

2. β_{CO_2} for 1 particle per cm^3 varies from $10^{-12} \rightarrow 10^{-6}$ m^{-1} sr^{-1} for naturally occurring aerosols, the lowest values being associated with the smaller particles.

3. β_{CO_2} for an aerosol volume concentration of 1 μm^3 per cm^3 varies from 10^{-10} to 10^{-8} m^{-1} sr^{-1} for naturally occurring aerosols. In certain circumstances, analysis in terms of aerosol mass distribution rather than number distribution may be preferred.

4. Shape is not an important factor in the calculation of β_{CO_2}, except possibly near an absorption line. (It may affect extrapolation from shorter wavelengths.)

5. Accurate calculation of β_{CO_2} requires accurate knowledge of dn/d log r to at least 1 μm and probably 2 μm for stratospheric aerosols and to at least 5 μm and probably 10 μm for tropospheric aerosols.

6. Composition is an important factor only for aerosols with a number mode radius greater than 1 μm. For a mode radius of 5 μm the difference in β_{CO_2} between a water soluble and a non-water soluble aerosol may approach an order of magnitude.

7. Extrapolation of aerosol size distributions to large sizes may lead to significant errors.

TABLE 8.2 LIDAR AND EXTINCTION MEASUREMENTS

I. Lidar:

1. Mainly confined to U.S.A., Europe and Japan
2. Principal wavelengths are 0.6943 μm, 1.06 μm (and 10.6 μm)
3. Long term data sets exist for the stratospheric aerosol
4. Numerous boundary layer measurements exist
5. Due to normalization problems, data for the free troposphere (and particularly its upper levels) is of limited value
6. Recent measurements of aerosols, using airborne lidar systems, at both visible and infrared wavelengths, show that this is a powerful technique for investigating many aerosol characteristics.

II. Extinction:

1. The most significant extinction data set, with global coverage, is that obtained at a wavelength of 1 μm from the SAGE and SAM II satellite systems.
2. Although the majority of data obtained by SAGE and SAM II is confined to stratospheric regions below 30 km, under favorable conditions, extinction data to the earth's surface can also be obtained.

TABLE 8.3 DEDUCTION OF β_{CO_2} FROM BACK-SCATTERING MEASUREMENTS AT OTHER WAVELENGTHS AND FROM EXTINCTION MEASUREMENTS

1. Particle sizes responsible for most extinction and scattering at shorter wavelengths are not the same as those responsible for scattering at 10.6 μm.

2. Values for the ratios of β_{CO_2} to $\beta_{0.69}$, $\beta_{1.06}$ and $\sigma_{1.00}$ vary over 1.5 → 2 orders of magnitude. Some sub-division into aerosol class may be made, lowest values of the ratio occur for stratospheric aerosols.

3. Stratospheric lidar measurements may be used to give an approximate time history for β_{CO_2} in the stratosphere. Minimum values may be fixed fairly accurately.

4. The ratio β_{CO_2} to σ_{CO_2} varies over 1.5 → 2 orders of magnitude, lowest values occurring for stratospheric aerosols.

TABLE 8.4 GENERAL REMARKS CONCERNING THE MODELING OF β_{CO_2}

1. The qualitative behavior of β_{CO_2} can be modeled including, in particular the height variation and major geographical variations.

2. Given present published information on aerosols, errors are half to one order of magnitude, even for the best information.

3. Major information gaps are
   1. Composition and size distribution of large particles at all levels above the boundary layer
   2. Seasonal and geographical variations of the aerosol
   3. Aerosols properties at altitudes of 7-12 km
   4. Humidity effects on large aerosols

4. Considerable variation in the parameters as measured by different instruments now exists

5. Extrapolation of optical measurements at other wavelengths to 1.06 μm can lead to errors at least as large as an order of magnitude. The error is dependent upon aerosol size distribution and may be reduced if this is known more exactly.

6. It appears desirable to
   1. Make simultaneous measurements for comparison purposes, using different sensors in the free troposphere
   2. Attempt to fill the information gaps noted above
   3. Make simultaneous measurements of CO_2 back-scatter and aerosol properties to confirm and improve modeling.

TABLE 8.5

EFFECTS OF CO_2 WAVELENGTHS AND AMBIENT CONDITION CHANGES ON BACKSCATTERING FUNCTION

The variation of β_{CO_2}, the backscattering function at CO_2 wavelengths (9.1 to 11.0 μm) depends on the aerosol composition.

1. For aerosol particles other than water soluble and ammonium sulfate, the variation in β_{CO_2} is less than a factor of 2.
2. For water soluble and ammonium sulfate aerosols, there may be a one order of magnitude change in β_{CO_2}.

Effects of changes in relative humidity and temperature on β_{CO_2} depends on several parameters:

- Aerosol composition--changes in β_{CO_2} from H_2SO_4, $(NH_4)_2SO_4$ and NaCl aerosols are different.
- Aerosol mode radius--the smaller the mode radius, the larger the change in β_{CO_2}.
- Ambient temperature--the lower the ambient temperature, the larger the change in β_{CO_2}.
- Ambient water content--the higher the ambient water content, the larger the change in β_{CO_2}. However, aerosol deliquescence must occur before any change can be observed.
- Change in ambient condition--increase in ambient water content or decrease in temperature will in general increase β_{CO_2}, except near the point of deliquescence.

TABLE 8.6

SOURCES OF ERROR IN THE CALCULATION OF β_{CO_2}

Uncertainties in

1. Aerosol size distribution and concentration

   -- Lack of detailed knowledge of particles with radii > 1 μm make β_{CO_2} calculations totally invalid. Even using the best information available on these particles, order of magnitude errors may arise.

2. Aerosol refractive index

   -- Except for materials with very high or low refractive indices or near absorption lines, errors are not more than a factor of two or three.

3. Aerosol shape

   -- Not an important factor (errors $\leqslant$ a factor of two) except possibly near an absorption line.

4. Measurement uncertainties

   -- Sampling problems arise here, as well as uncertainties in the technique itself. Order of magnitude errors may occur.

5. Natural variations

   -- The altitude variation of aerosol concentration and composition is reasonably well-documented from 0-6 km and in the stratosphere. Geographical, seasonal and meteorological variations are not well-documented but concentration variations of aerosol orders of magnitude definitely occur.

TABLE 8.7 MODELED VALUES OF β_{CO_2} IN THE ATMOSPHERE

1. β_{CO_2} decreases from 10^{-6} m^{-1} sr^{-1} at the earth's surface to 10^{-11} m^{-1} sr^{-1} in the stratosphere.

2. Values determined from different data sets may differ almost as much as the range within a single data set.

3. There is a scarcity of data for heights between 7 km and the tropopause.

4. β_{CO_2} for stratospheric aerosols is very dependent upon the presence of large particles with radii $\geq$ 1.0 μm.

5. Significant differences exist between values for β_{CO_2} in the free troposphere over the land and over the remote ocean, the latter being an order of magnitude less, on the average.

6. The 10% and 90% probability levels for β_{CO_2} in the free troposphere lie 1 → 1-1/2 decades apart.

7. The height variation of β_{CO_2} and the probability distribution of β_{CO_2} agree reasonably well with measured values.

9. ACKNOWLEDGMENTS

This work was supported by Contract NAS8-34427 with NASA Marshall Space Flight Center (MSFC). It is a pleasure to acknowledge the many useful discussions with J. D. Bilbro, W. D. Jones and E. A. Weaver of NASA-MSFC on the various aspects of this work and for their providing part of the experimental lidar data shown in Fig. 7.1. The assistance of Dr. U. O. Farrukh, IFAORS, in the computer programming and data analysis is gratefully acknowledged.

10. REFERENCES

Bigg, E. K., Stratospheric particles, *J. Atmos. Sci. 32*, 910-917, 1975.

Bigg, E. K., Comparison of aerosols at four baseline atmospheric monitoring stations, *J. Appl. Met. 19*, 521-533, 1980.

Bigg, E. K. and Ono, A., Size distribution and nature of atmospheric aerosols. Paper presented at IAMAP/IAPSO Combined First Special Assembly, Melbourne, 1975.

Bilbro, J. M., 1981, private communication.

Blifford, I. H., Tropospheric aerosols, *J. Geophys. Res. 75*, 3099-3103, 1970.

Blifford, I. H. and Ringer, L. D., The size and number distribution of aerosols in the continental troposphere, *J. Atmos. Sci., 26*, 716-726, 1969.

Chylek, P., Grams, G. W., and Pinnick, R. G., Light scattering by irregular randomly oriented particles, *Science, 193*, 480-482, 1976.

Cress, T. S., Airborne measurement of aerosol size distributions over northern Europe. Volume 1. Spring and Fall, 1976, Summer 1977. Air Force Geophysical Laboratory, Hanscom Field, Mass., USA, Environmental Research Paper No. 702, 29 May 1980.

DeLuisi, J. J., Furukawa, P. M., Gillette, D. A., Schuster, B. G., Charlson, R. J., Porch, W. M., Fegley, R. W., Herman, B. M., Rabinoff, R. A., Twitty, J. T., and Weinman, J. A., Results of a comprehensive atmospheric aerosol-radiation experiment in the Southwestern United States. Part I: Size distribution, extinction optical depth and vertical profiles of aerosols suspended in the atmosphere, *J. Appl. Met. 15*, 441-454, 1976.

Duce, R. A., Unni, C. K., Ray, B. J., Prospero, J. M., and Merrill, J. T., Long range atmospheric tansport of soil dust from Asia to the tropical north Pacific: temporal varibility, *Science*, 1522-2524, 1980.

Elterman, L., An atlas of aerosol attenuation and extinction profiles for the troposphere and stratosphere, Office of Aerospace Research, United States Air Force, Hanscom Field, Mass, U.S.A., AFCRL-66-828, Environmental Research Papers, No. 241, December 1966.

Elterman, L., Vertical-attenuation model with eight surface meteorological ranges 2 to 13 kilometers, Office of Aerospace Research, United States Air Force, Hanscom Field, Mass, U.S.A., AFCRL-70-0200, Environmental Research Papers, No. 318, March 1970.

Farlow, N. H., Oberbeck, V. R., Colburn, D. S. and Ferry, G. V., Comparison of stratospheric aerosol measurements over Poker Flat, Alaska, July 1979, *Geophys. Res. Lett. 8*, 15-17, 1981.

Gras, J. L., Southern hemisphere mid-latitude stratospheric aerosol after the 1974 Fuego eruption, *Geophys. Res. Lett. 3*, 533-536, 1976.

Gras, J. L. and Ayers, G. P., On sizing impacted sulfuric acid aerosol particles, *J. Appl. Meteor. 18*, 634-638, 1979.

Gras, J. L. and Laby, J. E., Southern hemisphere stratospheric aerosol measurements 3. Size distribution 1974-1979, *J. Geophys. Res. 86*, 9767-9775, 1981.

Haberl, J. B., Stratospheric Aitken nuclei counter, *Rev. Sci. Instrum. 46*, 443-447, 1975.

Hale, G. M. and Querry, M. R., Optical constants of water in the 200-nm to 200-μm wavelength region, *Appl. Optics, 12*, 555-563, 1973.

Hanel, G., The properties of atmospheric aerosol particles as functions of the relative humidity at thermodynamic equilibrium with the surrounding moist air, in *Advances in Geophysics, 19,* edited by Landsberg, H. E. and Mieghem, J. V., 73, 1976.

Hanel, G. and Bullrich, K., Physical properties of four types of tropospheric aerosols, prepared for Radiation Commission for Intercomparison Studies, 1977.

Hobbs, P. V., Radke, L. F., and Hindman, E. E., II, An integrated airborne particle-measuring facility and its preliminary use in atmospheric aerosol studies, *J. Aerosol Sci. 7,* 195-211, 1976.

Hofmann, D. J. and Rosen, J. M., Balloon-borne observations of stratospheric aerosol and condensation nuclei during the year following the Mount St. Helens eruption, U. of Wyoming, Dept. of Physics and Astronomy, Report No. AP-63, July 1981.

Huffman, D. R., A survey of optical constants in the 5-25 micron spectral region, Final Technical Report, March 13, 1981.

Kneizys, F. X., Shettle, E. P., Gallery, W. O., Chetwynd, J. H., Jr., Abreu, L. W., Selby, J. E. A., Fenn, R. W. and McClatchey, R. A., Atmospheric transmittance/radiance: computer code LOWTRAN 5, Air Force Geophysics Laboratory, Hanscom AFB, Mass, U.S.A., AFGL-TR-80-0067, Environmental Research Paper No. 697, 21 February 1980.

Kuznetsov, G. I. and Izhovkina, N. I., Two models of the atmospheric aerosol, *Atmospheric and Oceanic Physics, 9,* 537-540, 1972.

Longhurst, R. S., *Geometrical and physical optics,* Longmans, London, p. 423, 1964.

Lundgren, D. A., Aerosol measurement methods, in "Atmospheric Aerosols: Their Optical Properties and Effects," a topical meeting on atmospheric aerosols, held at Williamsburg, Virginia, December 13-15, 1976. NASA CP-2004.

McClatchey, R. A., Fenn, R. W., Selby, J. E. A., Volz, F. E., and Garing, J. S., Optical properties of the atmosphere (third edition), Air Force Systems Command, Hanscom Field, Mass, U.S.A., AFCRL-72-0497, Environmental Research Papers, No. 411, 24 August 1972.

McCormick, M. P., Hamill, P., Pepin, T. J., Chu, W. P., Swissler, T. J., and McMaster, L. R., Satellite studies of the stratospheric aerosol, *Bulletin of the American Meteor. Soc. 60,* 1038-1046, 1979.

Newell, R. E., Kidson, J. W., Vincent, D. G., and Boer, G. J., The general circulation of the tropical atmosphere and interactions with extratropical latitudes, Volume 1, The M.I.T. Press, 1972.

Nilsson, B., Meteorological influence on aerosol extinction in the 0.2-40 μm wavelength range, *Appl. Opt. 18,* 3457-3473, 1979.

Palmer, K. F. and Williams, D., Optical constants of sulfuric acid; application to the clouds of Venus? *Appl. Opt. 14,* 208-219, 1975.

Patterson, E. M., Optical properties of the crustal aerosol: relation to chemical and physical characteristics, *J. Geophys. Res. 86,* 3236-3246, 1981.

Patterson, E. M. and Gillette, D. A., Commonalities in measured size distributions for aerosol having a soil-derived component, *J. Geophys. Res. 82,* 2074-2082, 1977.

Patterson, E. M. and Grams, G. W., Optical methods for in situ measurements of aerosol size distributions and optical properties, in Tropospheric Chemistry Measurements from Aircraft, *Atmospheric Technology,* No. 12, published by NCAR, 1980.

Patterson, E. M., Kiang, C. S., Delany, A. C., Wartburg, A. F., Leslie, A. C. D., and Huebert, B. J., Global measurements of aerosols in remote continental and marine regions: Concentrations, size distributions and optical properties, *J. Geophys. Res 85,* 7361-7375, 1980.

Pinnick, G. R., Rosen, J. M., and Hofmann, D. J., Stratospheric aerosol measurements, III: Optical model calculations, *J. Atmos. Sci. 33,* 304-314, 1976.

Post, M. J., Hall, F. F., Richter, R. A., and Lawrence, T. R., Aerosol backscattering profiles at λ = 10.6 μm. Submitted to *Applied Optics,* 1982.

Prospero, J. M. and Carlson, T. M., Vertical and areal distribution of Saharan dust over the west equatorial North Atlantic Ocean, *J. Geophys. Res. 77,* 5255-5215, 1972.

Pueschel, R. F., Condensation nucleus measurements in Tropospheric Chemistry measurements from aircraft, *Atmospheric Technology,* No. 12, published by NCAR, 1980.

Reagan, J. A., Shinhirne, J. D., Byrne, P. M., Thomson, P. W., de Pena, R. G., and Mamane, Y., Atmospheric particulate properties inferred from lidar and solar radiometer observations compared with simultaneous in situ aircraft measurements: A case study, *J. Appl. Met. 16,* 911-928, 1977.

Rosen, J. M. and Hofmann, D. J., Stratospheric condensation nuclei, Dept. of Physics and Astromony, U. of Wyoming, Report No. AP-61.

Rosen, J. M., Hofmann, D. J., and Laby, J., Stratospheric aerosol measurements II: The worldwide distribution, *J. Atmos. Sci. 32,* 1457-1462, 1975.

Russell, P. B., Swissler, T. J., McCormick, M. P., Chu, W. P., Livingston, J. M., and Pepin, T. J., Satellite and correlative measurements of the stratospheric aerosol. I: An optical model for data conversions, *J. Atmos. Sci. 38,* 1279-1294, 1981.

Sassen, K., Infrared (10.6-μm) scattering and extinction in laboratory water and ice clouds, *Appl. Opt. 20,* 185-193, 1981.

Savoie, D. L., Physical and chemical characteristics of Saharan aerosols over the tropical North Atlantic, Master's thesis, University of Miami, 137 p. 1978.

Selby, J. E. A., Shettle, E. P., and McClatchey, R. A., Atmospheric transmittance from 0.25 to 28.5 μm: Supplement LOWTRAN 3B, AFGL-TR-76-0258, Environmental Research Papers, No. 587, 1 November 1976.

Shaw, G. E., Transport of Asian desert aerosol to the Hawaiian Islands, *J. Appl. Met. 19,* 1254-1259, 1980.

Shettle, E. P., and Fenn, R. W., Models for the aerosols of the lower atmosphere and the effects of humidity variations on their optical properties, Air Force Geophysical Laboratory, Hanscom AFB, Mass., USA, AFGL-TR-79-0214, Environmental Research Papers No. 676, 20 September 1979.

Swissler, T. J., Hamill, P., Osborn, M., Russell, P. B., and McCormick, M. P., A comparison of lidar and balloon-borne particle counter measurements of the stratospheric aerosol 1974-1980, *J. Atmos. Sci. 39,* 909-916, 1982.

Toon, O. B., and Pollack, J. B., A global average model of atmospheric aerosols for radiative transfer calculations, *J. Appl. Met. 15,* 225-246, 1976.

Toon, O. B., Pollack, J. B., and Khare, B. N., The optical constants of several atmospheric aerosol species: Ammonium sulfate, aluminum oxide, and sodium chloride, *J. Geophys. Res. 33,* 5733-5748, 1976.

Volz, F. E., Infrared optical constants of ammonium sulfate, Sahara dust, volcanic pumice, and flyash, *Appl. Opt. 12,* 564-568, 1973.

Winkler, P., Die relative Zusammensetzung des atmospharischen Aerosols in Stoffgruppen, *Meteor. Rdsch. 27,* 129-136, 1974.

Woods, D. C., Examples of realistic aerosol particles collected in a cascade impactor, In *Light Scattered by Irregularly Shaped Particles,* edited by D. W. Schuerman, Plenum Press, New York and London, 1979.

World Meteorological Organization Report No. WGP-12, "Aerosols and Climate," report of the meeting of the JSC experts held in Geneva, 27-31 October 1980.

Yue, G. K., and Deepak, A., Modeling of growth and evaporation effects on the extinction of 1.0-μm solar radiation traversing stratospheric sulfuric acid aerosols, *Appl. Opt. 20,* 3669-3675, 1981.

11. APPENDIX

Lidar and Other Research Workers Supplying Information

We are glad to acknowledge the assistance of the following research workers who supplied information used in Table 4.1 and in other sections of this report.

L. Chanin	Service d'Aeronomie Centre National de la Recherche Scientifique 91370 Verrieres-le-Buisson, France
B. R. Clemesha	INPE-C.P 515 12200 Sao Jose dos Campos, Sao Paulo, Brazil
J. DeLuisi	NOAA Environmental Research Laboratories Boulder, Colorado 80303 USA
F. G. Elford	Department of Physics University of Adelaide Adelaide, South Australia 5001, Australia
F. Fredriksson	National Swedish Environment Protection Board S-611 82 Nyköping, Sweden
M. Hirono	Department of Physics Kyushu University 33 Fukuoka 812 Japan
R. Jaenicke	Johannes Gutenberg Universitat Fachbereick Physik Institut für Meteorologie Anselm. F. V. Bentzal-Weg 12 Mainz, Federal Rpublic of Germany
F. Kasten	Deutscher Wetterdienst Meteorologische Observatorium Hamburg Frahmredder 95 2000 Hamburg 65, Federal Republic of Germany
C. V. Lamberts	Physics Lab TNO P. O. Box 96864 2509 JG The Hague The Netherlands
S. Lundquist	Department of Electrical Measurements Chalmers University of Technology S-412, 96 Guteberg, Sweden

K. Nagaya	Water Research Institute Nagoya University Chikusa-hu, Nagoya, Japan
C. M. R. Platt	CSIRO, Division of Atmospheric Physics Aspendale, Victoria, Australia
H. Quenzel	Meteorologisches Institut der Universität Theresienstrasse, 37 D-8000, Munchen 2, Federal Republic of Germany
J. S. Randhawa	Atmospheric Sciences Laboratory White Sands Missile Range, New Mexico 88002 USA
R. Reiter	Fraunhofer Institute for Atmospheric Environmental Research D-8100 Garmisch-Partenkirchen, Federal Republic of Germany
D. Renger	Institrut fur Physik der Atmosphäere DFVLR 8031 Wessling, Federal Republic of Germany
R. Schotland	Institute of Atmospheric Physics University of Arizona Tucson, Arizona 85721, USA
C. F. Sechrist	Aeronomy Laboratory Department of Electrical Engineering University of Illinois Urbana, Illinois 61801 USA
L. Stefanutti	Instituto di Ricera sulle Onde Electro-magnetische of CNR Via Paniatichi 64 Firenze 50127, Italy
N. Takuchi	National Institute for Environmental Studies Yatabe, Tsukuba Ibaraki, 305, Japan
E. L. Thomas	Department of Applied Physics The University of Hull Hull, HU6 7RX, England
L. Thomas	The University College of Wales Aberystwyth, SY23 38Z, United Kingdom
J. M. Vaughan	Royal Signals and Radar Establishment St. Andrews Road Great Malvern Worcs. WR14 3PS, England
J. Weinman	University of Wisconsin Meteorology Department Madison, Wisconsin USA

C. H. Werner
Institut fur Ohtoelektronik
DFVLR
8031 Wessling
Federal Republic of Germany

R. A. Young
Department of Physics
University of Adelaide
Adelaide, South Australia, 5001 Australia

Y. Z. Zhao
Institute of Atmospheric Physics
Academia Sinica,
Beijing, China

V. E. Zuev
The Institute of Atmospheric Optics
USSR Academy of Sciences
Siberia Branch
Tomsk, USSR

F. F. Hall
NOAA/Environmental Research Laboratory
Wave Propagation Lab
Boulder, Colorado 80303 USA

1. REPORT NO.	2. GOVERNMENT ACCESSION NO.	3. RECIPIENT'S CATALOG NO.
NASA CR-3638		

4. TITLE AND SUBTITLE	5. REPORT DATE
Atmospheric Backscatter Model Development for CO_2 Wavelengths	October 1982
	6. PERFORMING ORGANIZATION CODE
7. AUTHOR(S)	8. PERFORMING ORGANIZATION REPORT #
Adarsh Deepak, Geoffrey S. Kent, and Glenn K. Yue	IFAORS Tech Report 189
9. PERFORMING ORGANIZATION NAME AND ADDRESS	10. WORK UNIT NO.
Institute for Atmospheric Optics and Remote Sensing P. O. Box P Hampton, VA 23666	M-390
	11. CONTRACT OR GRANT NO.
	NAS8-34427
	13. TYPE OF REPORT & PERIOD COVERED
12. SPONSORING AGENCY NAME AND ADDRESS	Contractor Report Final
National Aeronautics and Space Administration Washington, DC 20546	14. SPONSORING AGENCY CODE

15. SUPPLEMENTARY NOTES

Technical Monitor: William D. Jones, Marshall Space Flight Center

16. ABSTRACT

The results of investigations into the problems of modeling atmospheric backscatter from aerosols, in the lowest 20 km of the atmosphere, at CO_2 wavelengths are presented, along with a summary of the relevant aerosol characteristics and their variability, and a discussion of the measurement techniques and errors involved. The different methods of calculating the aerosol backscattering function, both from measured aerosol characteristics and from optical measurements made at other wavelengths, are discussed in detail, and limits are placed on the accuracy of these methods. The effects of changing atmospheric humidity and temperature on the backscatter are analyzed and related to the actual atmosphere. Finally, the results of modeling CO_2 backscatter in the atmosphere are presented and the variation with height and geographic location discussed, and limits placed on the magnitude of the backscattering function. Conclusions regarding modeling techniques and modeled atmospheric backscatter values are presented in tabular form.

17. KEY WORDS	18. DISTRIBUTION STATEMENT
aerosol backscattering tropospheric aerosol particles stratospheric aerosol particles particle sensors CO_2 lidar	Unclassified - Unlimited Subject Category 46

19. SECURITY CLASSIF. (of this report)	20. SECURITY CLASSIF. (of this page)	21. NO. OF PAGES	22. PRICE
Unclassified	Unclassified	87	A05

For sale by National Technical Information Service, Springfield, Virginia 22161

NASA-Langley, 1982